DESIGN AND SYNTHESIS OF FUNCTIONAL POROUS ORGANIC MATERIALS

by

Zachary M Smith

A thesis submitted to the Faculty of the University of Delaware in partial fulfillment of the requirements for the degree of Master of Science in Chemistry and Biochemistry

Summer 2020

DESIGN AND SYNTHESIS OF FUNCTIONAL

POROUS ORGANIC MATERIALS

by

Zachary M Smith

Approved: _____

Eric D. Bloch, Ph.D.
Professor in charge of thesis on behalf of the Advisory Committee

Approved: _____

Brian Bahnson, Ph.D.
Chair of the Department of Chemistry and Biochemistry

Approved: _____

John A. Pelesko, Ph.D.
Dean of the College of Arts and Sciences

Approved: _____

Douglas J. Doren, Ph.D.
Interim Vice Provost for Graduate and Professional Education and
Dean of the Graduate College

ACKNOWLEDGMENTS

First and foremost, I would like to thank Dr. Eric Bloch for providing the opportunity, resources, and support to improve my synthetic chemistry skillset and expand my knowledge of chemistry. I would also like to thank my fellow research group members both past and present, for their help both in and out of the lab: Alex Antonio, Jay Decker, Meaghan Deegan, Michael Dworzak, Eric Gosselin, Andrew Kuznicki, Greg Lorzing, Kyle Korman, Casey Rowland, Garrett Taggart, Omar Barreda, and Christina Charles. Without y'all my lab experience wouldn't have been the same.

Much love to my parents and family members for believing in me, and helping me navigate the strange world we live in.

-Zach Smith

TABLE OF CONTENTS

LIST OF FIGURES

ABSTRACT

Attempts to modify porous aromatic frameworks (PAFs) via altering reagent composition, such as the addition of substituents to its precursor molecules, has largely shown to be ineffective. However, porous aromatic frameworks (PAFs) can be post-synthetically modified by relatively simple processes to create catalytically active analogous structures for tailored applications. Using previously published and novel methods, our group has post synthetically modify PAF-1with Brønsted acid functional groups. These modified PAFs were used as catalysts in hydroxyalkylation alkylation (HAA) reactions, commonly used in the synthesis of alkylfuran precursors to industrially relevant bio-lubricant base oils. Base oils are a vital commodity to the production of commercial lubricants. Here we seek to optimize a step in the synthetic route of bio lubricant precursors by creating a more efficient catalyst that can be used in combination with cheap starting materials found in biomass like sugars, alcohols, and agricultural waste. This allows for cost cutting in lubricant production while improving desirable characteristics in the end product lubricants utilizing them.

As an alternative to PAFs, porous organic cages (POCs) can provide several benefits; mainly, their crystallinity and their compatibility with density modification strategies. An octahedral aldehyde and diamine-based imine cage, commonly referred to as CC3, has received a fair share of interest, becoming well known in POC based research into gas and small molecule storage and separations. While it excels at this application, its primary drawback is poor surface area when compared to other porous materials (MOFs, COFs, PAFs, etc.). Coupled with the moderately expensive starting

materials required for synthesis, namely 1,3,5-triformylbenzene, there is much room for improvement in both synthetic process and molecular structure. The work outlined here describes a strategy to modify the packing arrangement and density of CC3 to explore optimization of density, to ultimately improve volumetric methane uptake in POCs. This was achieved through the synthesis of film phase POCs, and the effects of phase change on gas adsorption characteristics and density were investigated.

Chapter 1

INTRODUCTION TO POROUS MATERIALS

For over a century, scientists have been investigating the properties of porous materials. This body of work even predates the advent of new synthetic materials to when porous materials were limited to natural porous rock found in the ground. Zeolites, for example, are a type of porous aluminosilicate mineral that can be found naturally throughout the earth. In 1896, French mineralogist Georges Friedel experimented with zeolite porosity by displacing water absorbed by zeolites with organic solvents such as ethanol, benzene, and chloroform.[1,2] Shortly thereafter, F. Grandjean demonstrated the adsorption of ammonia and hydrogen by a dehydrated a sample of chabazite zeolite.[2] In the hundred years since, both naturally occurring and synthetic porous materials have received considerable attention. This was largely motived by the promising industrial applications of these solids. Union Carbide demonstrated the first industrial-scale use of zeolites in 1953 when they employed Linde Type A zeolite to remove oxygen impurities from argon at one of their chemical plants.[3] More recently, particularly as a result of new designer materials, porous materials have been a promising area of research has provided society with a multitude of benefits. These have included processes for new and more efficient industrial productivity,[4] breakthroughs in medical care[5] and potentially lifesaving drug delivery systems.[6] Even beyond these, porous materials are responsible for many beneficial technologies humans utilize every day.[7,8,9]

Whether considering naturally occurring or synthetic porous materials, modern adsorbents are typically broadly split into 3 categories: microporous, which contain pores less than 2 nanometers in diameter, mesoporous, which contain pores between 2 and 50 nanometers, and microporous, which contain pores greater than 50 nanometers in diameter. As it is not uncommon for adsorbents to contain a combination of pore sizes, their classification is usually based on the largest type of pore present, rather than the most abundant. While all three of these classes of porous materials have several applications,[10,11] for the gas storage, chemical separation, and catalysis applications discussed in this work, microporous materials are of greatest interest as their pore size, shape, and surface functionalities can be tailored with the highest selectivity. To characterize porous materials a variety of methods can be used, some of the more prevalent methods include X-ray crystallography, infrared spectroscopy, and powder X-ray diffraction. X-ray crystallography is particularly useful because pore size and geometry can be inferred from the structural information it provides. However, since certain materials are insoluble and/or amorphous, surface area and porosity measurements are also important characterization methods for porous materials.

In analyzing gas adsorption data for the characterization of porous solids, the two most common methods of calculating surface areas involve either the Langmuir model or the adsorption models developed by Brunauer, Emmett, and Teller (BET Theory). The Langmuir adsorption model was developed over 100 years ago and is a relatively simple adsorption model, although it holds up to intense scrutiny in all but the most extreme cases. This model assumes that: adsorbates behave as an ideal gas when conditions are isothermal, all adsorbent sites are equivalent, adjacent adsorption

sites do not interact, and that only a single monolayer of coverage forms on the surface they adhere to. In using the Langmuir model to understand gas adsorption data, the saturation uptake of a gas under specific conditions can be calculated, and from this the material's Langmuir surface area (Langmuir surface area is denoted by S_{LANG}).[12] In complex adsorbents, however, the Langmuir model fails to account for multiple layers of adsorbent on a surface. The BET adsorption models, on the other hand, expand upon the Langmuir model by accounting for multilayer adsorption (BET surface area is denoted by S_{BET}), among other phenomena. This theory hypothesizes that gas molecules physically adsorb to surfaces in infinite layers, only interact with adjacent layers, Langmuir theory applies to each layer, adsorbents can form higher layers before the first layer is complete, and that adsorption enthalpy is highest for the first layer subsequently decreasing in each additional layer.[13] Despite their differences it is common for both to be used concurrently in characterization.

1.1 Porous Solids

Although this work focuses on porous aromatic frameworks (PAFs) and porous organic cages (POCs), two specific classes of porous *organic* materials, there are several classes of all-organic, all-inorganic, and hybrid organic/inorganic materials relevant to the work discussed here. Two notable examples of these materials important to the field of porous materials chemistry, zeolites and metal-organic frameworks (MOFs), will also be briefly discussed in addition to the exclusively organic materials outlined in this chapter.

1.1.1 Zeolites

Zeolites are the most well-known solids among the broader class of all-inorganic porous materials. The first documentation of a zeolite can be attributed to Axel Cronstedt, who upon discovering stilbite created the term zeolite itself for this newfound class of mineral.[14] By definition, zeolites, which are often present in hydrated forms, are crystalline aluminosilicate minerals commonly containing alkali or alkaline-earth metals.[15] While these microporous minerals can be naturally occurring, the majority of zeolites used today are synthesized via hydrothermal methods. In fact, of the 2.6 million hypothetically possible zeolite structures, just 230[16] have been isolated and of these, roughly 40 structure types are naturally occurring.[17] The first successful custom zeolite synthesis was reported in 1862 with the synthesis of levynite.[14,18]

The porous structures and thus adsorbent capabilities, in addition to their nearly unparalleled stability, of zeolites make them ideal candidates for industrial applications. Catalysis is the most common application where zeolites are used on a large scale, however other common applications include gas separations[19] and ion exchange.[20,21] A key factor in zeolites' capacity to serve as effective catalysts in numerous reactions lies in the ability to tune the material's acidity, which is often achieved through altering the ratio of silicon and aluminum in the framework to increase/decrease the number of available Brønsted acid sites.[22] In catalysis, the overwhelming majority of zeolite utilization can be attributed to the fluid catalytic cracking (FCC) process, which is used in petroleum refineries to convert the large hydrocarbons in crude oil into smaller hydrocarbons used in petroleum derivatives like gasoline and other distillate fuels.[23] These FCC zeolite catalysts account for approximately 95% of global annual zeolite catalyst consumption.[24] Although they

have proven incredibly useful in many large-scale industrial applications, their narrow, small diameter pores (<1.5 nm) result in diffusion limitations[25,26] which can hinder their use as catalysis or for separations involving bulkier molecules.[27]

1.1.2 Metal Organic Frameworks (MOFs)

Definitively speaking, a MOF is a material comprised of metal ions and organic linkers (ligands) that assemble to form a permanently porous crystalline solid. Although examples of structures that would currently be classified as MOFs had been previously synthesized,[28,29] the creation of the term Metal-Organic Framework (MOF) was credited to Omar Yaghi in 1995.[30] In the time since, MOFs have quickly found themselves at the forefront of porous material research due to their amenability to structural modification and often exceedingly high surface areas and porosity. The current record holder for surface area is DUT-60 (S_{BET} = 7839 m^2/g) which was synthesized in 2018.[31] While DUT-60 holds the record, there are several MOFs with BET surface areas in this range,[32] and many more in the S_{BET} = 3000-5000 m^2/g range,[33] establishing the MOF as a strong leader in the realm of ultrahigh surface area materials. Another impressive feature of the MOF is its structural variance, in terms of both metal ion and ligand composition. The Cambridge structural database (CSD) contains an estimated 70,000 unique MOF crystal structures,[34] and this number continues to grow rapidly. Such a wide variety of known structures and potential building blocks allows the MOF an extremely high degree of tunability, opening them to a wide array of applications in catalysis,[35,36] separations,[37,38] and gas storage.[39,40] However, a critical weakness of the MOF is that they often suffer from stability issues,[41] namely poor hydrostability, significantly decreasing in surface area and structurally deteriorating upon exposure to moisture (i.e. atmospheric conditions).[33]

Stability issues in MOFs can be partially attributed to the labile nature of the metal-ligand coordination bonds they are based on.[42] This is particularly the case for ultrahigh surface area MOFs. This renders them difficult or impossible to work with in most real-world applications where moisture free conditions are often impossible or unrealistic due to the financial implications.

1.2 Overview of Porous Organic Materials

The relatively poor stability of many MOFs is a debilitating drawback that severely limits their feasibility in many desired applications. To potentially overcome this disadvantage, many groups have turned to investigating porous materials that are all-organic in composition. Strong covalent and/or aromatic bonding could allow for increased stability while maintaining structural integrity and porosity. In MOFs, it is well known that the lower strength of the M-L bonds, as compared to the C-C bonds of their organic ligands, are a structural liability. Porous organic solids have been under investigation for decades. One of the earliest examples of a porous organic material is the hypercrosslinked polymer (HCP), first synthesized in 1969.[43] Surface areas for these amorphous materials range from 600 m^2/g - 2000 m^2/g BET.[44,45] Modification of precursor concentration and structure allows for moderate pore size tunability. HCPs have shown promise for CO_2 capture applications; however, their adsorption capabilities often degrade in wet conditions.[46]

Polymers of intrinsic microporosity (PIMs) represent another early class of all-organic porous solids. These amorphous materials, which are composed of rigid polymer chains were first synthesized in 2002 and have surface areas ranging from 450-950 m^2/g BET.[47] Through judicious functionalization, triptycene-based PIMs were able to reach surface areas up to 1760 m^2/g .[48] PIMs have seen success in gas

separations as their solubility in organic solvents allows for enhanced membrane formation capabilities.[49] Conjugated microporous polymers (CMPs) are similar to the previously mentioned polymers but feature π-conjugation arising from the alternating σ and π bonding systems they contain. CMPs were introduced by the Cooper group in 2007 with the synthesis of CMP 1-4 via Sonogashira-Hagihara cross-coupling reactions involving halogen and alkyne monomers.[50] Surface areas are usually around 1000 m^2/g BET for these materials but have been reported as high as 3180 m^2/g BET.[51] They too are amorphous due to inefficient packing and the rotational ability of the single bonds connecting their building blocks, but their electronic structure allows for use in electronic (optoelectronics and photocatalysis)[52] as well as traditional porous material applications (catalysis, separations, etc.).[53,54] It should be noted that polymer-type porous materials in general however, do present a unique downside compared to more structured materials: because their structures are completely random, it is difficult to meaningfully install functional groups and methods of functionalization must be designed accordingly.

Despite their impressive surface areas, the aforementioned limitations of MOFs led researchers towards creating materials with the desirable qualities of the MOF while possessing increased atmospheric stability and lower cost of synthesis. This was somewhat achieved with the creation of organic materials such as HCPs, PIMs, and CMPs, but they too suffer from stability issues. Additionally, they lack the ability to pack efficiently causing them to be amorphous, which can cause reduced adsorption capabilities at higher pressures due to flexibility, hindering gas storage application possibilities. The irreversibility of their bonds also leads to a lack of thermodynamic control during synthesis, often leading to formation of the less stable

product. With the creation of covalent organic framework (COFs), these crystallinity and bond reversibility issues were solved. COFs are 2D or 3D micro and mesoporous crystalline extended organic structures linked together by covalent bonds, first described by Adrien Cote and Omar Yaghi in 2005.[55] COFs improved upon the chemical and thermal stability issues seen in MOFs by replacing metal-ligand coordination bonds with stronger covalent bonds. Reversible bond formation during synthesis allows for thermodynamic control during polymer formation, leading to more stable products.[56] The relationships between reversible bonding, thermodynamics and kinetics in controlling COF formation has been investigated by several groups.

However, this increased stability comes at the price of reduced surface area when compared to MOFs, with the record COF surface area (DBA-3D-COF 1, S_{BET} = 5083 m^2/g)[57] falling significantly short in comparison to the highest recorded MOF (DUT-60, S_{BET} = 7839 m^2/g).[31] Despite this, they can serve a wide array of applications because of almost limitless tunability. This is due to the sheer number of available building blocks for synthesis and ease of functionalization, making it easy to create application specific materials. Some of the applications of COFs include drug delivery,[58] gas storage,[59,60] and catalysis.[61]

1.3 Porous Aromatic Frameworks (PAFs)

Efforts to create materials that combine the high surface area of MOFs with the stability of COFs led to the discovery of a new class of materials, porous aromatic frameworks (PAFs), also known as porous polymer networks (PPNs). PAFs are porous organic materials in which aromatic covalent bonding is used to create extended, rigid, molecular structures providing enhanced surface area and increased

stability vs. COFs and MOFs, respectively. Most often they are synthesized through coupling reactions using tetrahedral phenyl ring containing building blocks, or monomers. Common synthesis methods used to construct PAFs include, but are not limited to, Yamamoto-type Ullmann cross couplings,[62] Suzuki cross-couplings,[63] and ionothermal reactions.[64] The first reported PAF (PAF-1) was synthesized in 2009 by Zhu Et. Al. via a Bis(cyclooctadiene)nickel(0) catalyzed Yamamoto type Ullmann cross-coupling reaction.[65] PAF-1 is an amorphous three-dimensional polymer with an adamantane like pore structure featuring thermal stability up to 520°C, extreme hydrophobicity, and a surface area of $S_{B.E.T.}$= 5600 m^2/g.[65] Additionally, given its extended three-dimensional structure, it is insoluble in every organic solvent. Since the introduction of PAF-1, PAFs have quickly become materials of interest due to their unique properties, outstanding stability, and extremely high surface areas.

The majority of reported PAFs are comprised of interconnected tetrahedral carbon centered monomers, tetrakis(4-bromophenyl)methane being a prominent choice. Use of other central monomer atoms has also been explored, such as silicon[66] and germanium.[67] For example PPN-4 (also known as PAF-3), analogous to PAF-1 in structure, utilizes a tetrakis(4-bromosilyl)methane monomer and holds the record surface area for PAF materials at S_{BET} = 6461 m^2/g (S_{Lang} = 10063 m^2/g).[66] The nature of linkers between tetrahedral centers can also vary, in both length (i.e. number of phenyl rings), and composition (differing from the common biphenyl type linker). When composition is altered it is often to construct a secondary building unit (SBU) which is then interconnected as a monomer, this usually leads to a change in framework topology (differing from the theorized dia topology of PAF-1[65] and its analogs). Use of a SBU in PAF creation is exemplified in the synthesis of PAF-2,

where a triazine ring is used to create a SBU with tetrakis(4-cyanophenyl)methane to produce a material with ctn topology.[68] While deviation from the standard PAF structure of PAF-1, PAF-3, etc. in either topology or distance between tetrahedral center invariably causes changes in pore characteristics, it also often leads to a significant decrease in surface area.[63,69] The same can be said for functionalization of PAF linkers. A prime example of this is the functionalization of PAF-1 with amine groups to obtain BPP-1, which is discussed in greater detail in subsequent chapters. Addition of one amine substituent per linker decreases Langmuir surface area by ~ 5200 m^2/g. Ease of functionalization is a prime benefit in regard to structural tunability, but the severe decrease in surface area is something that must be kept in consideration when tailoring application specific materials.

A critical drawback of PAFs lies in their relative incompatibility with common porous material characterization methods. The lack of both crystallinity and solubility causes difficulties in the use of most conventional diffraction or spectroscopic techniques. Surface area measurements are a primary method of characterization and can provide insight into pore properties/characteristics, but they do not provide significant structural information. This has led to computational methods becoming a vital tool in predicting PAF structures, whereas traditional methods that provide more concrete information like X-ray diffractometry and mass spectrometry are unable to be of use. However, combining data from computations, IR spectrometry, solid-state NMR, elemental analysis, and surface area calculations have allowed for PAF structures to be known to an acceptable degree of certainty.

Despite being amorphous, PAFs have highly accessible pore structures that facilitate optimal adsorption properties for both gasses and liquids. Their somewhat

modular synthesis allows for diverse structural compositions and coupled with their stability and ability to be easily functionalized, PAFs have the opportunity to become essential materials for improving current processes/applications involving porous materials (i.e. catalysis, separations, gas storage, etc.).

1.4 Porous Organic Cages (POCs)

Porous organic cages (POCs) are a class of all-organic materials that have received heavy attention since their first report by Skowronek et. al.[70] They possess many of the desirable properties of the previously mentioned extended network porous organic materials. However, their molecular nature endows them with the added benefits of being crystalline and potentially ultra-tunable. An early iteration of a type of these materials was reported by Cooper *et. al.* in 2009.[71] These tetrahedral, imine-based cages are comprised of four equivalents of triformylbenzene and six diamine units which condense to form the resulting cage. Depending on particular crystal packing, this cage can display BET surface areas up to 624 m^2/g. This type of [A + B] formula allows for considerable tunability of imine-based cage structures. It is a common motif amongst POCs[72] and the possible combinations that have emerged are seemingly endless and include carbon-carbon[73] , boronic ester[74] , and porphyrin based[75] cages, with some configurations of POCs containing up to 20 components.[76]

Analogous to the relationship between the common synthesis methods for PAFs and COFs, POC syntheses can utilize either reversible or irreversible bond forming routes, though the latter is not as frequently utilized. Irreversible bonding routes include metal catalyst assisted cross coupling,[77] ester condensation,[78] and cycloaddition.[79] As previously discussed, cage syntheses that rely on irreversible bond forming reactions are not as ideal due to the lack of thermodynamic control they can

impart. Additionally, these reaction protocols often require multiple steps and purification processes, both of which lead to lower yields. However, cages with irreversible bonds often have increased stability over those based on reversible bonds (imine, boronic ester, etc.). For this latter, more common route, imine condensation is the most popular.[80,81] However, novel synthetic methods, such as those based on boronic ester formation[82,83] and alkyne metathesis[84,85] have recently been reported. Reversible bond forming routes are preferred because it allows for corrections in self-assembly leading to thermodynamic product formation. Cheaper cost of synthesis due to lack of added catalysts and reduced purification steps are also benefits of these routes. Most cages based on reversible bond forming reactions do not require any added catalysts, exceedingly hazardous chemicals, or extreme temperatures and/or pressures to synthesize, a benefit to both lab safety and budget. Many cages can be synthesized using cheap reagents and common organic solvents. Although, like irreversibly formed cages, cages formed via reversible bonding have potential issues in their design, synthesis, and implementation. Chiefly among these are relatively low hydrostability and the formation of interlocked cages during self-assembly due to solvent-cage interactions, reducing surface area and pore size. Therefore, it can be said that method of synthesis is an important factor and must be considered when designing cages for applications in specific conditions, or high throughput processes where excessive reaction times and purification steps could impede material production.

Regardless of their mode of synthesis, the molecular nature of POCs is a particular advantage in the production of crystalline structures. From a fundamental standpoint, this makes structure elucidation significantly easier in comparison to their amorphous porous organic counterparts. Their inherent solubility is another benefit, as

it permits co-crystallization with other cages,[86] incorporation into other materials to create composites like cage-MOFs,[87] or creation of new materials altogether.[88] Solubility can also be used to prepare thin layer or sheet-like formations, which can provide desirable qualities when applied to surfaces, such as stereospecific selectivity[89] and small molecule sensing capabilities.[90] Lastly, high solubility enables the use of solvent interactions as a means of control cage packing arrangements in the solid state, which can force the formation of alternative polymorphs and differing crystal structures. This is due to the somewhat weak intermolecular forces between cages. Their modular structures create the ability to design cages presynthetically with specific building blocks, functional groups, or desired properties in mind. One persistent negative aspect of POCs however, is that on average they tend to exhibit lower surface areas when compared to materials like PAFs and MOFs.[91] Although the highest reported surface area among cages is quite high at S_{BET} = 3758 m^2/g[92] they typically display BET surface areas below 1000 m^2/g. Despite this, with an extensive list of benefits over other porous organic materials and an almost limitless combination of structural components, POCs can be viewed as an ever-expanding class of materials that possess impressive tunability towards application specific molecules. They have already demonstrated functionality in sensing,[93] chemical separations,[94,95] and catalysis.[96]

1.5 Applications of Porous Organic Materials

The scope of applications for porous materials in general has seen considerable growth since the initial commercialization of synthetic zeolites by Union Carbide in in 1954. Early materials were used as drying agents for refrigerant and natural gasses.[2] Zeolites, porous silicas, and other inorganic porous materials are still heavily used in

industry today as adsorbents for separations and catalysis.[97,98] However, they suffer from issues that prevent a more widespread usage of these materials, including catalyst deactivation,[99] diffusion limitations,[100] and coking (carbon deposit buildup).[101] Metal-organic frameworks (MOFs) have received considerable recent attention as hybrid alternatives to all-inorganic porous materials. They have achieved some limited success in respect to these applications. However, their lackluster stability and relatively high reagent/synthesis cost has inhibited their widespread implementation. The necessity to create materials with the ability to perform these same processes, without the aforementioned limitations, has caused an immense uptake in research in the synthesis of new porous *organic* materials. Porous organic solids have already shown their utility for a variety of applications and their superb tunability has also led to them being considered for novel solutions to existing problems. A summary of current applications of porous organic materials will be discussed in three categories herein: separations, catalysis, and gas storage.

1.5.1 Separations

Separations play a vital role in virtually all industrial sectors; in fact, they account for an estimated 10-15 % of the world's total energy consumption,[102] and 40-90 % of industrial capital and operating costs.[103] The majority of separation methods used in industry today are energy intensive processes based on massive thermal inputs: distillation, drying, and evaporation. These alone account for 80 % of separations energy consumption.[104] Large energy inputs are required as most common thermal separation methods have terrible efficiency, typical distillation processes for example, have a thermodynamic efficiency of 5-20 %.[105] Distillation is the

highest source of separations related energy consumption by a large margin, it accounts for 90-95% of separations in both chemical and petroleum industries.[103] It is primarily used to separate large hydrocarbons in crude oil into smaller hydrocarbons for various uses (fuels, lubricants, etc.), separation of organic chemicals, and gas phase separations (i.e. oxygen and nitrogen production from air). Distillations have been relied on for so long, removing such a staple in the separations process and replacing it with alternative technology will be no easy feat. Adsorptive-based separations are inherently more energy efficient; adsorption and membrane separations could be used to decrease energy consumption by several orders of magnitude. However, these are contingent on the development of novel adsorbents for specific applications. This will require porous materials that provide equal separations efficiency with dramatically lower energetic cost to offset the costs of replacing current systems. However, there has been significant headway made towards developing materials that could make this task achievable. In addition to improving the separation efficiency of already employed industrial separations, there are a number of novel separations where advanced porous materials could have an impact. An important example of this is CO_2 capture associated with electricity generation, referring to the process of adsorbing CO_2 to prevent it from entering the atmosphere. Reducing CO_2 emissions is an important aspect of environmental protection, as it is a greenhouse gas that largely contributes to the climate change issues being encountered worldwide.

Progress made as of late involving separations centers around the formation of membranes purely comprised of porous organic materials or

formed by combining them with other porous materials to increase selectivity and gas permeability. Fu et al.[106] reported a promising example of this where they utilized a tetra-(4-anilyl)methane and terephthaldehyde based imine cage COF-300[107] and [$Zn_2(bdc)_2(dabco)$] to create a membrane, [COF-300]-[$Zn_2(bdc)_2(dabco)$], that shows exceptional H_2/CO_2 selectivity. This selectivity is desirable for application in pre-combustion CO_2 capture, where CO_2 would be captured and sequestered while H_2 is combusted. PIM-1 and PIM-7 membranes have also displayed high selectivity and permeability towards industrially relevant gas mixtures CO_2/O_2 and CO_2/CH_4,[108] whose separations are important in nitrogen generation and natural gas enrichment processes, respectively.[109,110] The porous, imine-based organic cage CC3 has shown aptitude in performing various types of separations. Notable examples include separation of rare gasses from air (Kr, Xe, Rn) at low concentrations,[94] and separation of sulfur hexafluoride from nitrogen.[111] Additionally, computational studies of mixed matrix membranes (MMMs) constructed with varying mixtures of POCs have shown impressive separations capabilities of H_2/N_2 and H_2/CO_2 gas mixtures[112] exceeding the upper bound of the empirical permeability/selectivity limit[113,114] of polymeric membranes. It has even been demonstrated that CC3 has the ability to act as a stationary phase for high resolution gas chromatography, allowing for the possibility of applications in analytical chemistry. When CC3 crystals were applied as a coating to a silica capillary gas chromatography column, the column was able to resolve n-alkanes, n-alcohols, aromatic hydrocarbons, as well as provide enantioselectivity that rivaled state-of-the-art commercial equipment.[115]

Light hydrocarbon separations are one of the primary processes in which distillation is used,[116] consuming a staggering amount of energy annually. As previously mentioned, the ability to carry out these separations with porous materials would conserve massive amounts of energy. The purification and separation of ethylene (C_2H_4) from ethane (C_2H_6) and acetylene (C_2H_2) is an example of a separation that is carried out on a massive worldwide scale. Ethylene is a vital commodity in many industrial applications and the production of polymers, rubbers, and plastics, at an average of 1.53 million barrels per day consumed in the U.S. alone.[117] PAFs have been investigated for the separation of ethylene from other C_2 hydrocarbons. As an illustrative example, PAF-1 was modified with sulfonyl groups and ion exchanged with Ag to afford PAF-1-SO_3Ag,[118] which demonstrated high C_2H_4/C_2H_6 selectivity. PAF-110[119] and PAF-120,[120] which feature naphthalene-1,4,5,8-tetracarboxylic dianhydride linkers coupled to tris(4-aminophenyl)amine and 1,3,5-tris(4-aminophenyl)benzene monomers, respectively, have been studied for C_2H_2/C_2H_4 separations. Both PAFs show noteworthy chemical and thermal stability, and have exceptional selectivity for C_2H_2 over C_2H_4, with PAF-120 being the highest among porous organic materials studied for C_2H_2/C_2H_4 separations. While research into light hydrocarbon separations with porous organic materials is relatively new, these materials show that there is potential for their use in energy efficient separations.

1.5.2 Catalysis

It's well known that catalysts play an imperative roll in all facets of chemistry, from small scale reactions encountered in research laboratories to the hundred plus kilogram scale processes seen in industry, catalysts are critical components in countless chemical reactions. Porous materials have long been investigated as catalysts due to their large available internal surface areas that are able to facilitate chemical reactions, as well as the ability to tune pore sizes and structures with functional groups to enable specific catalysis and minimize unwanted side reactions. The ease of which materials such as PAFs can be functionalized with metal ions or acidic/basic groups has garnered them considerable attention as potential catalysts for a wide array of reactions. POCs also have a degree of customizability in the fact that their assembly can be tailored by choosing catalytically active building blocks that have sites that retain their reactivity in the final assembled product. There are two strategies that focus on utilizing these tunable properties to develop catalysts using porous organic materials: direct synthesis using building blocks that feature catalytically active groups, and post-synthetic modification of the parent material to add catalytic functional groups or encapsulate the catalyst within the porous material.

Of the two methodologies for catalyst design, utilizing a combination of porous organic materials and reactive metal species has seen more interest, and often provides an easier synthesis route. The widely researched and understood nature of many metallic species allows for a more direct route to achieve the desired reactivity. Previous studies into established catalysis with zeolites, MOFs, or metal nanoparticles can be used as models towards intended

reactivity. Many catalysts have been developed for organic reaction schemes, where catalysts are essential to maintain high conversion rates. COFs in particular have seen success as active catalysts for a variety of organic transformations. COF-300 and COF-LZU1, two imine linked crystalline COFs, have been loaded with $Pd(OAc)_2$ to give $Pd(OAc)_2$@COF-300[121] and Pd/COF-LZU1[122] respectively, to achieve high reaction yields in Suzuki-Miyura coupling reactions for a wide array of starting materials (> 95% in most instances). $Pd(OAc)_2$@COF-300 also showed high yields in both Sonogashira and Heck cross-coupling reactions.[121]

Despite being relatively new materials, PAFs have also proved to have potential as efficient catalysts. Maximov *et al*.[123] used PAF-30 to support ruthenium nanoparticles and form the catalyst Ru-PAF-30 for the hydrogenation of arenes, which resulted in high percent conversions and size selective hydrogenation capabilities. PAFs containing N-heterocyclic carbenes were metallated with iridium or ruthenium (PAF-(NHC)Ir/PAF-(NHC)Ru) by Rangel-Rangel et al.[124] and showed exceptional catalytic activity for alcohol N-amine alkylation and transfer hydrogenation of ketones. These are but a few instances, but there are a myriad of examples where using porous organic materials to coordinate metal ions or support metallic catalysts combined the desirable qualities of porous organics with the reactivity of metal species to form efficient catalysts.

Compared to synthesizing porous organic catalysts that contain metal ions, the creation of efficient catalysts made exclusively of organic porous materials and functional groups has proven to be more challenging. However,

PAFs provide a strong parent structure for this method of catalyst design, as they feature high surface areas, extreme stability, and are amenable to functionalization to add active sites. For example, sulfonation of 1,3,5-tris(4-bromophenyl)benzene and tris(4-bromophenyl)amine based PAF structures (Sulfo-1 & Sulpho-2, respectively) lead to outstanding catalytic ability towards acid-catalyzed esterification of acetic acid with butanol.[125] When compared to a powerful esterification catalyst, Amberlyst-15,[126] the Sulfo-1 compound had higher activity over several recycles. Fine tuning pore characteristics within PAFs via substituents can provide specific selectivity as well as impart high catalytic activity. Chen et al.[127] created a chiral catalyst using L-prolinamide to functionalize PAF-1 for catalysis of the aldol condensation reaction between p-nitrobenzaldehyde and cyclohexanone. PAF-1-NHPro not only displayed good enantio- and diastereoselectivity but was also able to be recycled 10 times without a significant drop in performance. Taking advantage of pore morphology in a similar fashion, Sun et al.[128] exploited the large pore size of PAF-70 to bind a large thiourea functional group. PAF-70-thiourea was then used to catalyze the N-bromosuccinimide mediated oxidation of alcohols and impressively, displayed no decrease in catalytic ability after 36 cycles. Recyclability is an important aspect of all catalyst driven industrial processes, due to the cost of replacing deactivated catalysts becoming a financial burden.[129] The high chemical and thermal stability of PAFs gives them real potential as platforms to produce efficient, recyclable catalysts for industrial applications.

1.5.3 Gas Storage

Among the investigated uses for porous organic materials, gas storage has been the most thoroughly studied. This is primarily due to the increased interest towards developing alternatives to fossil fuels in the automotive sector. Alternative fuel research has seen a marked research in recent years as climate change intensifies and its effects become increasingly apparent. In 2017 CO_2 accounted for 81.6 percent of all greenhouse gas emissions at 5271 million metric tons of carbon dioxide equivalents, a 2.9 percent increase from 1990[130] Thirty seven percent of this massive number is a result of fossil fuel consumption by the transportation sector.[131] As these large numbers show, automobiles are a large contribution source of CO_2 emissions in the United States. Although passenger vehicles are constantly becoming more efficient, the ultimate efficiency of gasoline-based automobiles can only improve to a limited extent.[132,133] Even in the most efficient vehicles, the fuel being consumed still contributes heavily to CO_2 emissions. An alternative fuel to gasoline, such as compressed natural gas (CNG) could provide similar fuel economy and a up to a 15% decrease in greenhouse gas emissions.[134] Natural gas is currently being produced in record numbers in the US and around the world,[135] and mass adoption of CNG vehicles would also lead to decreased dependence on foreign oil imports, providing major economic benefits[136] in addition to reducing CO_2 emissions. However, in adopting a natural gas based transportation sector lies in the utilization of the fuel in mobile applications. Natural gas, primarily composed of methane, is a gas at room temperature and atmospheric pressure and is thus considerably less dense than gasoline (0.657 kg/m^3 and ~750 kg/m^3 respectively).[137,138] As a result of this, it has a much

lower energy density per liter of 0.04 MJ compared to gasolines 32.4 MJ.[139] To allow vehicles to store enough fuel to have a range comparable to gasoline powered vehicles, natural gas, the density of natural gas must be increased, typically either by compression or liquifaction. Pressures of 200 – 350 bar are required for adequate compression and liquid storage requires maintaining cryogenic temperatures of –162 °C.[140] In addition to the safety concerns of these methods, both are expensive which serves as a major deterrent towards widespread adoption of CNG vehicles, especially when compared to the cost of a traditional gasoline fuel system. In attempt to remedy this issue, porous materials have been investigated to provide a solution to the high compression required in today's natural gas vehicles.

Because of their high surface areas and promising methane adsorption capabilities, porous organic materials have been considered for improving current CNG fuel storage technology by facilitating adsorbed natural gas (ANG) technology. These materials have the capability to adsorb and desorb methane repeatedly, lowering the required pressure for adequate storage within the fuel tank to the pressure required for the material to adsorb sufficient quantities of methane. Pressures above atmospheric pressure would still be required but would be considerably lower than what is required in current CNG fuel systems. The Department of Energy (DOE) and the Advanced Research Projects Agency – Energy (ARPA-E) have set guidelines for materials intended to be used for this purpose, through their Methane Opportunities for Vehicular Energy (MOVE) program. The target set for adsorbent materials by the DOE is a total methane uptake of 350 cm^3(STP)/cm^3

at 65 bar. The ARPA-E target is a deliverable methane capacity of 315 cm^3(STP)/cm^3 over a 5.8 – 65 bar range.[141] Since researchers began focusing on making materials that meet or exceed these targets, there has been considerable progress made. The current leaders in total and deliverable methane capacity are the metal-organic frameworks HKUST-1[142] with a total methane capacity of 267 cm^3/cm^3 at 295 K / 65 bar,[143] and UTSA-76a with a deliverable capacity (65 – 5.8 bar) of 197 cm^3/cm^3 at 298 K.[144] While HKUST-1 and UTSA-76a are the closest to achieving the targets set by both the DOE and ARPA-E, both suffer from typical MOF stability issues, namely poor hydrolytic stability, that hinder their utilization for ANG storage. Several other MOFs[145] have also come close to the capacities of HKUST-1 & UTSA-76a, but they too suffer from stability problems. For this reason, many have invested in developing porous organic materials as more stable alternatives to meet these targets. Amongst organic materials, PPN-4 possesses the highest methane storage capability with a total uptake of 155 cm^3/cm^3 at 298 K and 55 bar with a deliverable capacity of 138 cm^3/cm^3.[146] COF-102 is another promising material with a total volumetric capacity of 145 cm^3/cm^3 at 298 K and 65 bar and a deliverable capacity of 123 cm^3/cm^3.[146] Unfortunately, aside from these two leading materials, the methane storage capacities of all-organic porous materials fall significantly short of those displayed by many MOFs.[143]

If focusing on the methane storage capacities alone, one could assume that porous organic materials fall significantly short of their MOF counterparts in terms of performance. However, their stability remains unparalleled. MOFs that cannot withstand atmospheric conditions face a very difficult path to

implementation, regardless of their methane uptake capabilities. Indeed, porous organic materials have a long way to go to overtake MOFs in terms of capacity, but the sheer number of resources available in organic synthesis in conjunction with vastly superior stability displayed by many porous organics offers them a sizeable advantage.

1.6 Outlook for Porous Organic Materials

There are many promising opportunities for porous all-organic materials to become staple materials in any number of applications, but there are several shortcomings that must be addressed before this is made a reality. Despite their impressive ability to be tuned in terms or pore size or the addition of desired functional groups, etc. a drawback remains in the fact that these modifications often severely decrease surface area, one of the most desirable properties of these materials. Beyond this, there are relatively few examples of pore size/shape tuning, particularly when compared to the vast reported body of literature concerning MOFs.

Perhaps the biggest obstacle these materials face in becoming real world industrial adsorbents, catalysts, etc. is ease and cost of synthesis. For many industrial processes, zeolites remain the most-used materials regardless of their relatively poor performance. This is because their cost is significantly lower than those of more designer materials. Many industrial processes require adsorbents or catalysts on the thousand plus kilogram scale, and they cannot operate in a financially successful manner if materials would need to be synthesized a couple hundred milligrams at a time or using extremely expensive catalysts. So even if there are alternatives that could provide significantly better performance and/or recyclability it would not cost effective to implement them in such massive scale processes.

For their ultimate utilization to be realized, the synthesis of these high performing porous organic materials must be able to be scaled up to be produced in large quantities and without the need for exotic catalysts. This challenge is no small feat, as some materials lose desirable properties when synthesis is scaled past a certain point, or alternatives synthesis routes that do not require catalysts have not yet been discovered. Many researchers focus primarily on material optimization which is undoubtedly important, however it must be considered hand in hand with overall cost and scalability if real-world industrial application is to be seriously considered.

Chapter 2

POROUS AROMATIC FRAMEWORKS

As a result of their impressive physical and chemical properties, porous aromatic frameworks (PAFs) are a class of porous materials that have garnered appreciable attention since their first report in 2009.[65] As interest in these materials, and the ever-increasing diversity of applications they have shown promise for continues to grow, it has become clear that this robust organic material is capable of being useful in a large assortment of applications.[147] When approaching the design of materials from a functionality standpoint, one must consider many factors that influence the end product's capability to be successfully implemented on a meaningful scale. First of course, is the ability for the material to perform optimally for the targeted application. Additionally, the material must be stable under, for example, the regeneration conditions required for reuse. What makes PAFs such interesting materials in this respect is not only their high surface areas, but also their remarkable stability which typically remains intact after modification and functionalization. In the areas where PAFs are sought to be applied (gas storage, separations, catalysis, etc.) longevity towards repeatedly performing the specified task is crucial. Because they offer such stability, combined with easy tunability, PAFs stand as ideal candidates to serve as application specific porous materials that provide resilience to harsh operating conditions and are also high recyclable.

2.1 Optimization of PAFs

The first step towards creating application-specific PAF derivatives was to optimize the synthesis and activation of the parent PAF structure, PAF-1. The majority of the work presented here involved the modification of PAF-1, so it was imperative to obtain the highest quality PAF-1 base materials prior to modification. Initial synthesis of PAF-1 was performed following the first published synthesis of the material by Ben et al.[65] and yielded a product with a Langmuir surface area of 6800 m^2/g and a total nitrogen uptake of 62 mmol/g at $P/P_0 = 0.95$. The initial wash and activation procedure consisted of washes with HCl, THF, and H_2O, followed by room temperature vacuum drying.

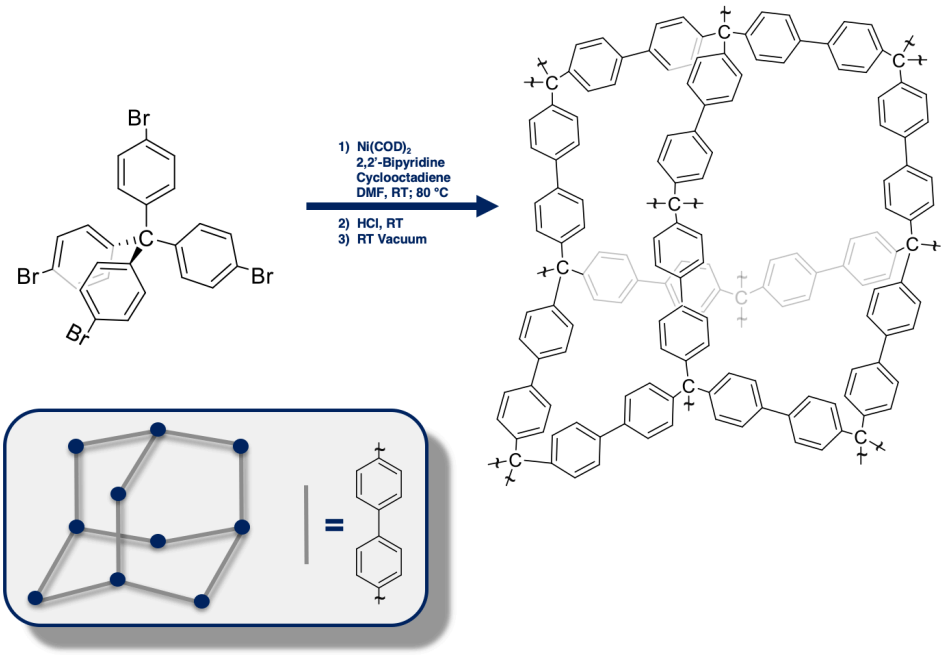

Figure 1: Reaction scheme of PAF-1 synthesis and representation of single diamondoid pore (main image). Simplified diagram of PAF-1 pore structure with biphenyl linker represented as stick, ball representing tetrahedral carbon node (bottom left).

However, consistently higher surface area material was able to be obtained through alteration of the wash and activation procedure. This new scheme consisted of washes with H_2O, anhydrous EtOH, and THF, followed by drying under vacuum at room temperature. Material worked up in this manner was able to consistently produce material with a Langmuir surface area ~7200 m^2/g and a total nitrogen uptake of 75 mmol/g at $P/P_0 = 0.95$. Additionally, to investigate the possibility of further enhancing surface area, post-wash material was subjected to Soxhlet extraction for 24 hours with THF prior to vacuum drying. However, surface area and nitrogen uptake gains proved to be negligible and Soxhlet extraction was deemed unnecessary.

2.2 PAF-1 Functionalization

Although PAFs feature high surface areas and large accessible pore space, aside from gas storage applications, basic PAF structures consisting of phenyl rings and uniform tetrahedral monomer centers (i.e. carbon, silicon) generally lack the necessary functional groups to be used for most applications. That is to say, functionalized PAF derivatives often outperform unfunctionalized PAFs in selectivity and separations capabilities and basic PAF structures, which are inherently homogenous in nature, are ordinarily unable to act as catalysts without the addition of functional groups. Therefore, to achieve the desired functionality PAFs must be synthesized with monomers or linkers containing the required functional groups or basic PAFs necessitate post-synthetic modification. These added groups are generally chosen to increase selectivity or to provide active sites for catalytic purposes.

2.2.1 Brønsted Acid Groups

The catalytic abilities of homogeneous Brønsted acids and solid materials containing Brønsted acid groups has been well documented, and there are several industrial processes driven by Brønsted acid catalysts. Processes that use homogenous Brønsted acids such as HF and H_2SO_4 in industry, however, consume massive amounts of these liquid acids and require energy intensive separations to remove and recycle them. In addition to this, the homogeneous nature of these acids necessitate considerable engineering solutions as they are incredibly corrosive to industrial infrastructure. Solid catalysts with Brønsted acid sites like zeolites also require costly regeneration due to the aforementioned issues with coking and deactivation.[99,101]

Previous publications have shown that PAFs can be used to create highly recyclable catalysts,[125,127,128] and we sought to evaluate the ability of a PAF-1 derivative functionalized with Brønsted acidic and/or basic sites to perform a catalytic process normally carried out by homogeneous Brønsted acid catalysts. The hypothesis behind this was that the PAF derivative would be able to perform the reaction with high turnover numbers and frequencies as it offers high internal surface area for reactions to take place and would be easily recyclable in a similar fashion to previously synthesized PAF-based catalysts. A proof of concept experiment was designed in which a PAF-1 derivative with anilinium chloride functional groups would be used to catalyze a hydroxyalkylation-alkylation reaction (HAA reaction). It was hypothesized that addition of the anilinium chloride functional group will provide the proton source necessary to drive the HAA reaction. We targeted the HAA of 2-alkylfurans with aldehydes to create furan containing lubricant base oils, which are used to create synthetic biolubricants.[148] Biolubricants can provide environmentally and cost friendly alternatives to traditional fossil fuel-based lubricants because their

starting materials can be derived from biomass sources such as C_5 sugars,[149] biomass-derived alcohols,[150] and cooking oil waste.[151] These starting materials are exceptionally cheap when compared to purchasing industrially synthesized bulk starting materials. Their use would take advantage of an ever-present supply of biomass components including crops specifically grown for renewable energy feedstock sources,[152] or materials regarded as waste products in their related industrial processes.[153]

First, PAF-1 was post synthetically modified to create Berkeley Porous Polymer-1 (BPP-1), a derivative in which each biphenyl linker in the framework contains one NH_2 functional group. BPP-1 was then further post synthetically modified to give BPP-2, where the amino functional groups are protonated using hydrochloric acid to produce anilinium chloride substituents. Due to the inherent insolubility of both BPP-1 and BPP-2, initial characterization involved the use of nitrogen adsorption isotherms and infrared spectroscopy.

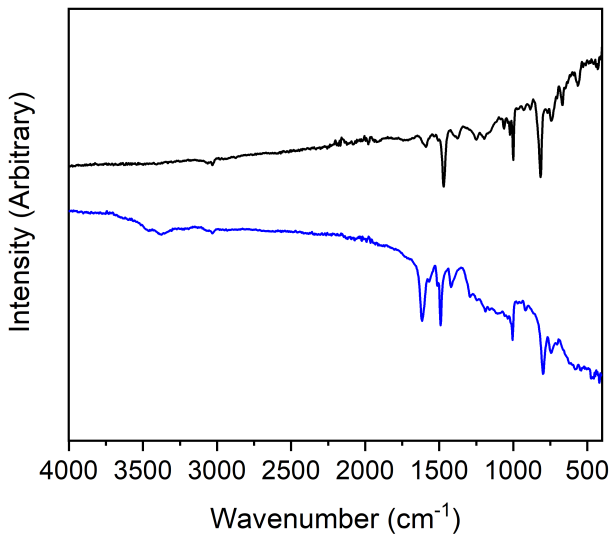

Figure 2: Infrared spectra of PAF-1 (black) and BPP-1 (blue)

For BPP-1 IR the spectrum showed a broad feature with two small peaks at 3400 and 3500 cm^{-1} characteristic of primary amine N-H stretching, a sharp peak at 1600 cm^{-1} of the N-H bend, at 1360 cm^{-1} of the C-N amine stretch, and a sharp peak at 800 cm^{-1} showing para substitution of benzene rings.

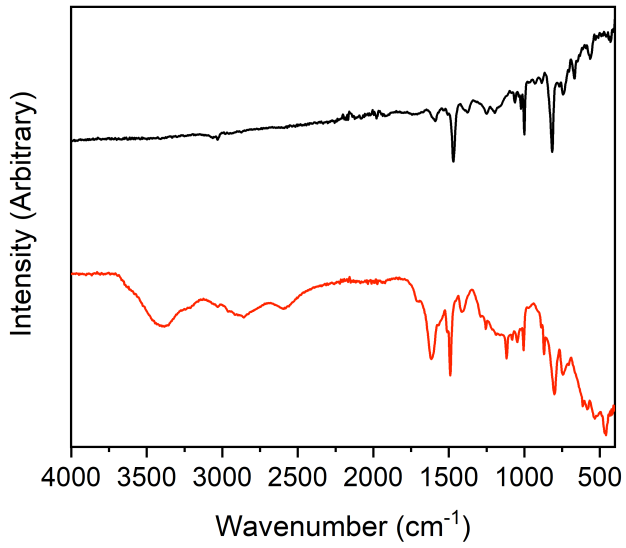

Figure 3: Infrared spectra of PAF-1 (black) and BPP-2 (red)

The IR spectrum of BPP-2 showed similar features, with a large broad single peak at 3360 cm^{-1} indicating amine N-H stretching, a slightly shifted sharp peak at 1560 cm^{-1} signifying the N-H bend, and at 1360 cm^{-1} corresponding to C-N amine stretching. For both BPP-1 and BPP-2 nitrogen adsorption isotherms aligned with published data for surface area and nitrogen uptake values.[154] BPP-1 possessed a Langmuir surface area of 2000 m^2/g and total nitrogen uptake of 21 mmol/g at $P/P_0 = 0.8$, BPP-2 Langmuir surface area was 1500 m^2/g with total nitrogen uptake of 15 mmol/g at $P/P_0 = 0.8$.

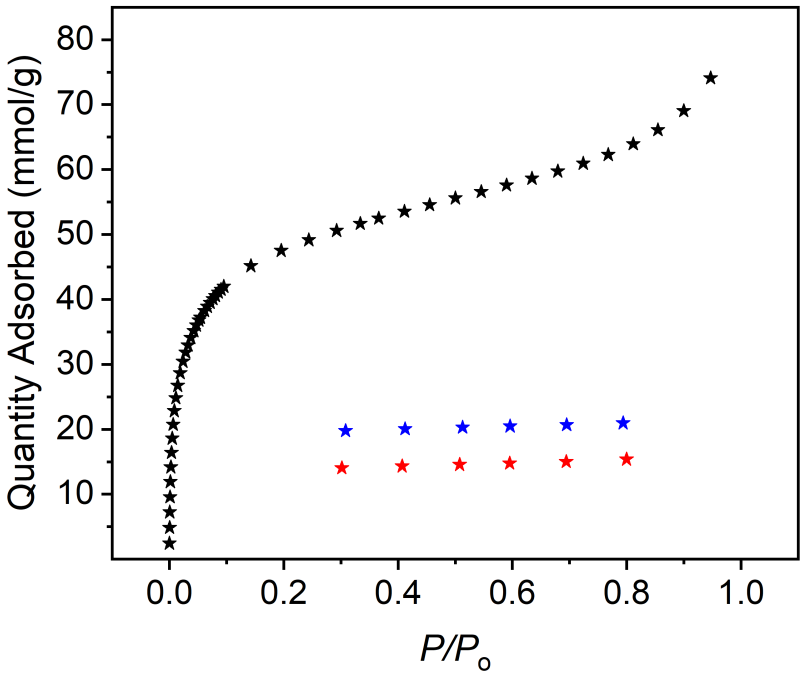

Figure 4: Nitrogen adsorption isotherms at 77 K for PAF-1 (black), BPP-1 (blue), BPP-2 (red)

This adsorption data also follows the trend of significant surface area and nitrogen uptake decrease resulting from PAF-1 functionalization, both values dropped by roughly 72 % for BPP-1 and 80 % for BPP-2. This trend can be rationalized by the fact that functionalization inevitably leads to obstruction in three-dimensional pore structures, with the extent of obstruction increasing with the use of larger functional groups. Once Synthesis and characterization of BPP-2 was completed, the trial experiment was run. Trial reactions were modeled after previous work by Liu et al.,[148,155] selected 2-alkylfurans and aldehydes were combined in a 2:1 furan-aldehyde ratio to form a stock solution. Stock solution was heated to 65° C, catalyst was added, and the reaction was left to stir overnight.

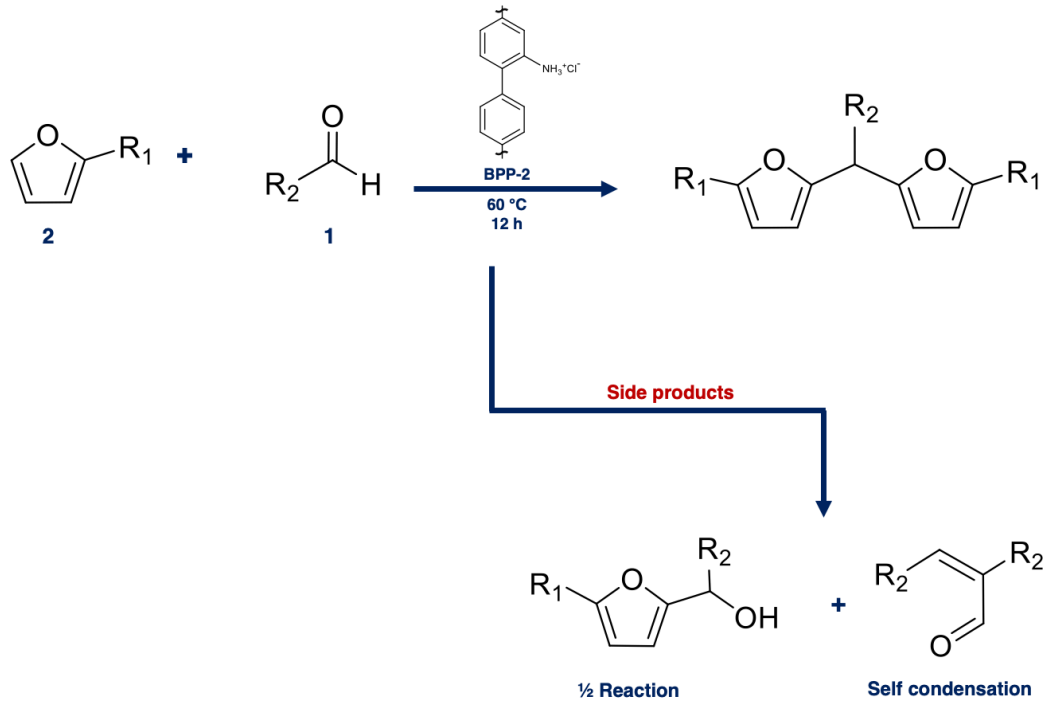

Figure 5: Hydroxyalkylation alkylation (HAA) reaction scheme showing furan and aldehyde starting materials (top left), structure of BPP-2 catalyst biphenyl linker (top center), furan containing lubricant product (top right), and predominant side products (bottom)

Product was filtered when heterogeneous catalysts were used, and then quantification was done via NMR. Control reactions were run with neat acids (phosphoric, sulfuric, and hydrochloric acids) to evaluate their ability to perform the reaction as homogeneous catalysts and compare to trials with BPP-2. Of the neat acids, phosphoric acid achieved the highest percent conversion and selectivity with both at 100 %. Phosphoric acid also had 100 % conversion but only obtained 40 % selectivity. Selectivity in this scenario was based on production of desired product vs known side products. Following the same reaction set up, stock solution was combined with

catalytic amounts of BPP-2 to evaluate its catalytic ability. BPP-2 was in fact able to perform the reaction with 100 % selectivity, but only achieved 28 % conversion of starting materials.

Data from these proof of concept experiments has shown that BPP-2 is in fact able to act as a catalyst in reactions where Brønsted acid catalysts are typically employed. Additionally, based off of the results using neat acid catalysts it can be hypothesized that PAF-1 functionalized with acidic phosphonate or sulfonate groups would provide enhanced percent conversion over BPP-2 in HAA or similar reactions. However, further testing in different reaction scenarios is needed, and would provide insight into how BPP-2 and other PAF derivatives could act as Brønsted acid catalysts. Furthermore, this data shows one of the ways that PAFs can be successfully utilized as a platform to create functional porous organic materials.

2.2.2 Tuning of Pore Morphology

An important property that governs the ability of a porous material to adsorb gases for storage or separation applications is the shape and size of pores that the material contains. For this reason, when designing a porous material for optimal gas adsorption capabilities a common strategy is to achieve a pore size that corresponds to the kinetic diameter of the gas that is to be adsorbed to facilitate a molecular sieving effect. This can be achieved through direct synthesis of materials containing pores of the desired size, or via adding functional groups to an existing material to achieve the required pore size. The latter method serves as a way to effectively decrease pore diameter in a material that would otherwise contain pores that are too large for optimal adsorption of a given gas. In addition to tuning pore size, functional groups can provide sites that enhance adsorption and desorption through selective surface

interactions, by increasing or decreasing heat of adsorption (Q_{st}). Strong interactions between adsorbate and adsorbent is one quality that endows porous materials with high uptakes capabilities for a given gas. Although it is important to note that strong interactions between adsorbent and adsorbate may also have detrimental effects on desorption properties, if surface interactions are too strong for adsorbates to be efficiently removed. Both adsorption, and desorption capabilities are necessary for porous materials to be successful in separations and gas storage applications.[156] Therefore, there is an ever-present need for a strategy that allows for precise tuning of adsorption enthalpies. However, obtaining the highest ability for gas adsorption or separations is not as simple as maximizing a single parameter. Studies have shown that the correct combination of surface area, pore size, pore volume, and heat of adsorption must be achieved for peak performance.[157]

It has been proven and is well understood that unsaturated metals provide strong adsorption sites in MOFs.[158,159] For example, HKUST-1,[142] UTSA-76a,[144] and NOT-101,[160] some of the leading materials in terms of methane uptake and deliverable capacity all contain a high density of open metal sites. Because porous organic materials lack these type of strong adsorption sites altogether, different approaches must be taken to increase adsorption and separation capabilities. As mentioned previously, one strategy to achieve this is through modifying the material to contain groups that create a suitable pore morphology and/or increase adsorbent-adsorbate interactions. Functionalization with alkyl groups allows for tuning of material adsorption properties through control over pore size and/or shape, where the length and bulk of the substituent governs the extent to which pores become obstructed.

There is an abundance of literature showing that introducing functional groups that vary in size and orientation are effective in tuning pore size.[161,162,163] Successful application of this method to PAFs was demonstrated by Garibay et. al,[164] where PAF-1 derivatives were synthesized containing methyl, hydroxymethyl, and phthalimidomethyl functional groups resulting in changes to pore volume and diameter. To tune adsorption properties via the strength of surface interactions, materials can be functionalized with polar groups such as amides or fluorinated substituents. Previous research has shown that the introduction of amide functional groups to porous materials can increase both gas uptake and selectivity.[165,166,167,168] This was exemplified by Zheng et. al[169] in the synthesis of the amide functionalized MOF $[Cu_{24}(TPBTM)_8(H_2O)_{24}]$, which showed increased CO_2 capacity and higher CO_2 selectivity in CO_2/N_2 and CO_2/CH_4 mixtures over the non-amide functionalized analogue PCN-61.[170] To evaluate these modification strategies in PAFs, we functionalized PAF-1 with a series of amide functional groups containing alkyl groups of varying sizes, to provide control of pore morphology while increasing adsorbate-adsorbent interactions for optimal adsorption and selectivity. This was achieved by reacting BPP-1 with select acyl chlorides: acetyl chloride, phenylacetyl chloride, butyrl chloride, and acryloyl chloride. Methane adsorption experiments were then run on the series of BPP-1-amides at 195 K to compare the resulting isotherms to PAF-1 methane adsorption at 195 K.

The best way to investigate the effect of functionalization on pore morphology would undoubtedly be to obtain a crystal structure via X-ray crystallography, so exact pore dimensions could be mapped. As PAFs are necessarily amorphous, diffraction methods cannot be used for their characterization and alternative methods must be

used to look for indications of alterations in PAF pore structure. For our materials, gas adsorption experiments were used to provide data exhibiting these changes. Gas adsorption isotherms and their related calculations are a critical piece of data needed to characterize pore structure, pore volume, and adsorbent properties in all porous materials. Besides the obvious differences in total uptake gathered from isotherms, the shape of an isotherm curve can indicate changes in pore structure or strength of adsorbent-adsorbate interactions.[171] This method is used extensively to compare adsorption characteristics between porous materials,[172,173] as well as the effects of functionalization on adsorption properties.[174,175] There are numerous literature examples in which comparative isotherms displaying differences in adsorption at certain pressure regions, or in total uptake are utilized to signify changes to pore morphology and/or adsorbate-adsorbent interactions.[176,177,178]

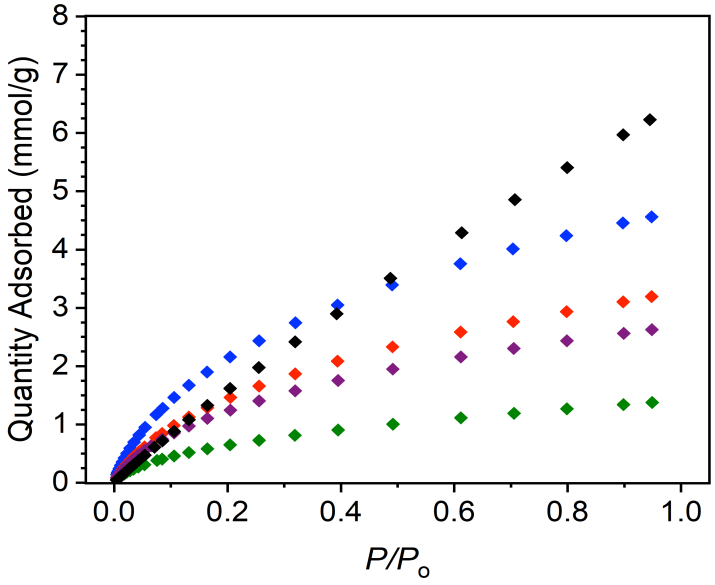

Figure 6: Methane Adsorption isotherms for select PAF-1-amides at 195 K, PAF-1 (black), PAF-1-acetamide (blue), PAF-1-butyrlamide (red), PAF-1-acryloylamide (purple), PAF-1-phenylacetamide (green)

Methane adsorption isotherms of the amide functionalized PAF-1 derivatives displayed changes in shape compared to unfunctionalized PAF-1, signifying the successful modification of pore morphology and adsorption characteristics. Although PAF-1 and PAF-1-amide derivatives all exhibited similar type I adsorption isotherms, differences in the slope of adsorption curves at certain pressure ranges are what indicated adsorbate-adsorbent interaction and pore morphology changes. Notably, quantities adsorbed from 0.0 – 0.45 bar in PAF-1-acetamide, 0.0 – 0.15 bar in PAF-1-butyrlamide, and 0.0 – 0.1 bar in PAF-1-acryloylamide were higher than in PAF-1 for these ranges. The positive increases in slope of PAF-1-amide derivatives at lower pressure ranges indicates increased micropore filling, which in this case can be attributed to the polar nature of amide functional groups causing increasing adsorbate-adsorbent interactions. This was displayed in all amide derivatives except PAF-1-phenylacetamide where the size of the amide functional group was too large, outweighing the positive adsorbate interaction effects of polarity. It is also possible that this was caused by the presence of the phenyl ring resulting in a lower difference in polarity across the phenylacetamide functional group. A decrease in surface area and total methane uptake occurred in all PAF-1-amides. The reduction of surface area and methane uptake were both correlated to alkyl group size, amides containing larger alkyl groups resulted in a more substantial decrease. PAF-1-acetamide had a Langmuir surface area of 1342 m^2/g (77 K N_2) and a total methane uptake of 4.6 mmol/g at P/P_0 = 0.95 (195 K), PAF-1-butyrlamide S_{Lang} = 1118 m^2/g (77 K N_2) with a total methane uptake of 3.2 mmol/g at P/P_0 = 0.95 (195 K), and PAF-1-Phenylacetamide S_{Lang} = 805 m^2/g (77 K N_2) with a total methane uptake of 1.4 mmol/g at P/P_0 = 0.95.

2.2.3 Conclusion and Outlook for Porous Aromatic Frameworks

If trends in porous materials research continue on as they have been, PAFs have a promising path ahead of them. Their impressive stabilities and surface areas put them at the forefront of interest in porous materials as few, if any, competing organic materials possess these qualities concurrently at such extremes. While statistically impressive, PAFs have major hurdles to overcome before their capabilities can be put to use in real world scenarios, most concerning being the high cost of synthesis. The amount of catalyst required to synthesize PAF-1 and PPN-4 at the gram scale, for example, is prohibitive to virtually any real world application due to the cost of $Ni(COD)_2$. Second, is the lack of concrete structural information available as almost all PAFs are amorphous. To fully utilize PAFS for the design of application specific porous organic materials more information on their structures is necessary, in order to optimize synthesis and modification methods. Nevertheless, the future looks bright for PAFs if these issues can be worked, making them more viable alternatives to porous materials currently implemented in industrial gas storage and catalysis applications.

2.3 Experimental Section

2.3.1 General Information

All solvents and reagents were obtained from commercial sources and used without any further purification (unless otherwise noted). Dry dichloromethane and N,N-dimethylformamide were obtained from a solvent purification/drying system and stored under a nitrogen atmosphere. H-NMR spectra were taken on a Bruker AV 400 spectrometer. Infrared spectroscopy measurements were collected under atmospheric conditions using a Bruker APLPHA II. Scanning electron microscope images were taken using a SEM/FIB Auriga 60 housed in the Advanced Materials Characterization

lab at the University of Delaware. All gas adsorption measurements were obtained using Micromeritics 3Flex and TriStar II gas adsorption analysis instruments. 3Flex and TriStar II tubes were heated in the oven at 120° C overnight to remove water. Once cooled the tubes were evacuated and backfilled with nitrogen using the Smart VacPrep system and weighed. Samples were loaded into the tubes and degassed overnight at their respective activation temperatures. Isothermal jackets were used on analysis tubes for cryogenic measurements. Surface areas for PAF-1 and PAF-1 derivatives were measured via Nitrogen adsorption isotherm measurements in a 77 K liquid nitrogen bath and calculated using the corresponding Micromeritics software for each instrument (TriStar II & 3 Flex). Surface areas for porous organic cages were measured in the same fashion as PAF-1 for Nitrogen adsorption isotherms. For porous organic cage surface area measurements utilizing carbon dioxide, isotherms were measured in a 195 K isopropanol / dry ice bath. Excluding high pressure measurements, methane isotherms for all materials were measured using a 195 K isopropanol / dry ice bath. High pressure methane measurements were collected on a Hy-Energy Scientific Instruments PCT-Pro-2000 at room temperature.

BET calculations were used on PAF-1 for initial characterizations. For BPP-1, BPP-2, and all porous organic cages Langmuir calculations were used in the interest of throughput, due to the drastically reduced time of measurement.

2.3.2 Synthesis Procedures

2.3.2.1 Synthesis of tetrakis(4-bromophenyl)methane

32 ml of bromine was added to a 3 neck round bottom flask containing a stir bar. 10 g tetraphenylmethane was added in small portions under vigorous stirring and

left to stir at room temperature for 20 minutes. The flask was then cooled to - 78° C in a CO_2 /isopropanol bath, and 75 ml anhydrous ethanol was added slowly. The resulting mixture was left in the bath to warm to room temperature and stir overnight. The precipitate was filtered and washed with a saturated solution of sodium bisulfite, then water, to obtain a beige powder which was dried overnight under vacuum at room temperature.

2.3.2.2 Synthesis of PAF-1

Inside of a glovebox under nitrogen atmosphere 2.25 g bis(1,5-cyclooctadiene)nickel(0), 1.28 g 2,2'-bipyridine, 1.12 g 1,5-cyclooctadiene, and 120 mL anhydrous N,N-dimethylformamide were combined in a 500 mL Schlenk flask. The flask was then removed from the glovebox and placed under nitrogen atmosphere on a Schlenk line. The deep purple mixture was stirred at 80° C for 1 hour then 1 g tetrakis(4-bromophenyl)methane was added under positive nitrogen flow. The reaction was sealed and left to stir at 80° C for 24 hours under nitrogen. Once cooled to room temperature, 70 mL concentrated (18 M) hydrochloric acid was added and the solution was left to stir overnight at room temperature. The resulting emerald green suspension was filtered, and the precipitate was washed with water, anhydrous ethanol, and tetrahydrofuran followed by 24 hours of Soxhlet extraction with tetrahydrofuran. The resulting beige solid was dried for 24 hours at room temperature under vacuum to obtain a bright white solid.

2.3.2.3 Synthesis of BPP-1

100 mg PAF-1 and a stir bar were placed in a 300 mL three neck round bottom flask equipped with a solid addition tube containing 3.0 g copper nitrate hemi-penta

hydrate. The flask was then placed under nitrogen atmosphere utilizing a Schlenk line. 14 mL acetic anhydride and 14 mL anhydrous dichloromethane were added and the flask was cooled to 0° C in an ice bath. Once cooled the copper nitrate hemi-penta hydrate was added over a period of 5 minutes, the ice bath was removed, and the mixture was left to stir 24 hours at room temperature. The resulting dark blue solution was filtered and washed with 3 normal hydrochloric acid (causing a color change to beige), 80° C water, and 60° C methanol and left to dry on a vacuum funnel for 15 minutes. Obtained solid was placed in a 100 mL Schlenk flask under nitrogen atmosphere with 48 mL of 50/50 methanol:water and 2.9 g sodium dithionite and left to stir for 24 hours. Solid was filtered and suspended in 80° C water for one hour, water decanted and replaced with fresh hot water. This was repeated for a total of 5 cycles, followed by suspension in 60° C anhydrous ethanol followed by decanting and replacing with fresh hot ethanol twice. Product was obtained via filtration, washed with warm tetrahydrofuran, and dried under vacuum at 80° C overnight.

2.3.2.4 Synthesis of BPP-2

100 mg BPP-1 was placed in a 50 mL Schlenk flask under nitrogen atmosphere with 4 mL 1,4-dioxane and 1.5 mL 4 M hydrochloric acid in 1,4-dioxane. The solution was left to stir overnight at room temperature. Product was obtained via filtration and washed with 1,4-dioxane followed by anhydrous ethanol. The tan colored solid was then dried under vacuum at room temperature for 24 hours.

2.3.2.5 Synthesis of PAF-1-Acetyl Chloride

100 mg BPP-1, 10 mL tetrahydrofuran, and 1mL acetyl chloride combined in a 25 mL round bottom flask. The mixture was refluxed at 90°C for 3 days. Solid was

isolated via filtration, washed with tetrahydrofuran, and dried under vacuum at room temperature.

2.3.2.6 Synthesis of PAF-1-Phenylacetyl Chloride

100 mg BPP-1, 10 mL tetrahydrofuran, and 2 mL phenylacetyl chloride combined in a 25 mL round bottom flask. The mixture was refluxed at 90°C for 3 days. Solid was isolated via filtration, washed with tetrahydrofuran, and dried under vacuum at room temperature.

2.3.2.7 Synthesis of PAF-1-Butyrl Chloride

100 mg BPP-1, 10 mL tetrahydrofuran, and 1.6 mL butyrl chloride combined in a 25 mL round bottom flask. The mixture was refluxed at 90°C for 3 days. Solid was isolated via filtration, washed with tetrahydrofuran, and dried under vacuum at room temperature.

2.3.2.8 Synthesis of PAF-1-Isobutyrl Chloride

100 mg BPP-1, 10 mL tetrahydrofuran, and 1.6 mL phenylacetyl chloride combined in a 25 mL round bottom flask. The mixture was refluxed at 90°C for 3 days. Solid was isolated via filtration, washed with tetrahydrofuran, and dried under vacuum at room temperature.

2.3.2.9 Synthesis of PAF-1-Acroloyl Chloride

100 mg BPP-1, 10 mL tetrahydrofuran, and 1.2 mL acroloyl chloride combined in a 25 mL round bottom flask. The mixture was refluxed at 90°C for 3 days. Solid was isolated via filtration, washed with tetrahydrofuran, and dried under vacuum at room temperature.

2.3.2.10 Hydroxyalkylation Alkylation (HAA) Reactions

In a typical reaction set up the selected 2-alkylfuran and aldehyde were combined in a 2:1 furan-aldehyde ratio to form a stock solution. 0.5 mL or 3.5 mL (depending on catalyst) stock solution was placed in a vial sealed with a Teflon lined cap and heated to 65° C, catalyst and stir bar were added, and the reaction was left to stir overnight at 65° C. Product was filtered when solid catalyst was used, and analyzed via ^{1}H-NMR.

2.3.3 Nuclear Magnetic Resonance Spectra

Determination of percent conversion of starting material was carried out using a simplified method in which the peak at 7.3 ppm corresponding to the furan component of the starting material stock solution was compared to the main product peak at 3.9 ppm. Percent selectivity in this case is a comparison of side product peaks at 3.7 ppm and 9.3 ppm, and the main product peak at 3.9 ppm. This method was used to determine a rough percent selectivity and conversion to screen for catalytic ability. Complete quantification of the previously mentioned values will require mass spectrometry and more comprehensive analysis of product mixture(s) utilizing gas chromatography methods. In the interest of time these methods are to be performed once the best catalyst is identified and optimized. Peaks used in calculations shown in Figure 7.

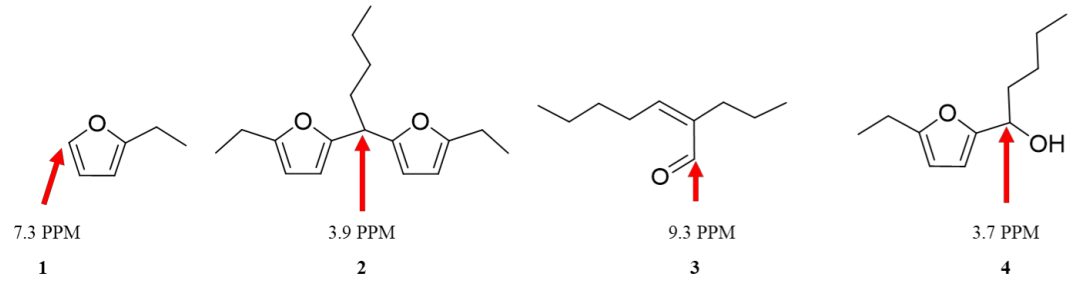

Figure 7: Peaks of interest denoted by red arrows for the furan starting material (1), final product (2), condensation side product (3), ½ reaction side product (4)

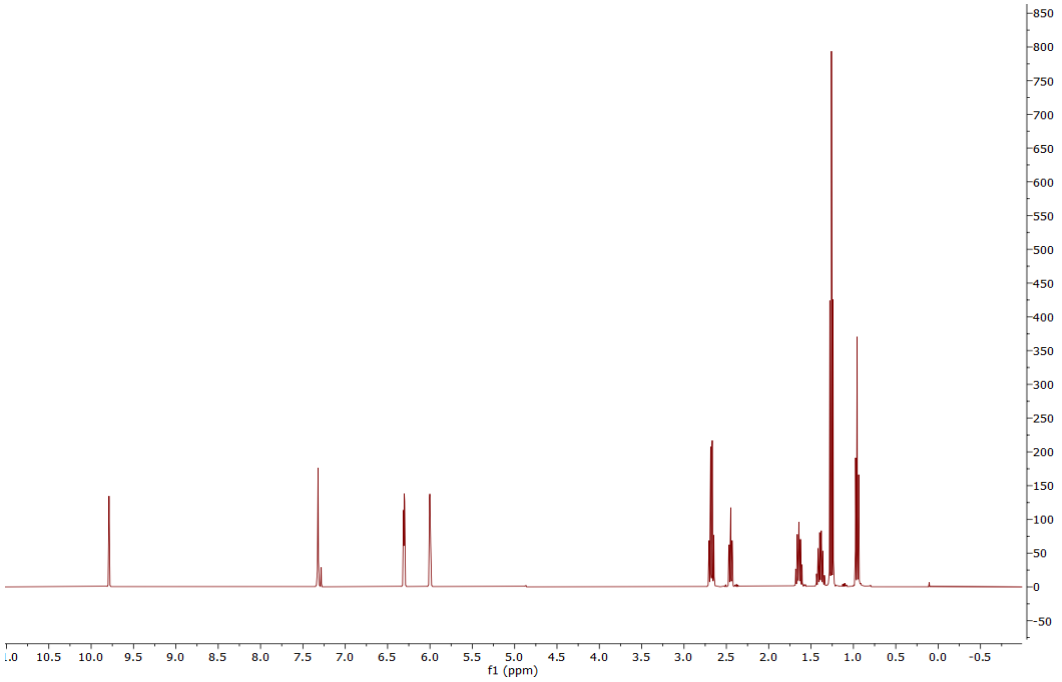

Figure 8: ^{1}H-NMR spectra of 2-ethylfuran & pentanal stock solution (2:1 ratio)

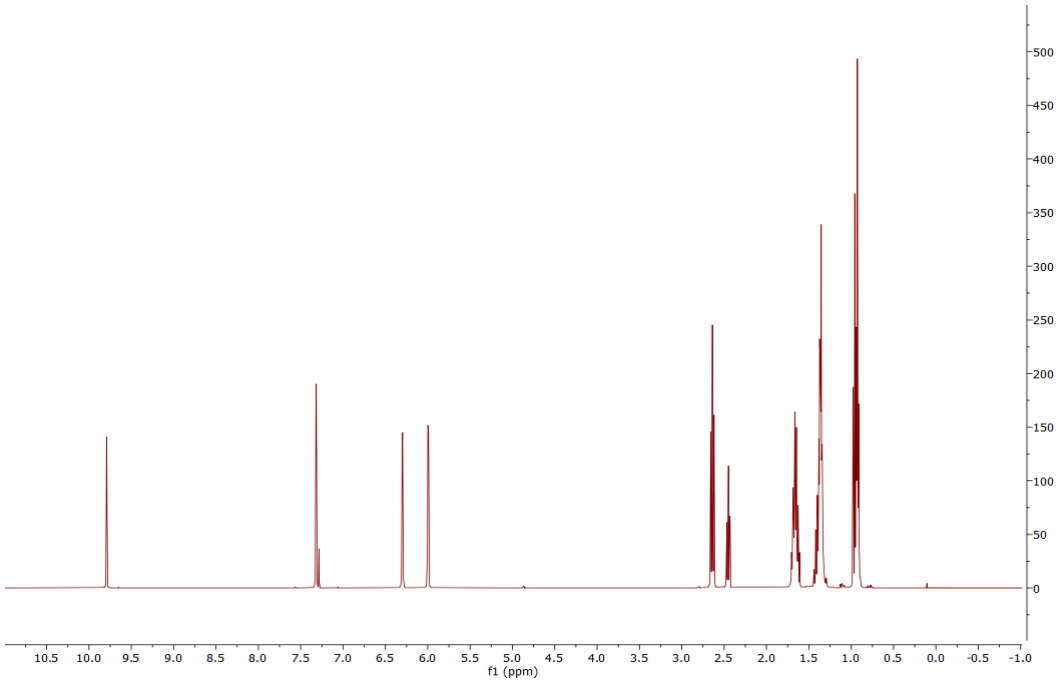

Figure 9: ^{1}H-NMR spectra of 2-pentylfuran & pentanal stock solution (2:1 ratio)

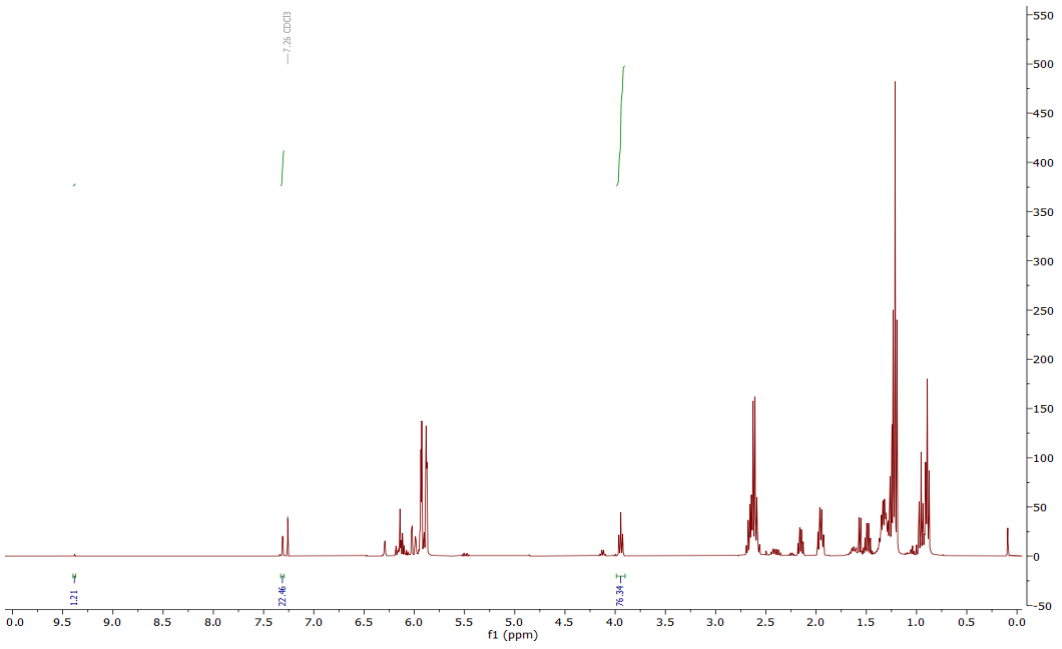

Figure 10: ^{1}H-NMR of product from HAA reaction with 0.5 mL stock solution (2:1 ethylfuran/pentanal) and concentrated HCl

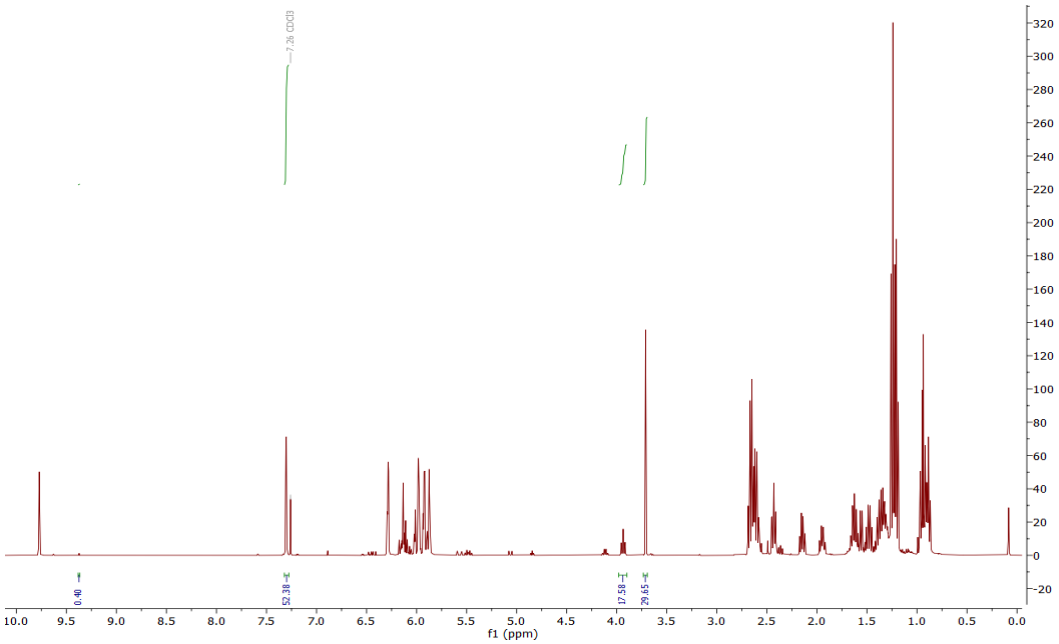

Figure 11: ^{1}H-NMR of product from HAA reaction with 0.5 mL stock solution (2:1 ethylfuran/pentanal) and 4 M HCl in Dioxane

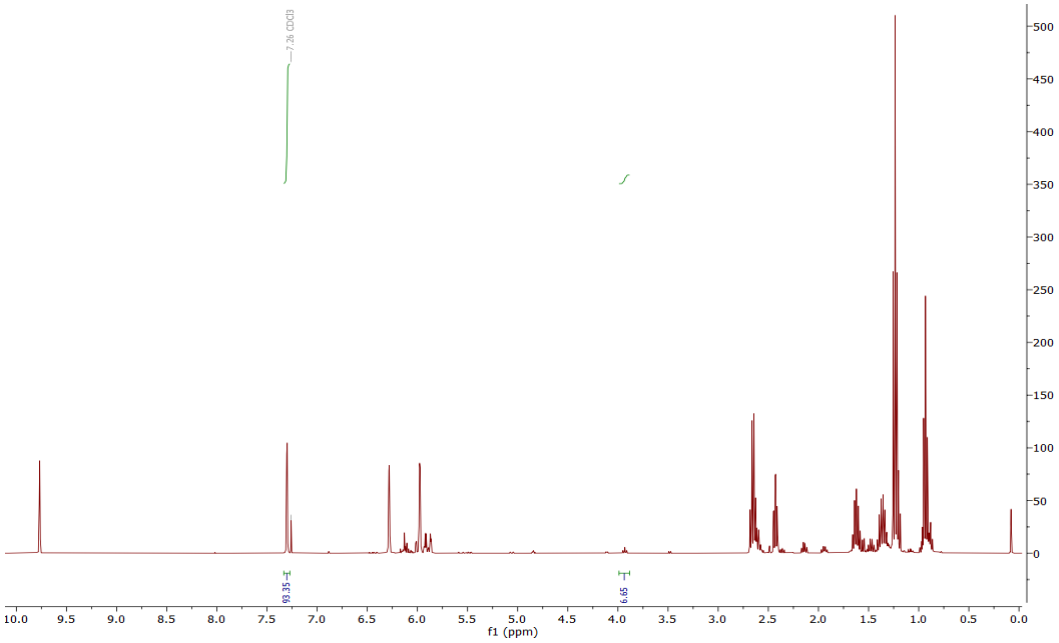

Figure 12: ^{1}H-NMR of product from HAA reaction with 0.5 mL stock solution (2:1 ethylfuran/pentanal) and 2 M HCl in ether

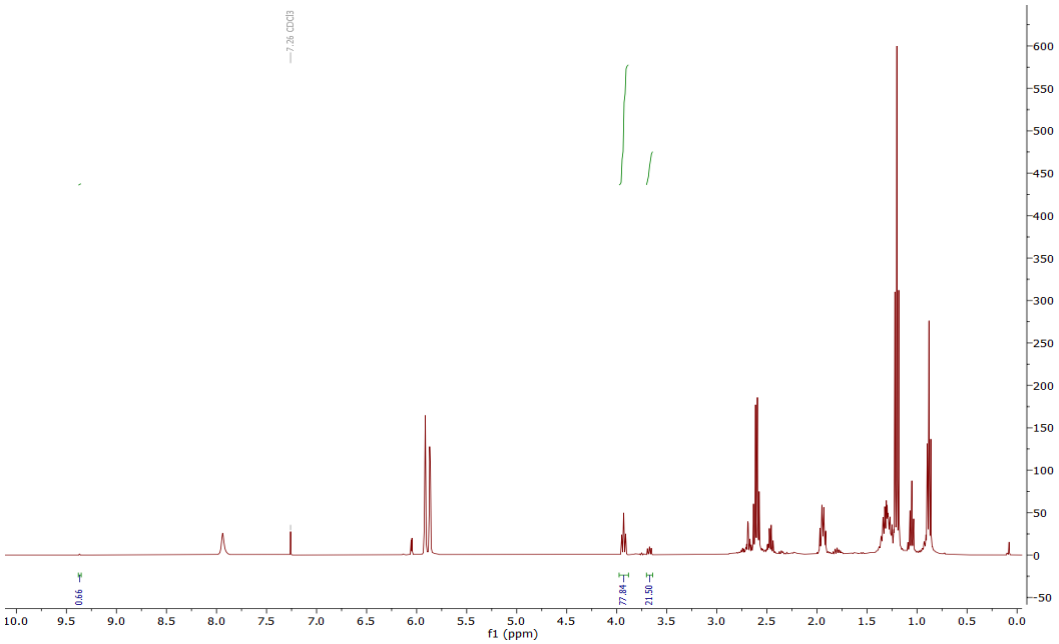

Figure 13: ^{1}H-NMR of product from HAA reaction with 0.5 mL stock solution (2:1 ethylfuran/pentanal) and concentrated H_2SO_4

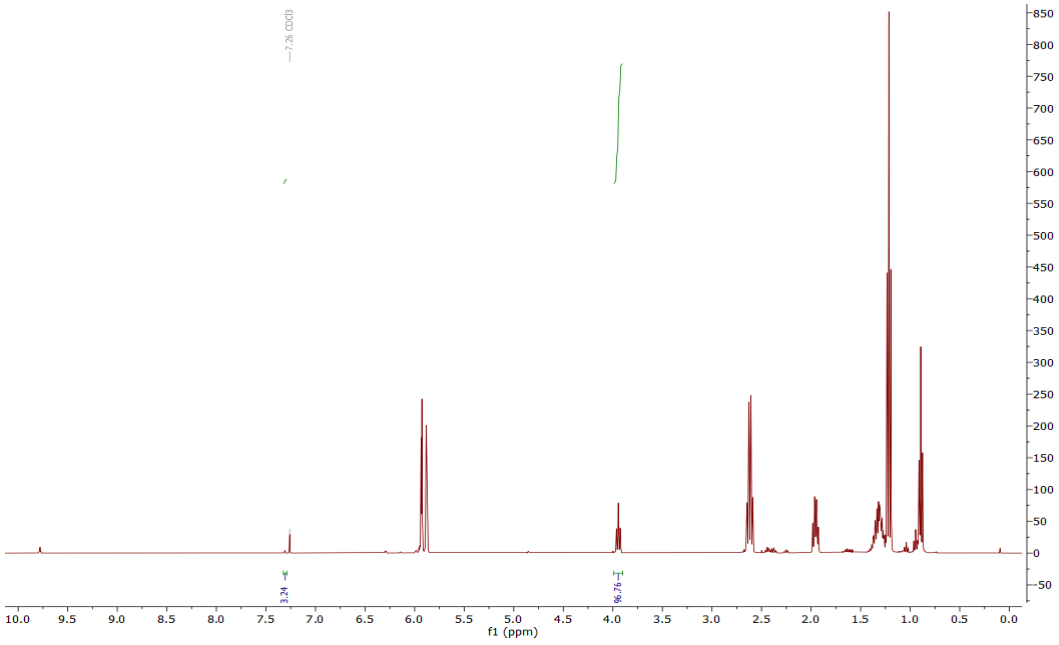

Figure 14: ^{1}H-NMR of product from HAA reaction with 0.5 mL stock solution (2:1 ethylfuran/pentanal) and H_3PO_4

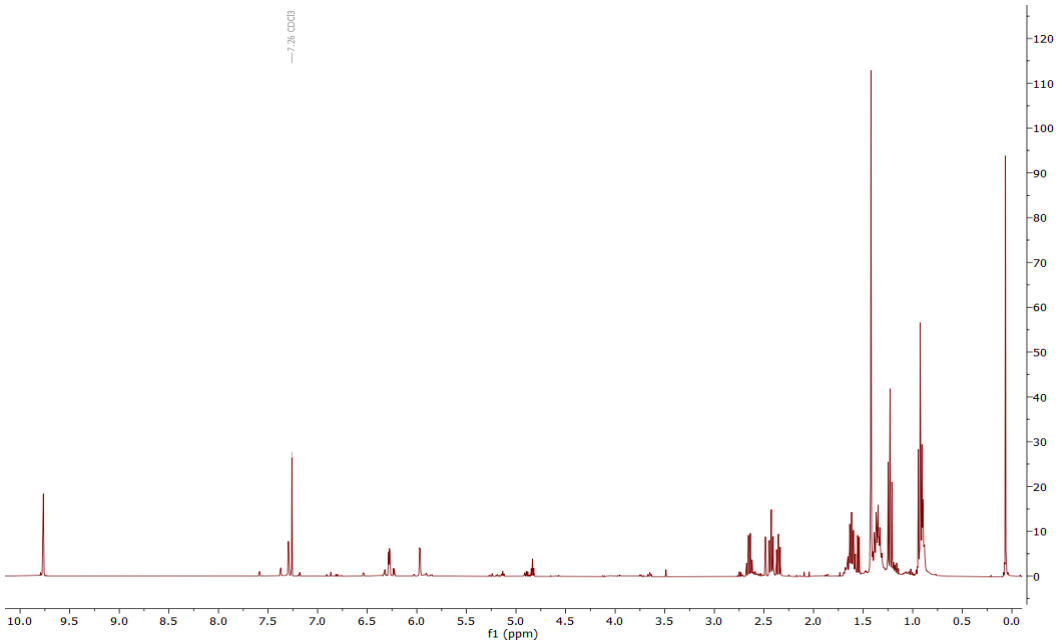

Figure 15: ^{1}H-NMR of product from HAA reaction with 0.5 mL stock solution (2:1 ethylfuran/pentanal) and PAF-1 without the presence of acid catalyst

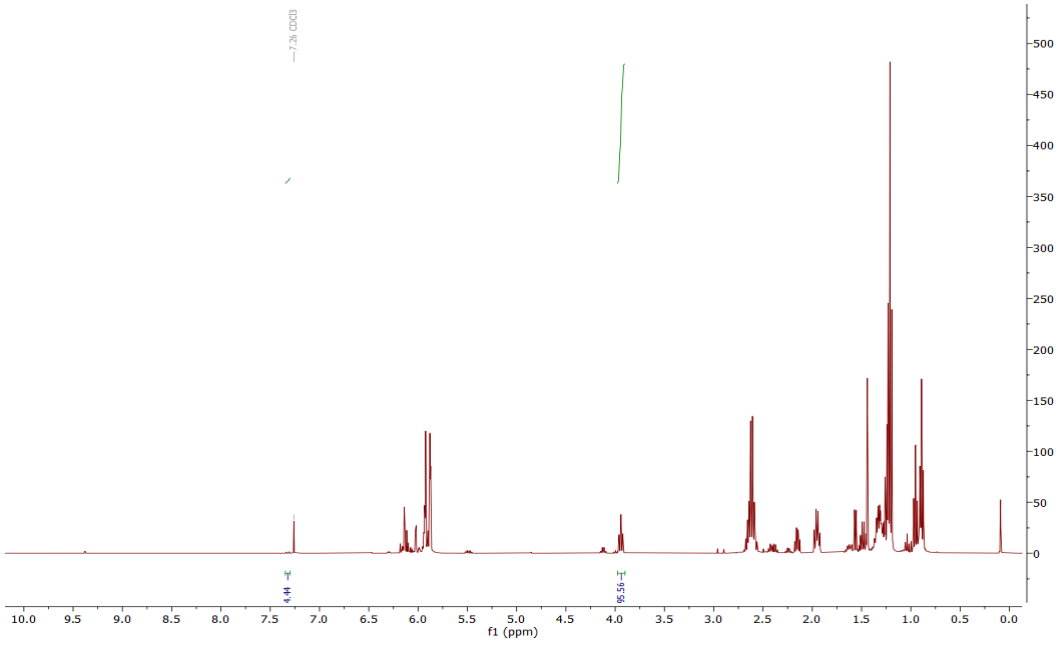

Figure 16: ^{1}H-NMR of product from HAA reaction with 0.5 mL stock solution (2:1 ethylfuran/pentanal), PAF-1, and HCl

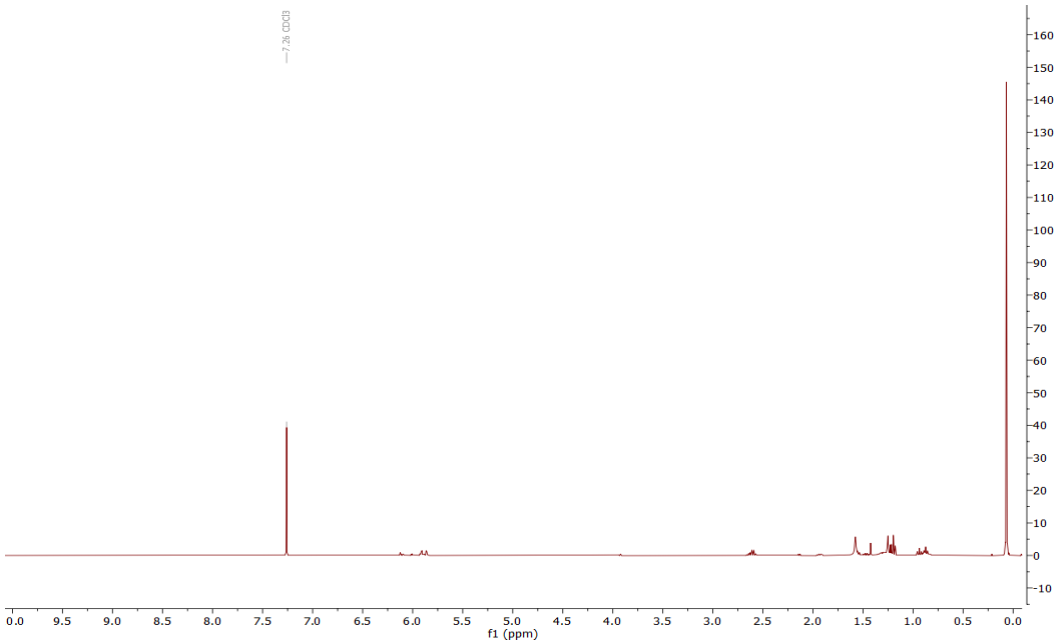

Figure 17: ^{1}H-NMR of product from HAA reaction with 0.5 mL stock solution (2:1 ethylfuran/pentanal), PAF-1, and 4 M HCl in dioxane

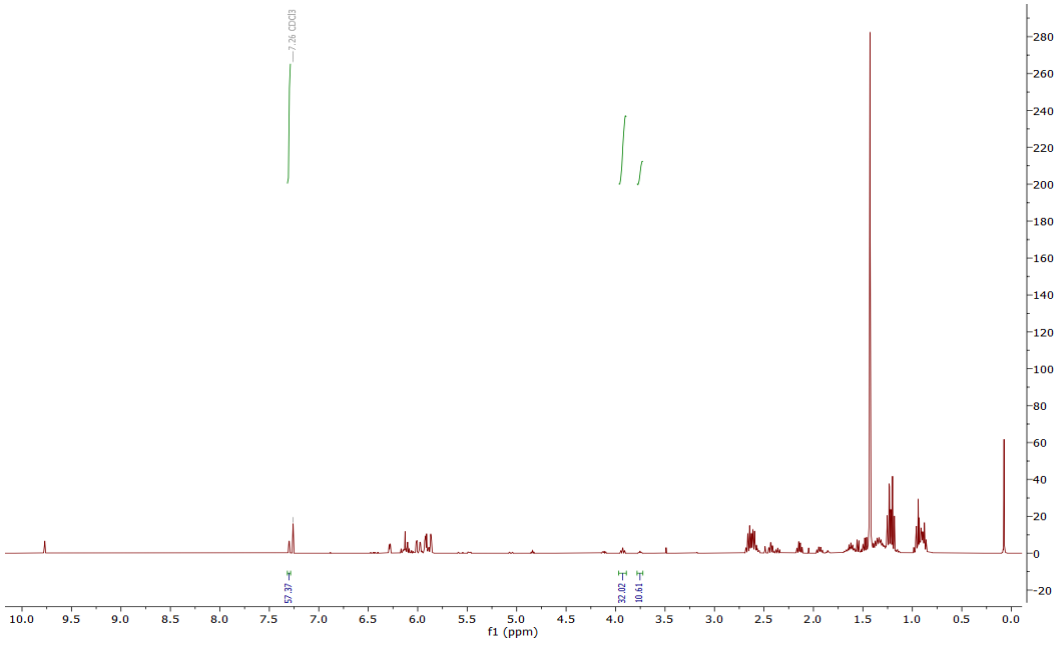

Figure 18: ^{1}H-NMR of product from HAA reaction with 0.5 mL stock solution (2:1 ethylfuran/pentanal), PAF-1, and 2 M HCl in ether

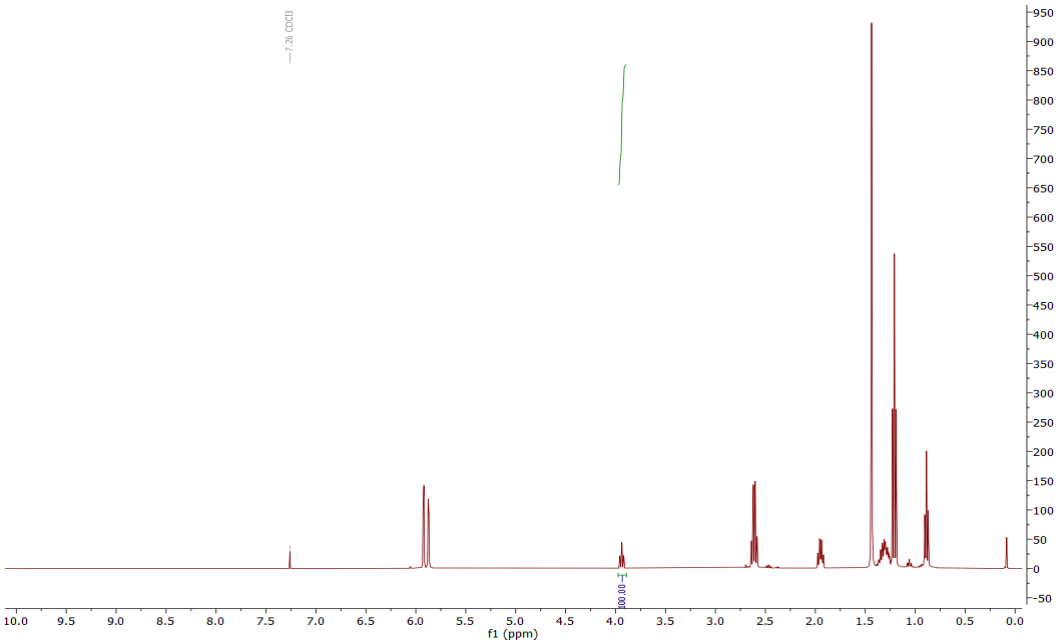

Figure 19: ^{1}H-NMR of product from HAA reaction with 0.5 mL stock solution (2:1 ethylfuran/pentanal), PAF-1, and H_2SO_4

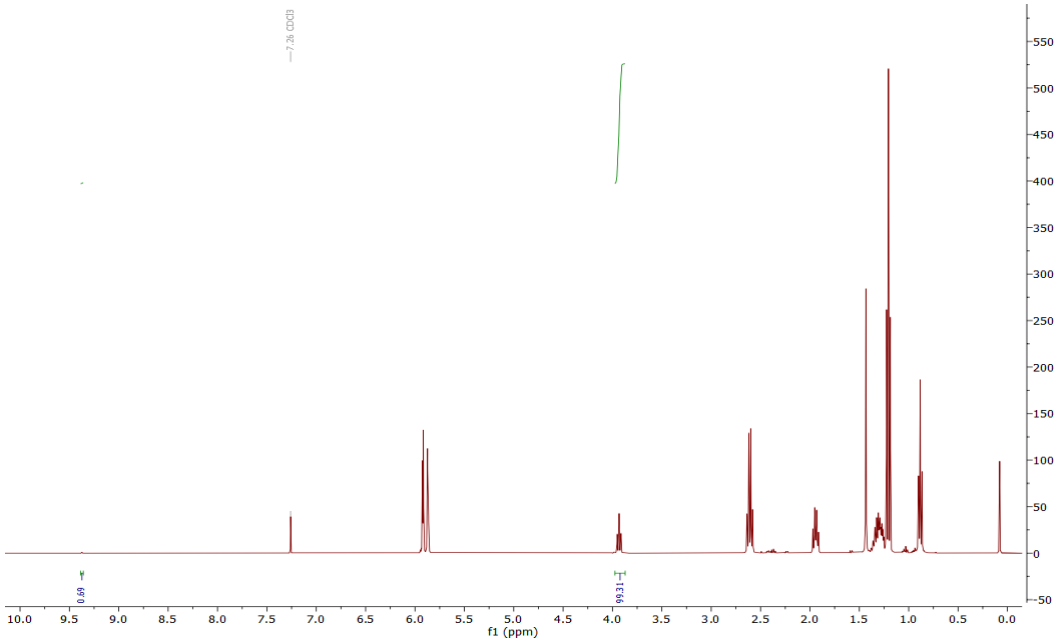

Figure 20: ^{1}H-NMR of product from HAA reaction with 0.5 mL stock solution (2:1 ethylfuran/pentanal), PAF-1, and H_3PO_4

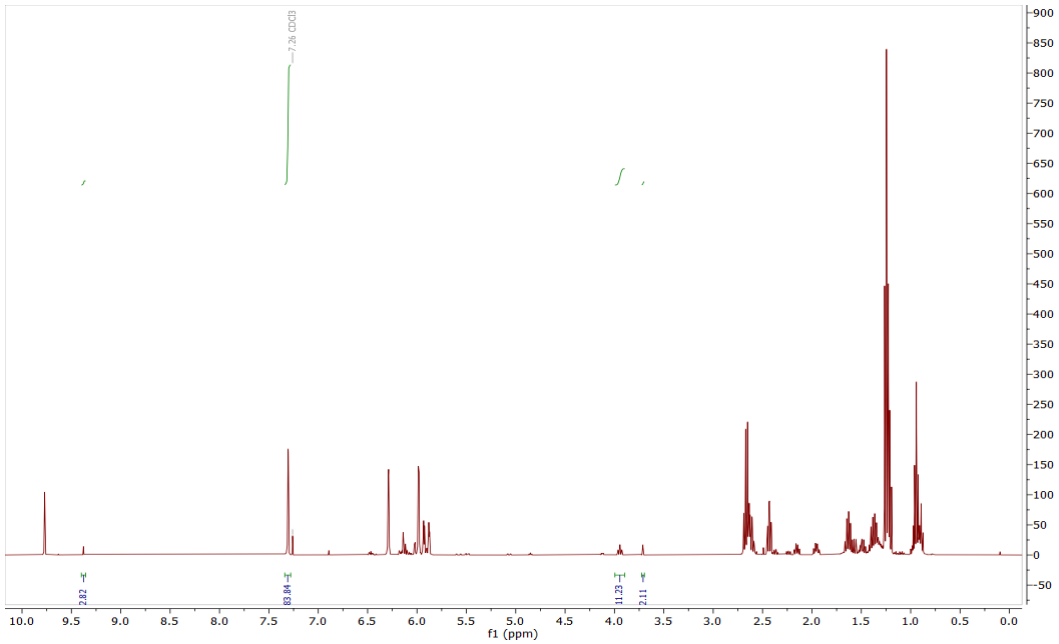

Figure 21: ^{1}H-NMR of product from HAA reaction with 3.5 mL stock solution (2:1 ethylfuran/pentanal) and BPP-2

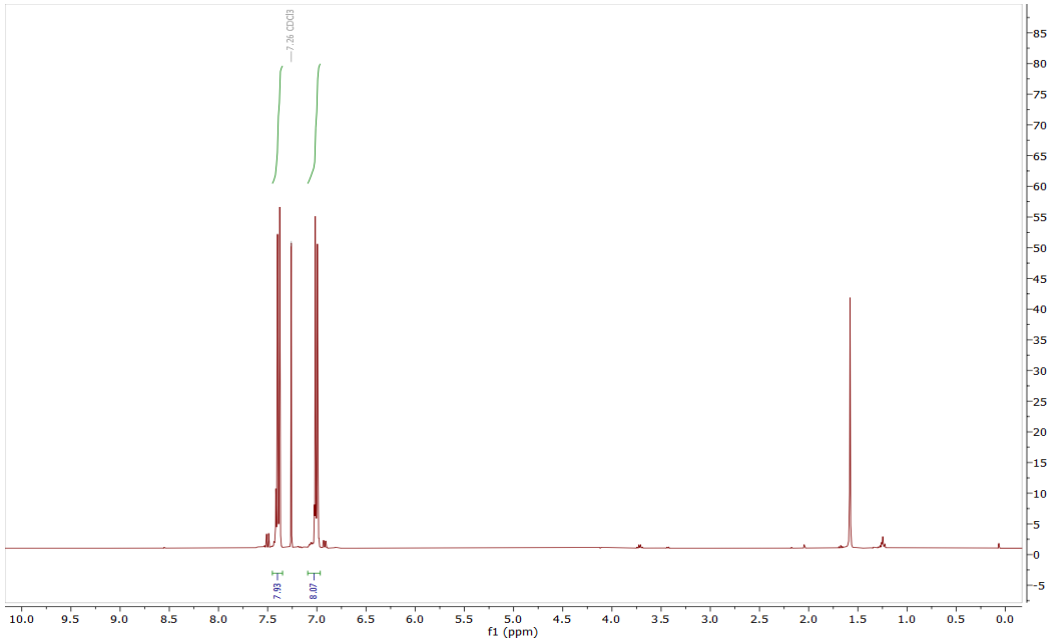

Figure 22: ^{1}H-NMR of tetrakis(4-bromophenyl)methane

2.3.4 Infrared Spectra

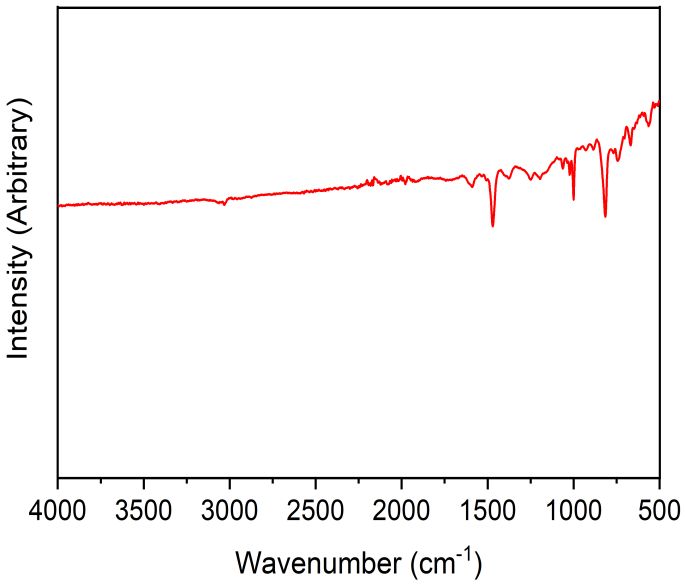

Figure 23: Infrared spectrum of activated PAF-1

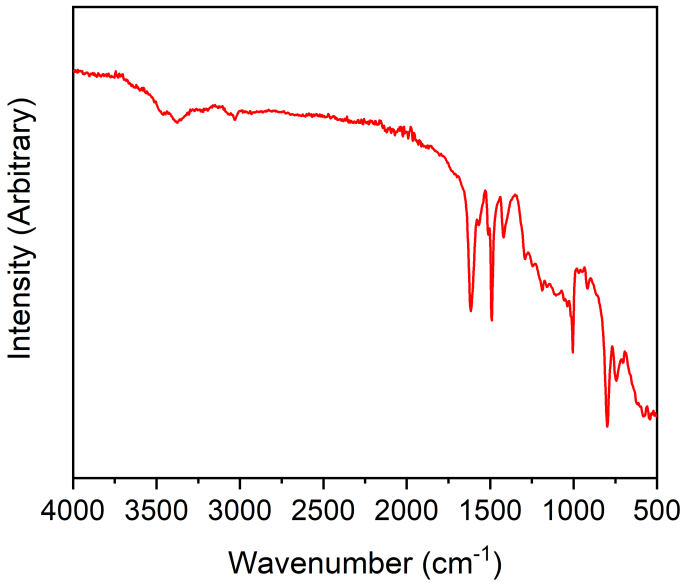

Figure 24: Infrared spectrum of activated BPP-1

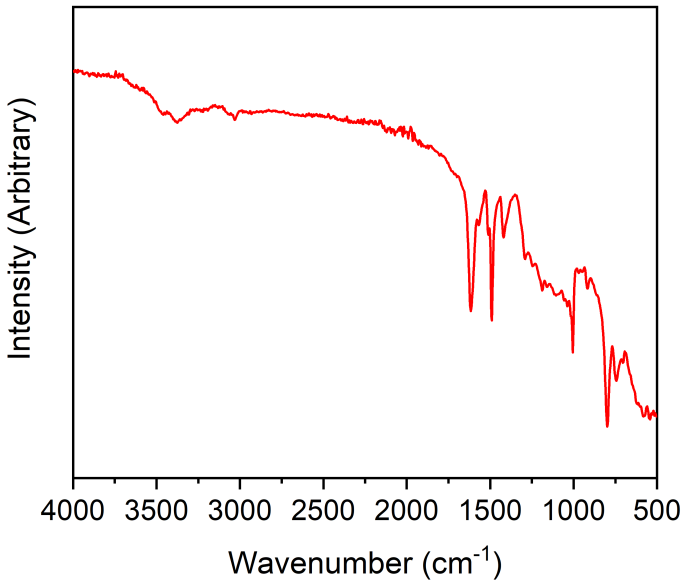

Figure 25: Infrared spectrum of activated BPP-2

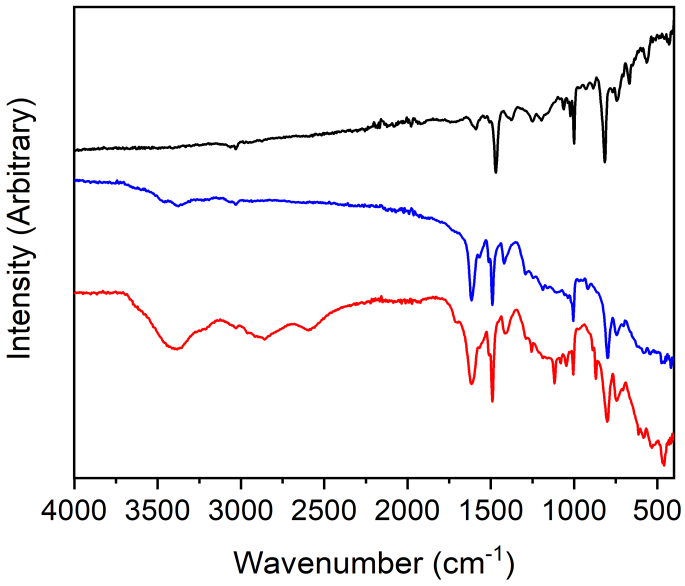

Figure 26: Infrared spectra of PAF-1 (black), BPP-1 (blue), and BPP-2 (red)

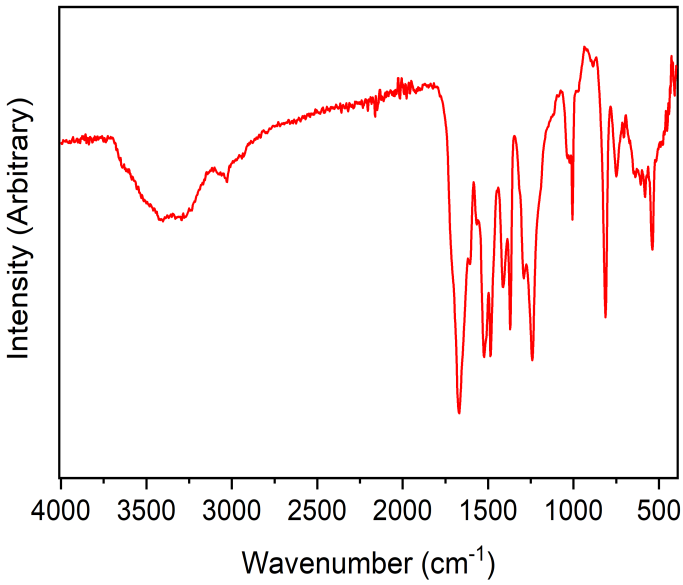

Figure 27: Infrared spectrum of activated PAF-1-acetamide

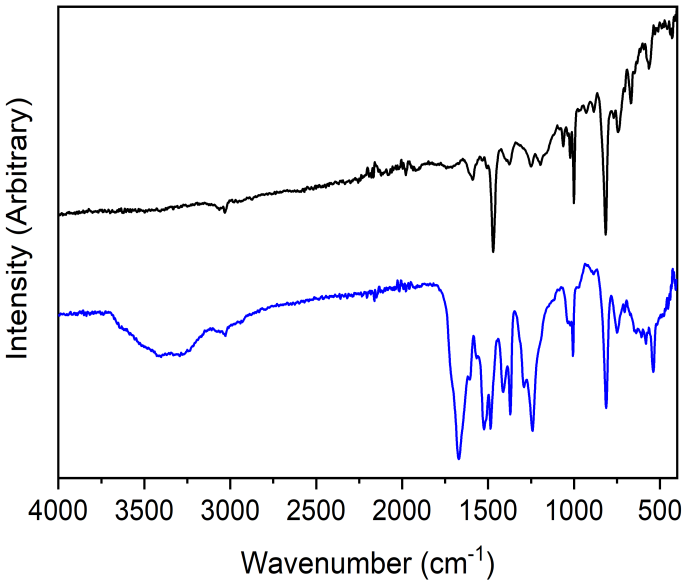

Figure 28: Infrared spectra of PAF-1 (black) and PAF-1-acetamide (blue)

2.3.5 Gas Adsorption Isotherms

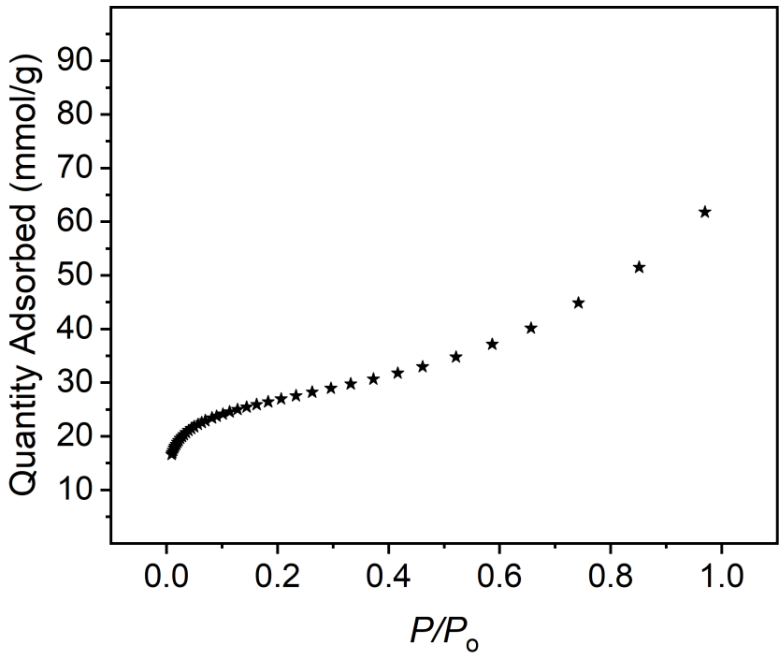

Figure 29: N_2 adsorption at 77 K for activated PAF-1 using original wash and activation methods (see experimental section)

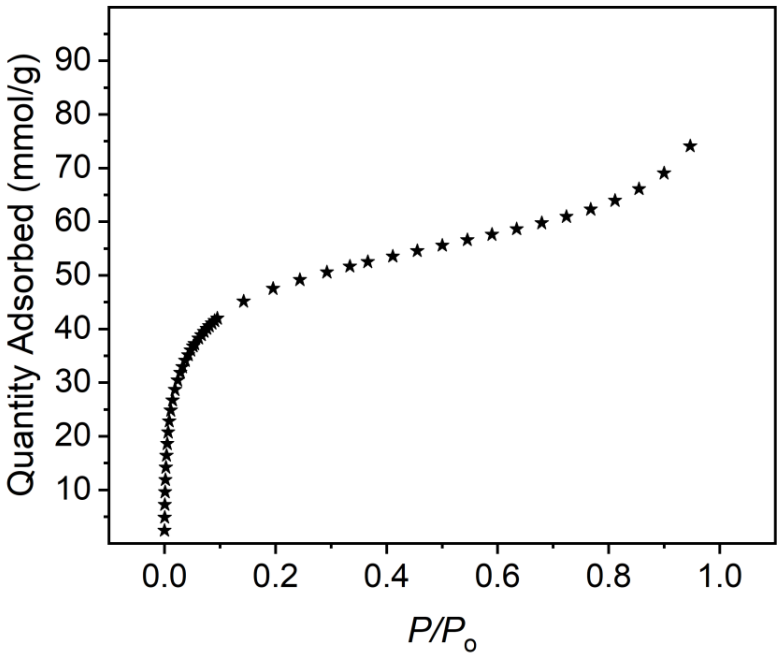

Figure 30: N_2 adsorption at 77 K for activated PAF-1 using altered wash and activation methods (see experimental)

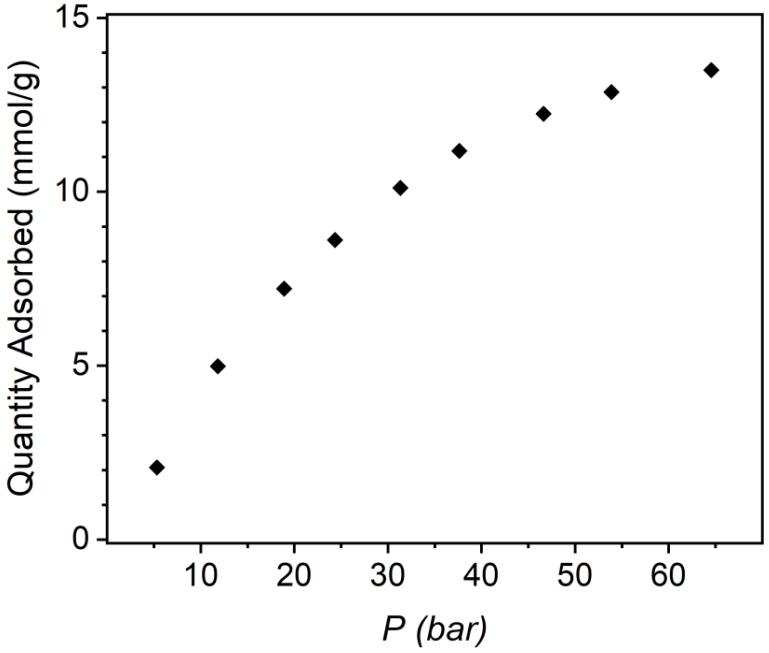

Figure 31: High pressure CH_4 adsorption at 298 K for PAF-1

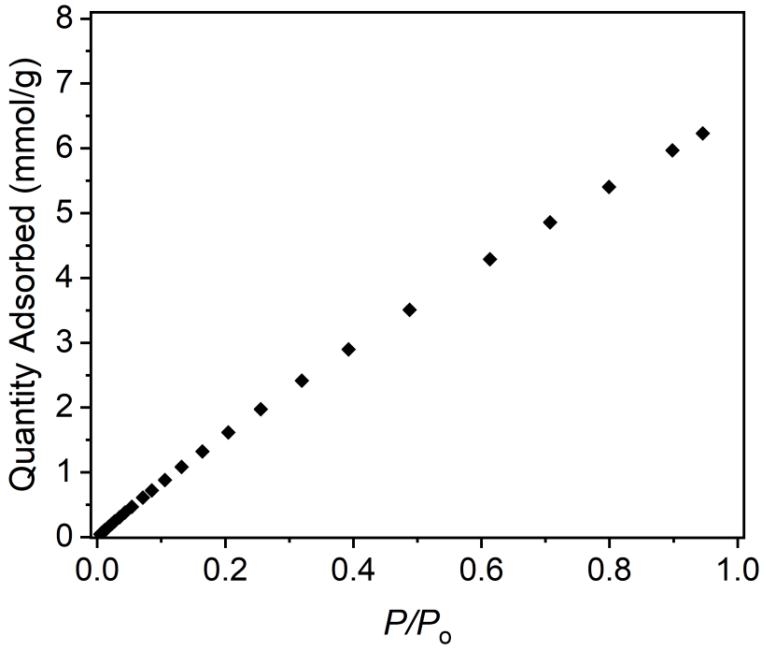

Figure 32: CH_4 adsorption at 195 K for PAF-1

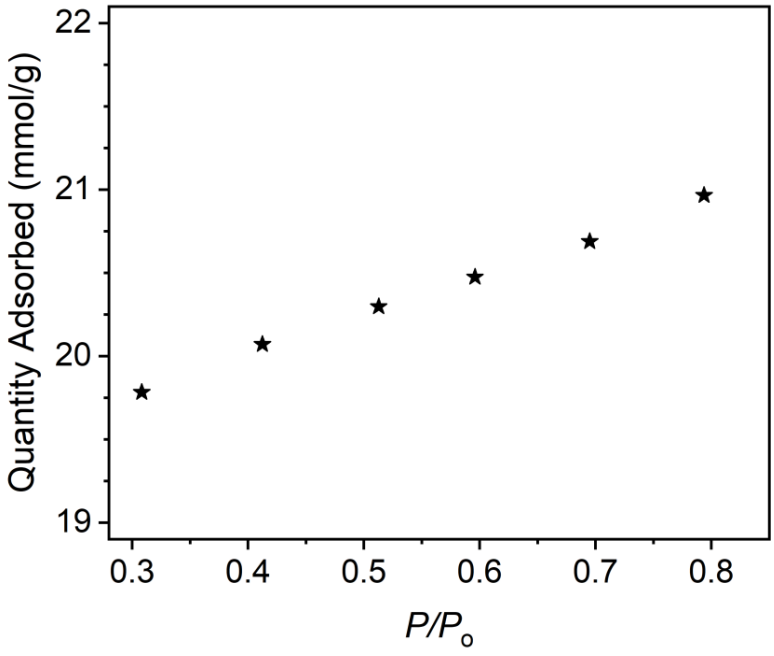

Figure 33: N_2 adsorption at 77 K for BPP-1

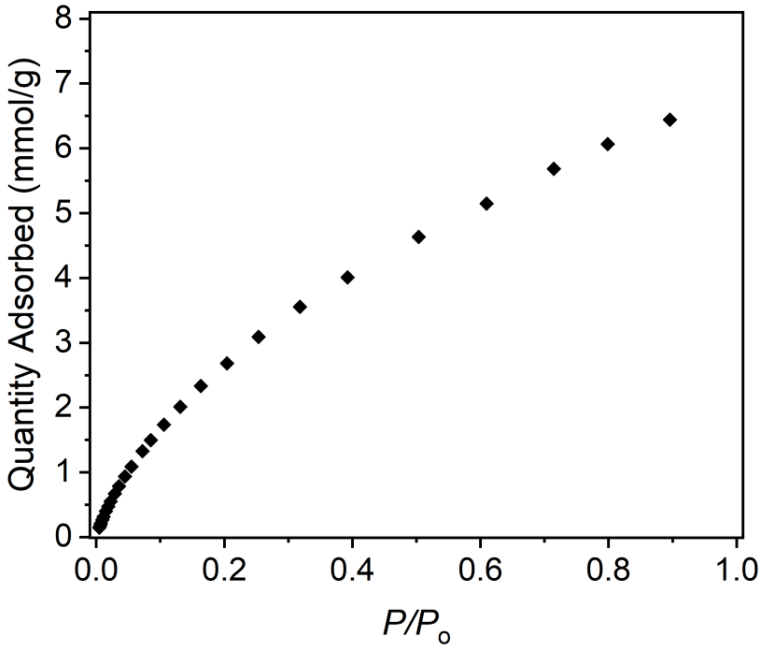

Figure 34: CH_4 adsorption at 195 K for BPP-1

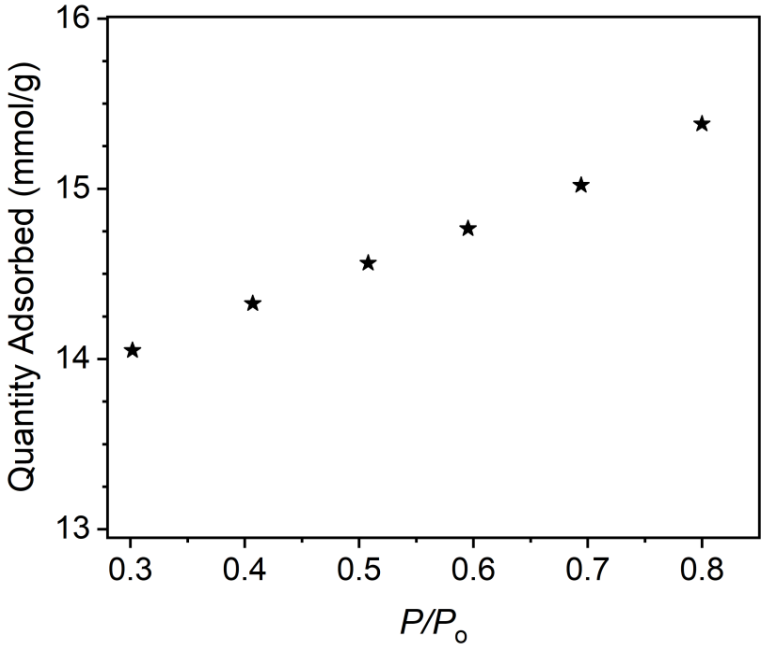

Figure 35: N_2 adsorption at 77 K for BPP-2

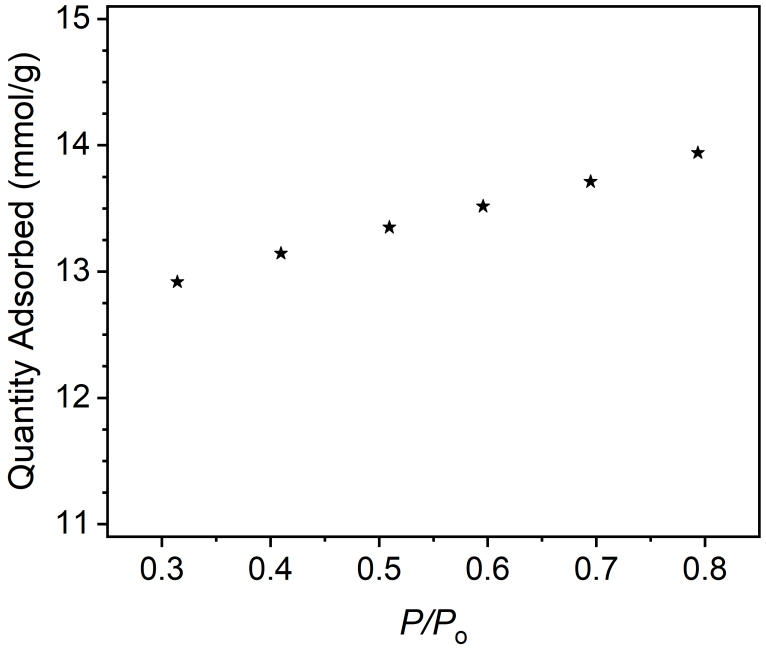

Figure 36: N_2 adsorption at 77 K for PAF-1-aceteamide

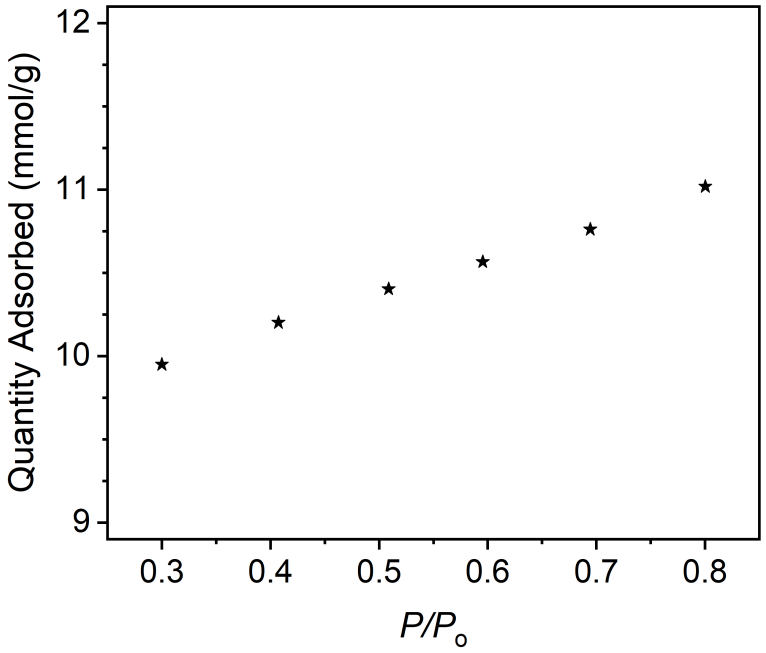

Figure 37: N_2 adsorption at 77 K for PAF-1-butyrlamide

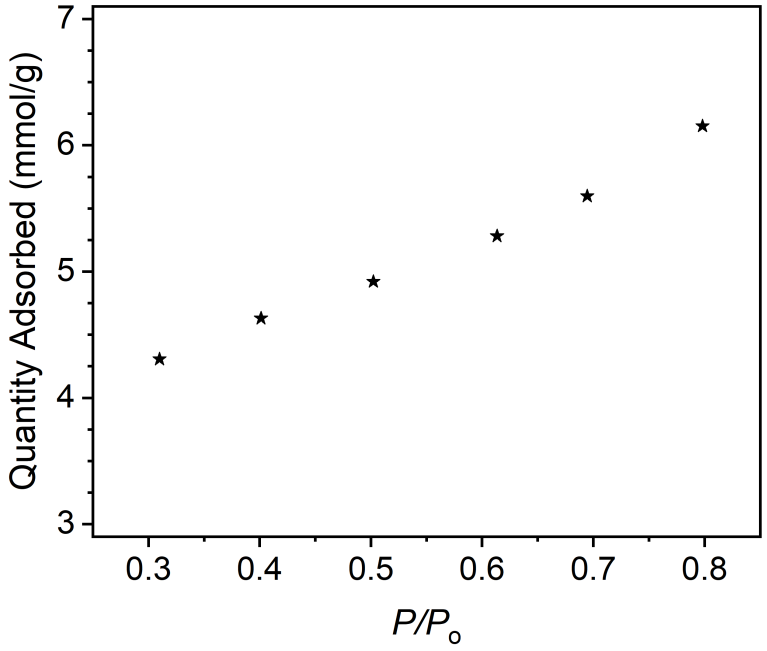

Figure 38: N_2 adsorption at 77 K for PAF-1-phenylacetamide

2.3.6 Scanning Electron Microscope Images

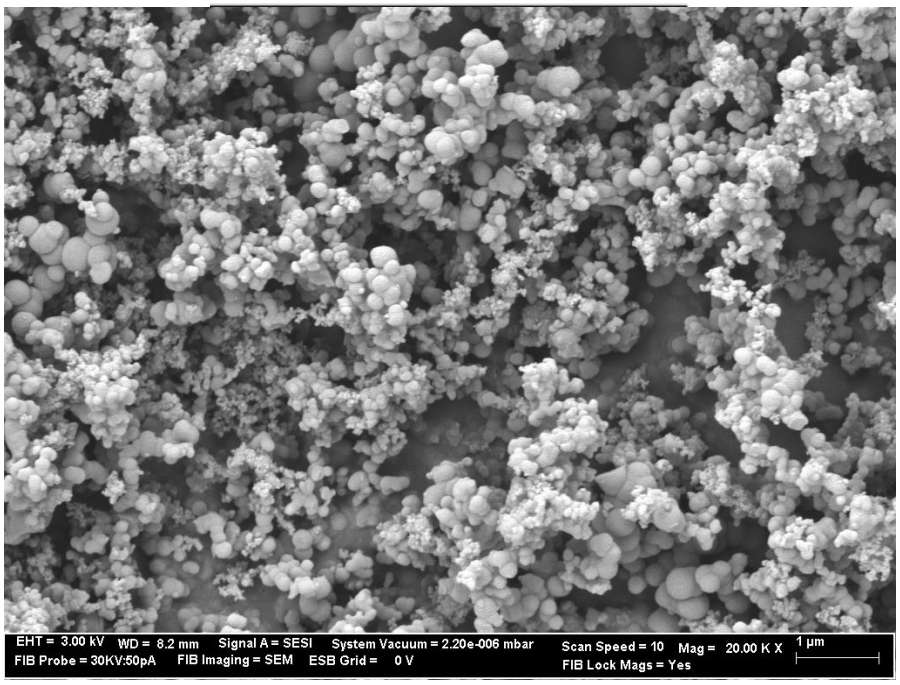

Figure 39: Scanning electron microscope image of PAF-1 at 20,000 x magnification

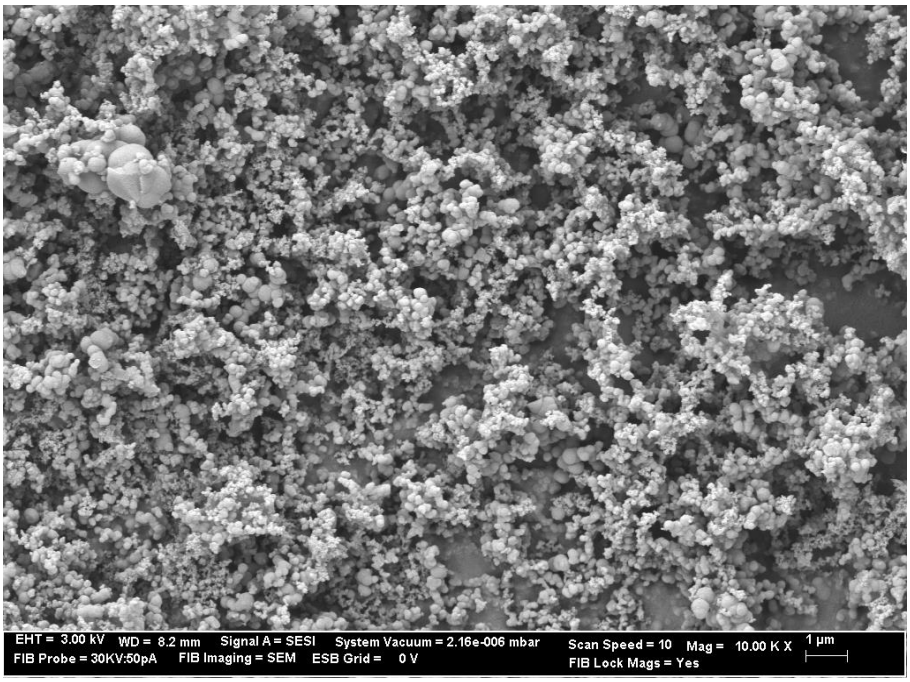

Figure 40: Scanning electron microscope image of PAF-1 at 10,000 x magnification

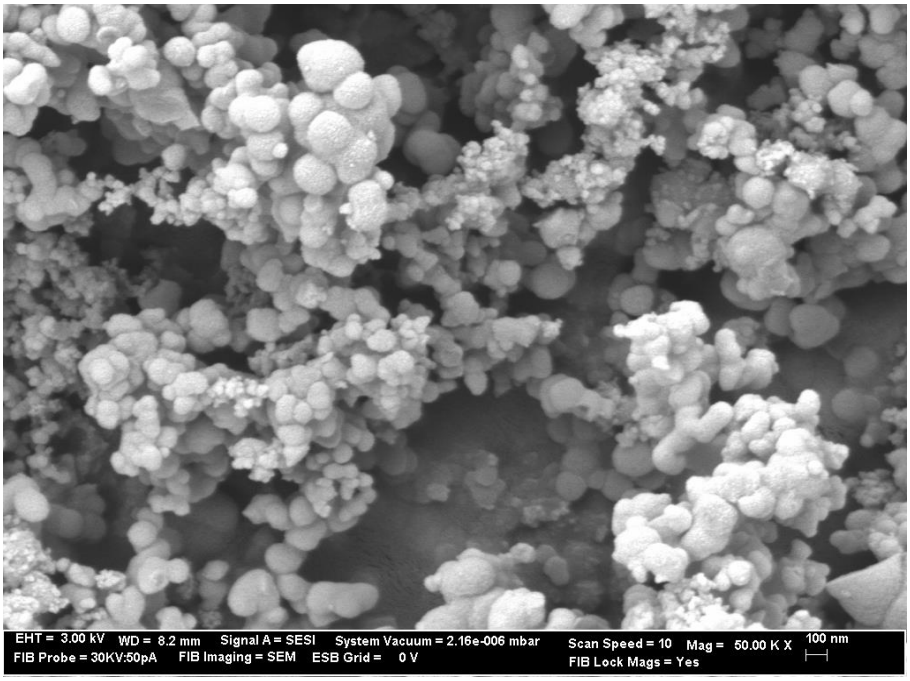

Figure 41: Scanning electron microscope image of PAF-1 at 50,000 x magnification

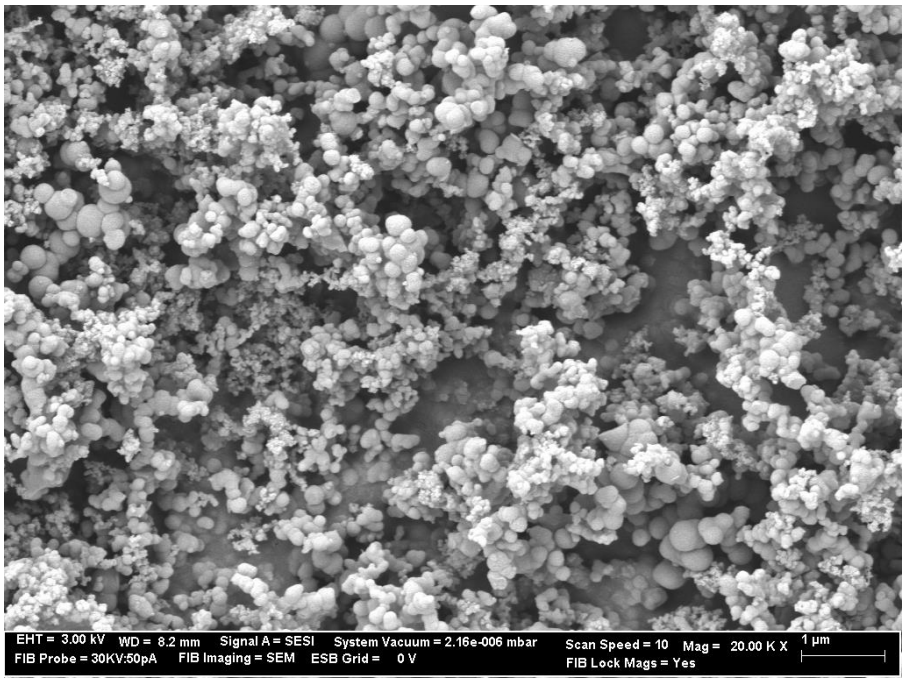

Figure 42: Scanning electron microscope image of PAF-1 at 20,000 x magnification

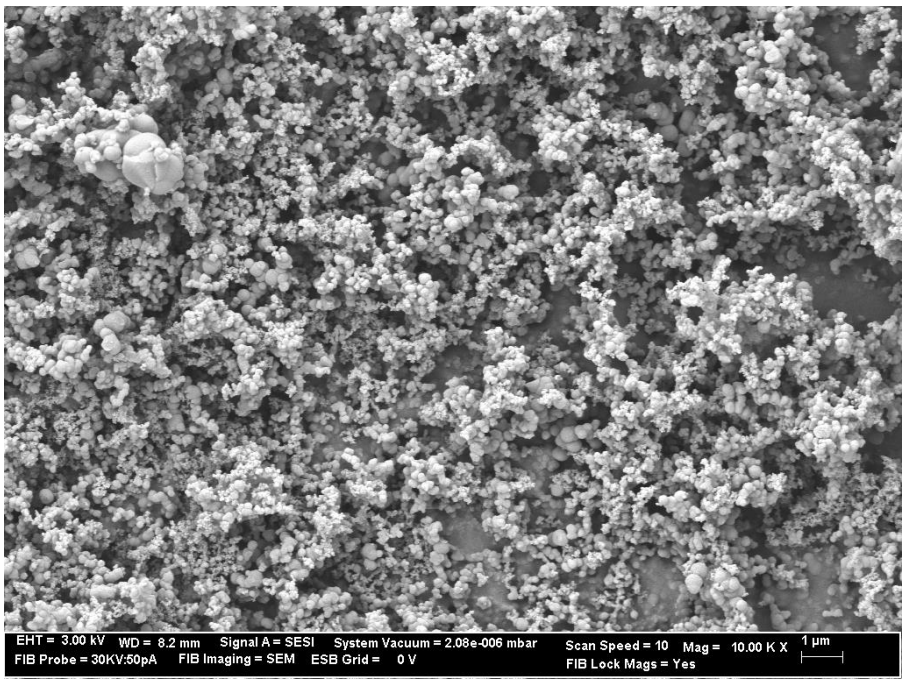

Figure 43: Scanning electron microscope image of PAF-1 at 10,000 x magnification

Chapter 3

POROUS ORGANIC CAGES

In the field of porous materials, porous organic cages are a diverse class that offer the desired qualities seen in other porous organic materials (HCPs, PIMs, CMPs, etc.) with the added advantage of being crystalline, and the potential to be ultra-tunable due to their molecular nature. These two qualities have played an integral role towards the explosion of research POCs have seen in the years since Skowronek et. al[70] reported the first assembly of an imine based POC in 2008. The ability to use covalent chemistries and readily obtainable organic reagents to synthesize porous and highly tunable organic materials has opened up a wealth of possibilities for applications of porous organic materials. Organic cages also satisfy key requirements for materials used in large scale industrial operations, namely low-cost synthesis and high scalability. Factors such as these are of high priority in industry when selecting porous materials to serve as adsorbents and catalysts, where throughput and cost of operation are considered in every step of the process.

3.1 Current Interest in Porous Organic Cages

Research in the Bloch group concerning porous organic cages has primarily revolved around methane storage. Although the gravimetric surface areas of most POCs fall short of the record values displayed by other porous solids, their span of pore sizes lie within the ideal range for methane molecules, allowing them to possess good volumetric methane storage capacities. Of particular interest to our group is the porous organic cage CC3, which was among the first organic cages reported by Cooper et. al.[71] in 2009 and is by far the most widely studied POC. As previously

mentioned, it has been studied for its potential use in a variety of applications,[87,90,93,96] but most involve its impressive separation abilities.[94,95,111,115] What makes CC3, more specifically CC3-R, a target in our research is its facile synthesis, tunability, and methane storage capacity. When crystallized to form the CC3β polymorph this cage closely resembles the smallest pore in the MOF HKUST-1, one of the leading materials in methane storage.[143] Both are octahedral in shape, with CC3-R containing edge lengths of 9.46 Å and the HKUST-1 pore 9.29 Å. Being similar in morphology, it comes as no surprise that CC3β possesses the ability to store impressive amounts of methane given its surface area (S_{BET} 652 m^2/g), with a volumetric storage capacity of 83.0 cm^3/cm^3 at 65 bar and 298 K based off a crystallographic density of 0.922 g/cm^3.[179] While this capacity is lower than seen in high capacity MOFs, CC3β does have a significantly higher crystallographic density than many MOFs[139] due to close packing of cage molecules. Another desirable characteristic of CC3β is its solubility, which can be used to increase its bulk density. Taking advantage this high solubility prior work in the Bloch group showed that dissolving CC3β in dichloromethane and upon solvent evacuation with flowing nitrogen, its bulk density increased from 0.139 g/cm^3 to 0.309 g/cm^3 with no resulting loss of surface area. When calculated using the initial bulk density of CC3β its volumetric capacity was 12.35 cm^3/cm^3, after the increase in bulk density volumetric capacity rose to ~29 cm^3/cm^3.[179] Although this increased capacity also falls short of record holding MOF materials,[145] the capability to employ solubility as a method of significantly increasing density and, in turn, volumetric capacity allows for an added degree of cage tunability. Material bulk density is an important factor for gas storage applications as basing volumetric capacity calculations on crystallographic density is unrealistic, it is not feasible to synthesize a

single crystal large enough to use in a storage tank scenario. The implications of this on the development of porous materials for gas storage applications will be discussed in subsequent sections within this chapter.

3.2 Imine Based Porous Organic Cage CC3 and Derivatives

One of the significant benefits of CC3, and porous organic cages in general, is it their ease of synthesis when compared to other porous materials such as MOFs or PAFs. Most MOFs require lengthy synthesis times, high temperatures, extensive solvent exchanging procedures that can take several days, and air free conditions during synthesis and after activation to maintain porosity. On the other hand, PAFs usually require multi-day synthesis procedures that involve many reagents and expensive catalysts, like $Ni(COD)_2$ in the case of PAF-1 and PPN-4.

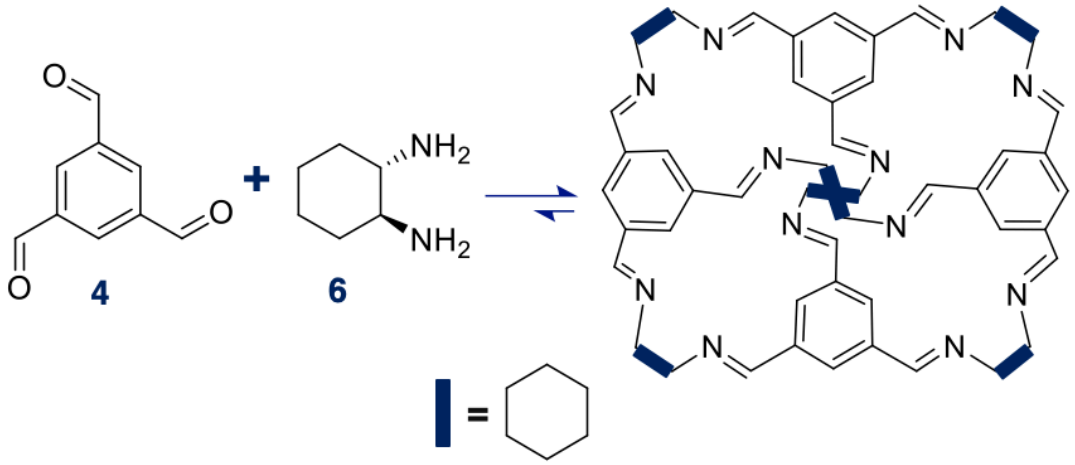

Figure 44: Scheme showing the reaction of a 4:6 ratio of 1,3,5-triformylbenzene to 1,2-diaminopropane and the resulting CC3 cage structure.

In contrast, synthesis of CC3 and related structures takes place in a one-pot reaction that simply involves combining reagents in solvent, purging the reaction vessel with nitrogen, and leaving the reaction mixture to stir at room temperature for a few days under nitrogen atmosphere. Additionally, activation procedures are simple, only requiring removal of solvent to afford activated product with satisfactory surface areas. There is no need for high temperatures or solvent exchanges like with MOFs or extensive vacuum drying like there is with PAFs. This not only makes it easier to obtain pristine cage but enables POCs to be easily synthesized in high yields. Lastly, the route of CC3 activation offers an additional degree of tunability, where the method and conditions of solvent evacuation can be utilized to alter cage packing, morphology, and crystallinity in the product. Their simple, cost effective, and efficient synthesis combined with an exceedingly high degree of tunability towards both intra- and intercage space, makes CC3 and organic cages in general perfect platforms for gas storage applications.

3.2.1 Tuning Cage Packing and Density

Our group has previously shown that by functionalizing parent cage molecules the packing arrangement of cages, and thus volumetric gas storage capacity, can be altered. Additionally, we have manipulated charge in coordination cage structures to get precisely targeted functional group mixtures.[180] Tuning the packing arrangement of POCs can be accomplished in a similar fashion through functional group addition, or via mixing two different types of cage structures. Our groups prior work with CC3 and its derivatives led to it being the primary cage of interest in regard to investigating alterations to cage packing formations. To explore routes of adjusting cage packing while best preserving the structure of CC3 two distinct methods can be utilized:

combining CC3 with analogous porous organic cages or alternate diamine caps to solutions of the CC3 parent cage. The Cooper group[181] investigated the synthesis of POCs created via the mixing of two different cage structures, and by reacting ratios of two differing diamine caps with a 1,3,5-triformylbenzene linker. This resulted in mixtures of "scrambled" amorphous cage structures where the extent of porosity is attributed to both intercage pore volume and internal cage volume. Though these processes were shown to be effective, it results in a highly mixed product containing combination ratios of each cap and linker present. This causes isolation of particular cage species of interest to be exceedingly difficult. Additionally, monitoring reaction kinetics to obtain specific ratios of cap to linker during the reaction is difficult to monitor in a normal synthesis scenario. Because we sought to achieve products with more finely tuned amounts of CC3 diaminocyclohexane cap being replaced, we focused on how packing arrangement changes effect surface area and porosity when varying amounts of diamine are added to a parent solution of CC3.

As stated above, when diamine is added to cage solution products do not consist of a 1:1 ratio of CC3 to the cage with the added diamine cap. The product consists of an amalgam of pure CC3 and cage with all added diamine cap, as well as cages containing intermittent ratios of CC3 with between 1 to 6 diaminocyclohexane caps replaced by the added amine. By altering the amount of diamine added one can control the extent of cap replacement, where increasing amounts of diamine lead to higher ratios of product with all caps replaced. Changing the ratio of substituted diamines allows for the tuning of packing structure in the resultant compound in two ways: through control of intercage void space and differences in the pore sizes of cages where caps from the parent structure have substituted. Higher rates of

substitution increase disorder among the molecules leading to increasingly disordered packing, creating a larger number of voids between cages. Size of the additional diamine introduced to the parent cage solution permits for an additional degree of control, as it determines the size of the resulting intercage voids. To investigate this, experiments were set up where CC3-R was dissolved in dichloromethane and 1,3-diaminopropane was added in different amounts. The reaction vessel was sealed with a septum, solution was purged with nitrogen, then 1,3-diaminopropane was added via syringe through a septum, and the reaction mixture was left to stir for 3 days at room temperature under nitrogen atmosphere. When targeting this approach, it was difficult to get crystals for analysis, as all products obtained were amorphous due to their inefficient packing. Despite this, the methodology showed that it is possible to tune of density through altering the level of disorder amongst cage molecules.

3.2.2 Density Tuning to Create Film Phase Cages

The aforementioned experiments on tuning cage resulted in difficulties in obtaining crystals for structural analysis, attempts to evacuate solvent led to the formation of a highly viscous liquid phase product. Being able to only obtain products of this nature, we then turned attention to using these amorphous compounds to synthesize organic cages in a film like phase to optimize density. Although its crystallographic density is relatively high the bulk density of CC3 in its CC3β polymorph is very low, at just 0.139 g/cm^3. For porous materials intended to be used as adsorbents volumetric capacity is typically the most important metric for its true capacity to store a gas, in both transportation and stationary applications. In the transportation sector, for example, methane storage in porous materials is being extensively researched for application as a clean fuel. As discussed in prior sections of

this work, the DOE and ARPA-E have set targets for porous materials to be used for compressed natural gas (CNG) storage. Materials have been synthesized that possess the ability to store volumes of methane approaching these targets, but their use for vehicular CNG storage becomes unrealistic when their density is taken into account.

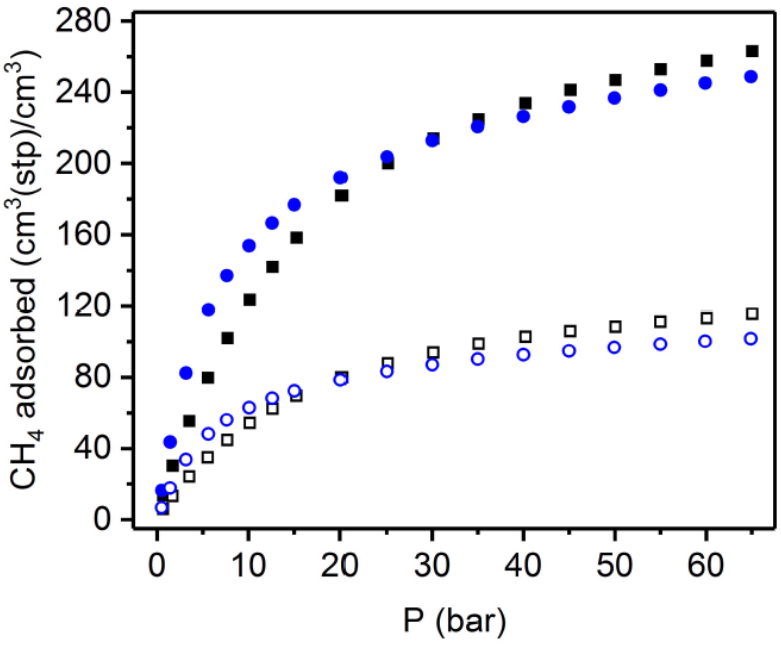

Figure 45: High pressure methane isotherms at 195 K showing crystallographic (shaded) vs. bulk density (open) adsorption for HKUST-1 (black squares) and Co-MOF-74 (blue circles)

For example, two of the leading materials in methane storage, HKUST-1 and Co-MOF-74, are reported to have total methane uptakes of 267 and 248 cm^3(STP)/cm^3 at 65 bar, respectively.[143] The problem lies in the fact that these uptakes are calculated using crystallographic density instead of bulk density (also known as volumetric density), which fails to account for the volume the material occupies in the phase that

it would be in when used in an actual vehicle fuel tank. Essentially these high uptake examples are misleading because the adsorbent material would be packed into a fuel tank in a powder like solid phase, not as one large crystal. When the bulk density of HKUST-1 and Co-MOF-74 are taken into account their deliverable capacity falls to around 100 cm^3(STP)/cm^3,[182] less than half of what is commonly reported. Vehicles would require prohibitively large fuel tanks to store the required amount of natural gas within these low-density materials, or the material would have to be made denser. Gas storage capabilities in porous materials are often diminished when they are made denser via forceful methods like compression, due to pores essentially being crushed.[183,184] Since porous materials cannot be compressed enough to provide sufficient density without loss of porosity, other methods to obtain higher density must be explored. In order to achieve higher density in a porous organic cage, we took advantage of the tunability of packing and density of CC3 to create a film phase porous material.

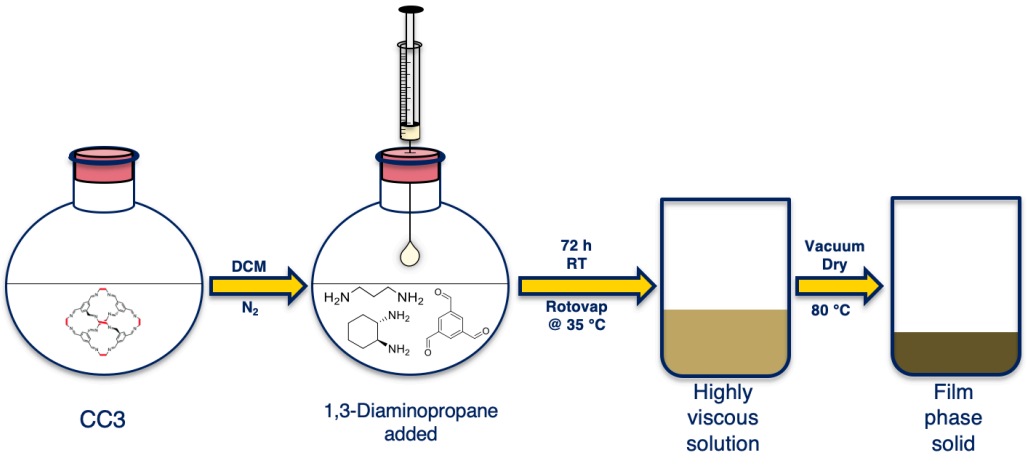

Figure 46: Diagram depicting the method used to create a film phase CC3-R and 1,3,-diaminopropane based film phase porous organic cage

To create the film phase cage, we took the amorphous products from the reactions of CC3 and 1,3-diaminopropane and slowly evaporated solvent in vacuo at 30° C followed by vacuum drying at 80° C to form a dense film. Gas adsorption experiments of these materials resulted in all being effectively nonporous. They were, however, able to adsorb quantities of CO_2 which correlated to the amount of 1,3-diaminopropane added to solution, higher diamine content resulted in higher CO_2 uptake. Total CO_2 uptake at 195 K for the film phase cages from least diamine added to most were as follows: 6.1 cm^3/g STP at $P/P_0 = 0.95$, 7.8 cm^3/g STP at $P/P_0 = 0.95$, and 28.3 cm^3/g STP at $P/P_0 = 0.95$. These values represent uptakes of film phase cages created in mmol ratios of CC3-R:1,3-diaminopropane of 0.1:3, 0.1:6, and 0.05:6, respectively. Although largely nonporous, the ability to uptake CO_2 in these film phase materials is possible due to the intercage space resulting from disordered packing caused by the introduction of 1,3-diaminopropane. Additional experimentation is needed to quantify the exact amount of diamine needed to obtain specific densities, however these proof of concept experiments show that density tuning is possible through the creation of film phase porous organic cages.

Finally, although the well-known POC, CC3-R, shows incredible utility for a variety of applications, the cost of the trialdehyde used in the synthesis of this cage is often viewed as prohibitive. Instead, we targeted the synthesis of porous organic cages using a 1,3,5-tricetylbenzene linker and various diamine caps. The primary reason for this being that 1,3,5-triacetylbenzene is cheaper than 1,3,5-triformylbenzene, at $34 and $174 per gram respectively. Such a significant difference in price makes a triformylbenzene based cage scalable at a more reasonable price, an important aspect when looking forward to potential large scale or industrial application.

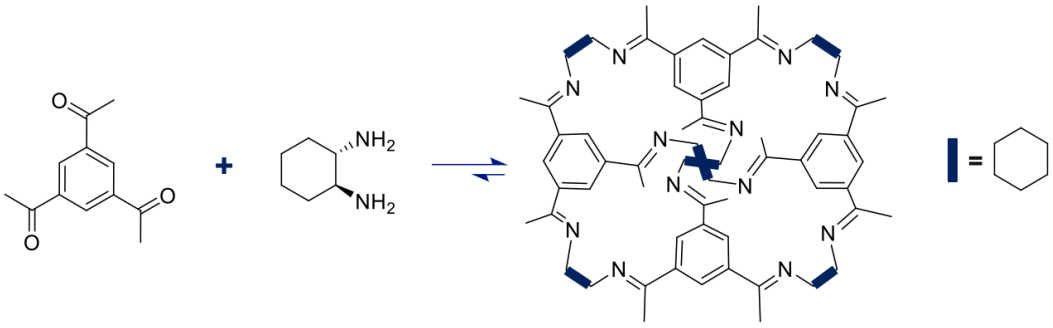

Figure 47: Scheme showing the reaction of a 4:6 ratio of 1,3,5-triacetylbenzene to 1,2-diaminopropane and the resulting CC3 cage structure.

Although their surface area and gas uptake were negligible compared to the CC3 cage, with the best solid phase product having a Langmuir surface area of just 297 m^2/g, many of the combinations of triacetylbenzene and diamines resulted in an extremely viscous liquid when in vacuo concentration was attempted to obtain solid. This is likely not due to a change in the cage structure, as the triacetylbenzene linker creates an analogous cage to CC3. Therefore, as results from the previous CC3-R experiments showed, it can be said that this amorphous structure is also caused by disordered packing. At that time, the adsorption properties of these triacetylbenzene solutions when transformed into films was not investigated. Future work on this project will provide insight into the structure and tunability of density and packing in triacetylbenzene based cage structures, along with properties of amorphous or film phase cage mixtures of both triformylbenzene and triacetylbenzene based cages.

3.3 Conclusion and Outlook for Porous Organic Cages

Porous Organic Cages present a highly tunable and easily synthesized platform for the creation of application specific molecules. With a seemingly unlimited number

of reagents that can be considered for cage synthesis, future research into POCs could very well reveal an unprecedented amount of cage structures as time goes on and computational power increases. The ability to create film phase materials with POCs also opens the possibility for instant membrane creation, where the cage itself would serve as the membrane, eliminating the need for surface deposition or mixing with other materials to create composite membranes. One future direction our lab intends to take is the mixing of two cages that have structures based on irreversible bonds, resulting in an actual mixture of the two parent cages without any scrambling taking place. This would allow for the combination of cages with two specific functionalities in exact ratios for finely tuned separation or catalysis capabilities. Despite their relatively low surface areas, it can be said that POCs show a more realistic promise towards large scale applications in comparison to other porous materials like MOFs or PAFs. This is due to their cheap and easily scalable synthesis, as well as their unmatched structural versatility, allowing them the ability to serve a wide range of functions.

3.4 Experimental Section

3.4.1 General Information

See section 3.1.1 for general information

3.4.2 Synthesis Procedures

3.4.2.1 Synthesis of Porous Organic Cage CC3

1.0 g triformylbenzene, 1.2 g 1,2-diaminocyclohexane, and 450 mL anhydrous dichloromethane were combined in a 500 mL round bottom flask equipped with a

septum. The flask was purged with nitrogen for 30 minutes then left under nitrogen atmosphere to stir for 3 days at room temperature. The resulting pale-yellow solution was concentrated in vacuo, redissolved in dichloromethane, and filtered to remove contaminants. This solution was then concentrated in vacuo again and the resultant solid was washed with ethyl acetate, redissolved once more in anhydrous dichloromethane, concentrated in vacuo, and dried under vacuum at 90° C for 24 hours to afford a slightly pale yellow solid.

3.4.2.2 Synthesis of Triacetylbenzene-diaminocyclohexane imine cage

210 mg triacetylbenzene, 175 mg 1,2-diaminocyclohexane, and 60 mL anhydrous dichloromethane were combined in a 100 mL round bottom flask and purged for 30 min with nitrogen. The solution was then stirred at 45° C under nitrogen atmosphere for 3 days equipped with a condenser to prevent evaporation of solvent. The resultant solution was concentrated in vacuo to obtain a burnt orange film like substance, which was then left to dry under vacuum at room temperature 24 hours to obtain a flakey tan powder-like substance.

3.4.2.3 Synthesis of Scrambled Film Phase CC3 Based Cage

50 mg CC3 cage and 50 mL dry dichloromethane were combined in a 100 mL round bottom flask equipped with a septum. The solution was stirred at room temperature for 30 minutes while purging with nitrogen. 0.50 mL 1,3-diaminopropane was then added via syringe and the solution was left to stir for 3 days under nitrogen atmosphere. The solution was then concentrated in vacuo, redissolved in anhydrous dichloromethane, filtered to remove contaminants, concentrated again in vacuo and dissolved in ethyl acetate, then concentrated in vacuo again. Solid dissolved in

anhydrous dichloromethane once more and concentrated in vacuo again to obtain a highly viscous liquid. This liquid was then slowly heated to 80° C inside of a TriStar II gas adsorption tube under vacuum for 24 hours to produce a thin film-like solid.

3.4.3 Gas Adsorption Isotherms

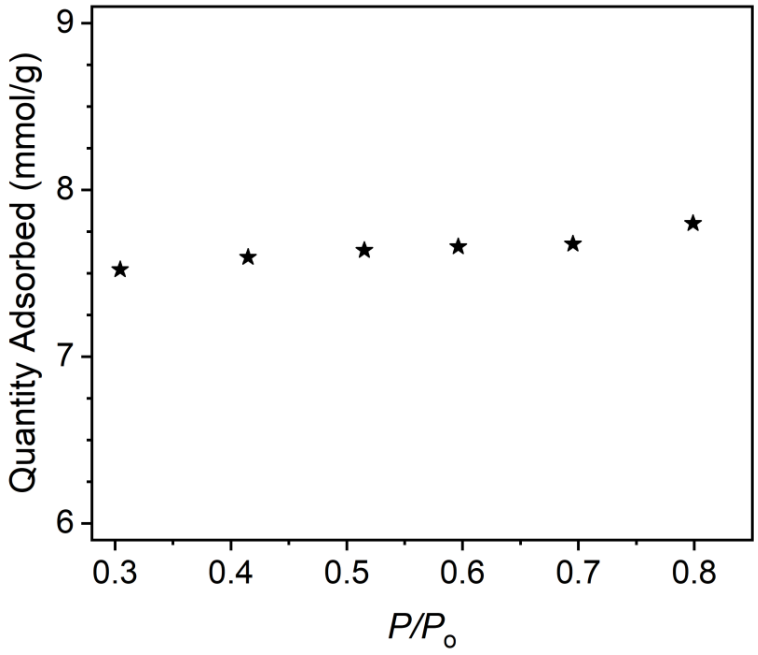

Figure 48: N_2 adsorption at 77 K for porous organic cage CC3

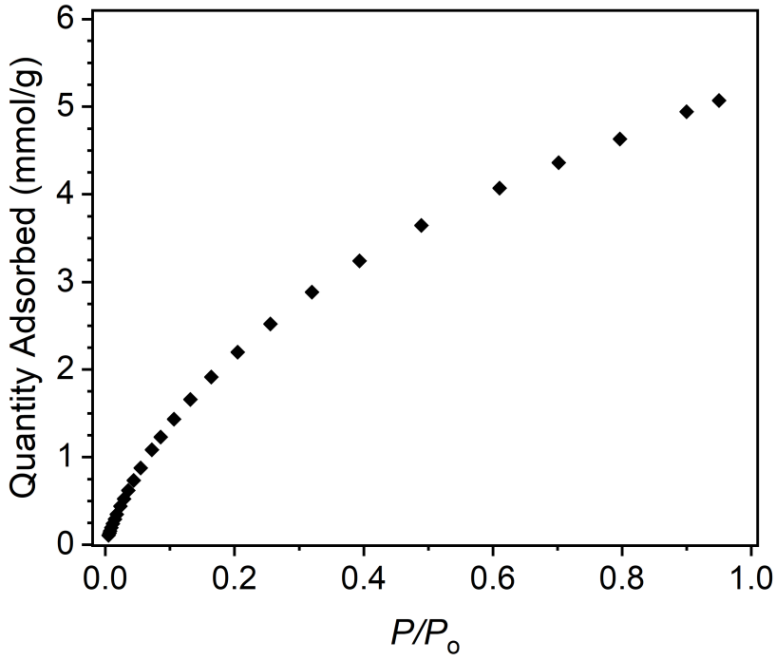

Figure 49: CH_4 adsorption at 195 K for porous organic cage CC3

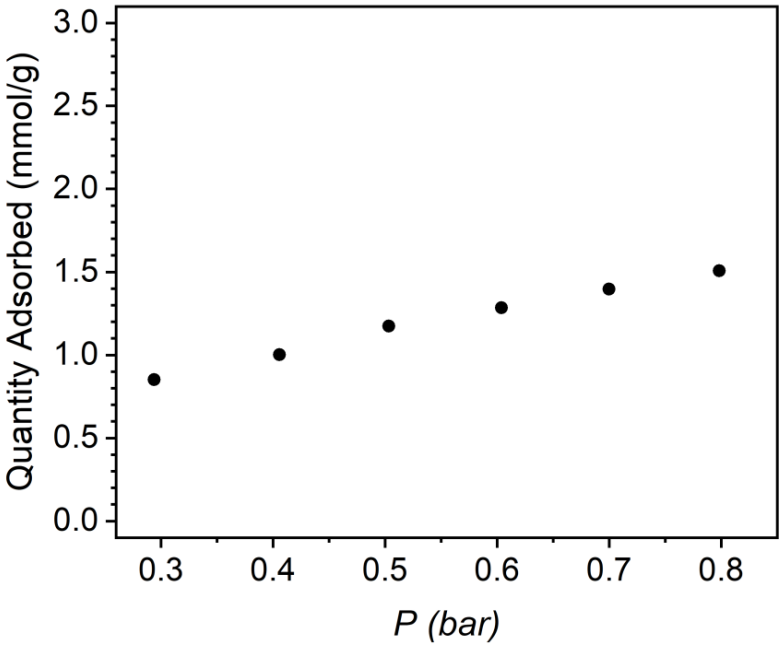

Figure 50: CO_2 adsorption at 195 K for 1,3,5-triacetylbenzene and 1,2-diaminocyclohexane porous organic cage

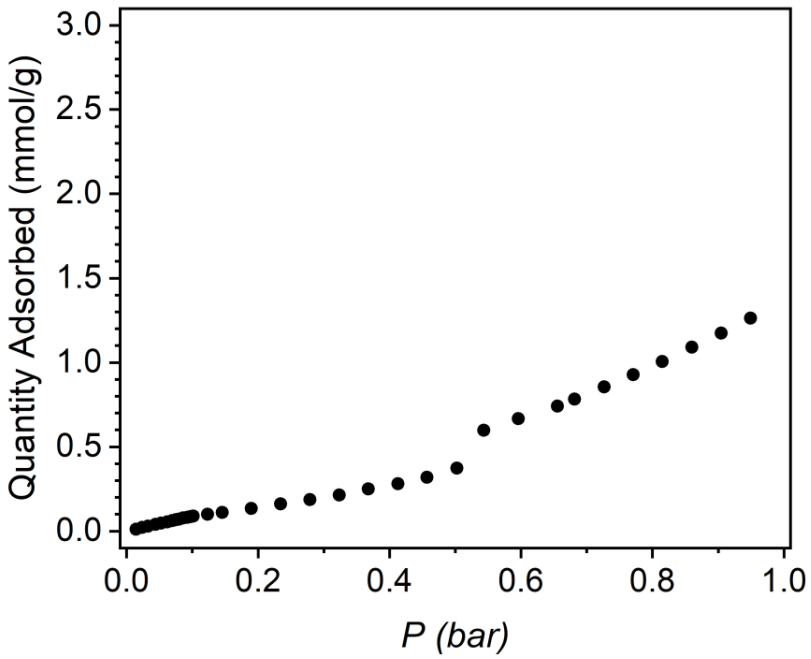

Figure 51: CO_2 adsorption at 195 K for scrambled film phase CC3 & 1,3-diaminopropane porous organic cage

REFERENCES

1- Donnay, J. D. H. Memorial of Georges Friedel. *Am. Mineral* **1934,** *19*, 329–335.

2- Kulprathipanja, S. *Zeolites in Industrial Separation and Catalysis*; Wiley-VCH: Weinheim, 2010. Pg 3

3- Sherman, J. Synthetic Zeolites and Other Microporous Oxide Molecular Sieves. *Proc. Natl. Acad. of Sci. U.S.A*. **1999**, *96*, 3471-3478.

4- Izumi, Y.; Ichihashi, H.; Shimazu, Y.; Kitamura, M.; Sato, H. Development and Industrialization of the Vapor-Phase Beckmann Rearrangement Process. *Bull. Chem. Soc. Jpn*. **2007**, *80*, 1280–1287.

5- Baril, E.; Lefebvre, L. P.; Hacking, S. A. Direct Visualization and Quantification of Bone Growth into Porous Titanium Implants Using Micro Computed Tomography. *J. Mater. Sci.: Mater. Med*. **2011**, *22*, 1321–1332.

6- Arruebo, M. Drug Delivery from Structured Porous Inorganic Materials. *Wiley Interdiscip. Rev.: Nanomed. Nanobiotechnol*. **2011**, *4*, 16–30.

7- Phillips, K.; England, G.; Sunny, S.; Shirman, E.; Shirman, T.; Vogel, N.; Aizenberg, J. A Colloidoscope Of Colloid-Based Porous Materials And Their Uses. *Chem. Soc. Rev.* **2016**, *45*, 281-322.

8- Nakhli, S.; Delkash, M.; Bakhshayesh, B.; Kazemian, H. Application Of Zeolites For Sustainable Agriculture: A Review On Water And Nutrient Retention. *Water, Air, & Soil Pollut.* **2017**, *228*, 464

9- Jiang, N.; Shang, R.; Heijman, S.; Rietveld, L. High-Silica Zeolites For Adsorption Of Organic Micro-Pollutants In Water Treatment: A Review. *Water Res.* **2018**, *144*, 145-161.

10- Wang, B.; Prinsen, P.; Wang, H.; Bai, Z.; Wang, H.; Luque, R.; Xuan, J. Macroporous Materials: Microfluidic Fabrication, Functionalization and Applications. *Chem. Soc. Rev.* **2017**, *46*, 855–914.

11- Cecilia, J. A.; Tost, R. M.; Millán, M. R. Mesoporous Materials: From Synthesis to Applications. *Int. J. Mol. Sci.* **2019**, *20*, 3213.

12- Langmuir, I. The Adsorption of Gases On Plane Surfaces of Glass, Mica And Platinum. *J. Am. Chem. Soc.* **1918**, *40*, 1361–1403.

13- Brunauer, S.; Emmett, P. H.; Teller, E. Adsorption of Gases in Multimolecular Layers. *J. Am. Chem. Soc.* **1938**, *60*, 309–319.

14- Smart, L.; Moore, E. *Solid State Chemistry,* 3rd Ed.; CRC Press: London, 2005; p 301.

15- Kulprathipanja, S. *Zeolites in industrial separation and catalysis*; Wiley-VCH Verlag GmbH & Co.: Weinheim, 2010; pp 1-20.

16- Ch. Baerlocher and L.B. McCusker. Database of Zeolite Structures. http://www.iza-structure.org/databases (accessed June 2nd 2020)

17- Flanagan D. M.; Zeolites. *Minerals Yearbook, volume I, Metals and Minerals*; U.S. Geological Survey: Reston, VA, 2018; pp 84.1-84.4

18- Mumpton, F. Using Zeolites in Agriculture. *Innovative Biological Technologies for Lesser Developed Countries*, OTA-13P-F-29; US Congress: Washington DC, 1985

19- Kosinov, N.; Gascon, J.; Kapteijn, F.; Hensen, E. J. Recent Developments in Zeolite Membranes for Gas Separation. *J. Membr. Sci.* **2016**, *499*, 65–79.

20- Ćurković, L.; Cerjan-Stefanović, Š.; Filipan, T. Metal Ion Exchange by Natural and Modified Zeolites. *Water Res.* **1997**, *31*, 1379–1382.

21- Calabria, J. L.; Lens, P. N.; Yeh, D. H. Zeolite Ion Exchange to Facilitate Anaerobic Membrane Bioreactor Wastewater Nitrogen Recovery and Reuse for Lettuce Fertigation in Vertical Hydroponic Systems. *Environ. Eng. Sci.* **2019**, *36*, 690–698.

22- Verdoliva, V.; Saviano, M.; Luca, S. D. Zeolites as Acid/Basic Solid Catalysts: Recent Synthetic Developments. *Catalysts* **2019**, *9*, 248.

23- Gary, J. H.; Handwerk, G. E.; Kaiser, M. J. *Petroleum refining: Technology and Economics*, 5th ed.; CRC Press: Boca Raton, 2007; pp 121-140.

24- Komvokis, V.; Tan, L.; Clough, M.; Pan, S.; Yilmaz, B. Zeolites in sustainable chemistry: synthesis, characterization and catalytic applications; Xiao, F.-S., Meng, X., Eds.; Springer-Verlag: Berlin, 2016; pp 271-291.

25- Jensen, N. K.; Rufford, T. E.; Watson, G.; Zhang, D. K.; Chan, K. I.; May, E. F. Screening Zeolites for Gas Separation Applications Involving Methane, Nitrogen, and Carbon Dioxide. *J. Chem. Eng. Data* **2011**, *57*, 106–113.

26- Donk, S. V.; Janssen, A. H.; Bitter, J. H.; Jong, K. P. D. Generation, Characterization, and Impact of Mesopores in Zeolite Catalysts. *Catal. Rev.* **2003**, *45*, 297–319.

27- Perot, G.; Guisnet, M. Advantages and Disadvantages of Zeolites as Catalysts in Organic Chemistry. *J. Mol. Catal.* **1990**, *61*, 173–196.

28- Hoskins, B. F.; Robson, R. Infinite Polymeric Frameworks Consisting of Three Dimensionally Linked Rod-like Segments. *J. Am. Chem. Soc.* **1989**, *111*, 5962–5964.

29- Venkataraman, D.; Gardner, G. B.; Lee, S.; Moore, J. S. Zeolite-like Behavior of a Coordination Network. *J. Am. Chem. Soc.* **1995**, *117*, 11600–11601.

30- Yaghi, O. M.; Li, G.; Li, H. Selective Binding and Removal of Guests in a Microporous Metal–Organic Framework. *Nature* **1995**, *378*, 703–706.

31- Hönicke, I. M.; Senkovska, I.; Bon, V.; Baburin, I. A.; Bönisch, N.; Raschke, S.; Evans, J. D.; Kaskel, S. Balancing Mechanical Stability and Ultrahigh Porosity in Crystalline Framework Materials. *Angew. Chem., Int. Ed.* **2018**, *57*, 13780–13783.

32- Farha, O. K.; Eryazici, I.; Jeong, N. C.; Hauser, B. G.; Wilmer, C. E.; Sarjeant, A. A.; Snurr, R. Q.; Nguyen, S. T.; Yazaydın, A. Ö.; Hupp, J. T. Metal–Organic Framework Materials with Ultrahigh Surface Areas: Is the Sky the Limit? *J. Am. Chem. Soc.* **2012**, *134*, 15016–15021.

33- Yuan, S.; Feng, L.; Wang, K.; Pang, J.; Bosch, M.; Lollar, C.; Sun, Y.; Qin, J.; Yang, X.; Zhang, P.; Wang, Q.; Zou, L.; Zhang, Y.; Zhang, L.; Fang, Y.; Li, J.; Zhou, H.-C. Stable Metal-Organic Frameworks: Design, Synthesis, and Applications. *Adv. Mater.* **2018**, *30*, 1704303.

34- Moghadam, P. Z.; Li, A.; Wiggin, S. B.; Tao, A.; Maloney, A. G. P.; Wood, P. A.; Ward, S. C.; Fairen-Jimenez, D. Development of a Cambridge Structural

Database Subset: A Collection of Metal–Organic Frameworks for Past, Present, and Future. *Chem. Mater.* **2017**, *29*, 2618–2625.

35- Burgess, S. A.; Kassie, A.; Baranowski, S. A.; Fritzsching, K. J.; Schmidt-Rohr, K.; Brown, C. M.; Wade, C. R. Improved Catalytic Activity and Stability of a Palladium Pincer Complex by Incorporation into a Metal–Organic Framework. *J. Am. Chem. Soc.* **2016**, *138*, 1780–1783.

36- Gao, D.; Wang, Z.; Wang, C.; Wang, L.; Chi, Y.; Wang, M.; Zhang, J.; Wu, C.; Gu, Y.; Wang, H.; Zhao, Z. CrPd Nanoparticles on NH2-Functionalized Metal-Organic Framework as a Synergistic Catalyst for Efficient Hydrogen Evolution from Formic Acid. *Chemical Engineering Journal* **2019**, *361*, 953–959.

37- Yang, L.; Cui, X.; Zhang, Y.; Wang, Q.; Zhang, Z.; Suo, X.; Xing, H. Anion Pillared Metal–Organic Framework Embedded with Molecular Rotors for Size-Selective Capture of CO_2 from CH_4 and N_2. *ACS Sustainable Chem. Eng.* **2019**, *7*, 3138–3144.

38- Van De Voorde, B.; Damasceno Borges, D.; Vermoortele, F.; Wouters, R.; Bozbiyik, B.; Denayer, J.; Taulelle, F.; Martineau, C.; Serre, C.; Maurin, G.; De Vos, D. Isolation of Renewable Phenolics by Adsorption on Ultrastable Hydrophobic MIL-140 Metal-Organic Frameworks. *ChemSusChem* **2015**, *8*, 3159–3166.

39- Alezi, D.; Belmabkhout, Y.; Suyetin, M.; Bhatt, P. M.; Weseliński, Ł. J.; Solovyeva, V.; Adil, K.; Spanopoulos, I.; Trikalitis, P. N.; Emwas, A.-H.; Eddaoudi, M. MOF Crystal Chemistry Paving the Way to Gas Storage Needs: Aluminum-Based Soc-MOF for CH4, O2, and CO2 Storage. *J. Am. Chem. Soc.* **2015**, *137*, 13308–13318.

40- Tian, T.; Zeng, Z.; Vulpe, D.; Casco, M. E.; Divitini, G.; Midgley, P. A.; Silvestre-Albero, J.; Tan, J.-C.; Moghadam, P. Z.; Fairen-Jimenez, D. A Sol–Gel Monolithic Metal–Organic Framework with Enhanced Methane Uptake. *Nat. Mater.* **2017**, *17*, 174–179.

41- Ding, M.; Cai, X.; Jiang, H.-L. Improving MOF Stability: Approaches and Applications. *Chem. Sci.* **2019**, *10*, 10209–10230.

42- Howarth, A. J.; Liu, Y.; Li, P.; Li, Z.; Wang, T. C.; Hupp, J. T.; Farha, O. K. Chemical, Thermal and Mechanical Stabilities of Metal–Organic Frameworks. *Nat. Rev. Mater.* **2016**, *1*, 15018.

43- Rogozhin, S. V.; Davankov, V. A.; Tsyurupa, M. P. Patent USSR 299165, 1969.

44- Huang, J.; Turner, S. R. Hypercrosslinked Polymers: A Review. *Polymer Reviews* **2018**, *58*, 1–41.

45- Ahn, J.-H.; Jang, J.-E.; Oh, C.-G.; Ihm, S.-K.; Cortez, J.; Sherrington, D. C. Rapid Generation and Control of Microporosity, Bimodal Pore Size Distribution, and Surface Area in Davankov-Type Hyper-Cross-Linked Resins. *Macromolecules* **2006**, *39*, 627−632.

46- Dawson, R.; Stevens, L. A.; Drage, T. C.; Snape, C. E.; Smith, M. W.; Adams, D. J.; Cooper, A. I. Impact of Water Coadsorption for Carbon Dioxide Capture in Microporous Polymer Sorbents. *J. Am. Chem. Soc.* **2012**, *134*, 10741−10744.

47- McKeown, N. B.; Makhseed, S.; Budd, P. M. Phthalocyanine-based nanoporous network polymers. *Chem. Commun*. **2002**, *23*, 2780−2781.

48- Ghanem, B. S.; Hashem, M.; Harris, K. D. M.; Msayib, K. J.; Xu, M.; Budd, P. M.; Chaukura, N.; Book, D.; Tedds, S.; Walton, A.; McKeown, N. B. Triptycene-Based Polymers of Intrinsic Micro- porosity: Organic Materials That Can Be Tailored for Gas Adsorption. *Macromolecules* **2010**, *43*, 5287−5294.

49- Wang, Y.; Ma, X.; Ghanem, B.; Alghunaimi, F.; Pinnau, I.; Han, Y. Polymers of Intrinsic Microporosity for Energy-Intensive Membrane-Based Gas Separations. *Materials Today Nano* **2018**, *3*, 69–95.

50- Jiang, J.-X.; Su, F.; Trewin, A.; Wood, C. D.; Campbell, N. L.; Niu, H.; Dickinson, C.; Ganin, A. Y.; Rosseinsky, M. J.; Khimyak, Y. Z.; et al. Conjugated Microporous Poly(aryleneethynylene) Networks. *Angew. Chem., Int. Ed*. **2007**, *46*, 8574−8578.

51- Holst, J. R.; Stöckel, E.; Adams, D. J.; Cooper, A. I. High Surface Area Networks from Tetrahedral Monomers: Metal-Catalyzed Coupling, Thermal Polymerization, and “Click” Chemistry. *Macromolecules* **2010**, *43*, 8531−8538.

52- Jiang, J. X.; Trewin, A.; Adams, D. J.; Cooper, A. I. Band Gap Engineering in Fluorescent Conjugated Microporous Polymers. *Chem. Sci*. **2011**, *2*, 1777−1781.

53- Li, A.; Lu, R.-F.; Wang, Y.; Wang, X.; Han, K.-L.; Deng, W.-Q. Lithium-doped Conjugated Microporous Polymers for Reversible Hydrogen Storage. *Angew. Chem., Int. Ed*. **2010**, *49*, 3330−3333.

54- Dawson, R.; Adams, D. J.; Cooper, A. I. Chemical Tuning of CO_2 Sorption in Robust Nanoporous Organic Polymers. *Chem. Sci*. **2011**, *2*, 1173−1177.

55- Cote, A. P.; Yaghi, O. Porous, Crystalline, Covalent Organic Frameworks. *Science* **2005**, *310*, 1166–1170.

56- Zhu, L.; Zhang, Y. Crystallization of Covalent Organic Frameworks for Gas Storage Applications. *Molecules* **2017**, *22*, 1149.

57- Baldwin, L. A.; Crowe, J. W.; Pyles, D. A.; Mcgrier, P. L. Metalation of a Mesoporous Three-Dimensional Covalent Organic Framework. *J. Am. Chem. Soc.* **2016**, *138*, 15134–15137.

58- Fang, Q.; Wang, J.; Gu, S.; Kaspar, R. B.; Zhuang, Z.; Zheng, J.; Guo, H.; Qiu, S.; Yan, Y. 3D Porous Crystalline Polyimide Covalent Organic Frameworks for Drug Delivery. *J. Am. Chem. Soc.* **2015**, *137*, 8352–8355.

59- Furukawa H.; Yaghi O. M. Storage of Hydrogen, Methane, and Carbon Dioxide in Highly Porous Covalent Organic Frameworks for Clean Energy Applications. *J. Am. Chem. Soc*. **2009**, *131*, 8875-8883.

60- Doonan C. J.; Tranchemontagne D. J.; Glover, T. G.; Hunt J. R.; Yaghi O. M. Exceptional Ammonia Uptake by a Covalent Organic Framework. *Nat. Chem.* **2010**, *2*, 235-238.

61- Ding S. Y.; Gao J.; Wang Q.; Zhang Y.; Song W.-G.; Su C.-Y.; Wang W. Construction of Covalent Organic Framework for Catalysis: Pd/COF-LZU-1 in Suzuki-Miyaura Coupling Reaction. *J. Am. Chem. Soc.,* **2011**, *133*, 19816-19822.

62- Demirocak, D. E.; Ram, M. K.; Srinivasan, S. S.; Goswami, D. Y.; Stefanakos, E. K. A Novel Nitrogen Rich Porous Aromatic Framework for Hydrogen and Carbon Dioxide Storage. *J. Mater. Chem. A* **2013**, *1*, 13800.

63- Yuan, Y.; Sun, F.; Ren, H.; Jing, X.; Wang, W.; Ma, H.; Zhao, H.; Zhu, G. Targeted Synthesis of a Porous Aromatic Framework with a High Adsorption Capacity for Organic Molecules. *J. Mater. Chem.* **2011**, *21*, 13498-13502.

64- Wang, W.; Ren, H.; Sun, F.; Cai, K.; Ma, H.; Du, J.; Zhao, H.; Zhu, G. Synthesis of Porous Aromatic Framework with Tuning Porosity via Ionothermal Reaction. *Dalton Trans.* **2012**, *41*, 3933-3936.

65- Ben, T.; Ren, H.; Ma, S.; Cao, D.; Lan, J.; Jing, X.; Wang, W.; Xu, J.; Deng, F.; Simmons, J. M.; Qiu, S.; Zhu, G. Targeted Synthesis of a Porous Aromatic Framework with High Stability and Exceptionally High Surface Area. *Angew. Chem., Int. Ed.* **2009**, *48*, 9457–9460.

66- Yuan, D.; Lu, W.; Zhao, D.; Zhou, H.-C. Highly Stable Porous Polymer Networks with Exceptionally High Gas-Uptake Capacities. *Adv. Mater.* **2011**, *23*, 3723–3725.

67- Yuan, Y.; Liu, J.; Ren, H.; Jing, X.; Wang, W.; Ma, H.; Sun, F.; Zhao, H. Synthesis And Characterization Of Germanium-Centered Three-Dimensional Crystalline Porous Aromatic Framework. *J. Mater. Res.* **2012**, *27*, 1417-1420.

68- Ren, H.; Ben, T.; Wang, E.; Jing, X.; Xue, M.; Liu, B.; Cui, Y.; Qiu, S.; Zhu, G. Targeted Synthesis of a 3D Porous Aromatic Framework for Selective Sorption of Benzene. *Chem. Commun.* **2010**, *46*, 291–293.

69- Jing, L.; Sun, J.; Sun, F.; Chen, P.; Zhu, G. Porous Aromatic Framework With Mesopores As A Platform For A Super-Efficient Heterogeneous Pd-Based Organometallic Catalysis. *Chem. Sci.* **2018**, *9*, 3523-3530.

70- Skowronek, P.; Gawronski, J. Chiral Iminospherand Of A Tetrahedral Symmetry Spontaneously Assembled In A [6 + 4] Cyclocondensation. *Org. Lett.* **2008**, *10*, 4755-4758.

71- Tozawa, T.; Jones, J. T. A.; Swamy, S. I.; Jiang, S.; Adams, D. J.; Shakespeare, S.; Clowes, R.; Bradshaw, D.; Hasell, T.; Chong, S. Y.; Tang, C.; Thompson, S.; Parker, J.; Trewin, A.; Bacsa, J.; Slawin, A. M. Z.; Steiner, A.; Cooper, A. I. Porous Organic Cages. *Nat. Mater.* **2009**, *8*, 973–978.

72- Jelfs, K. E.; Eden, E. G. B.; Culshaw, J. L.; Shakespeare, S.; Pyzer-Knapp, E. O.; Thompson, H. P. G.; Bacsa, J.; Day, G. M.; Adams, D. J.; Cooper, A. I. In Silico Design of Supramolecules from Their Precursors: Odd–Even Effects in Cage-Forming Reactions. *J. Am. Chem. Soc.* **2013**, *135*, 9307–9310.

73- Avellaneda, A.; Valente, P.; Burgun, A.; Evans, J. D.; Markwell-Heys, A. W.; Rankine, D.; Nielsen, D. J.; Hill, M. R.; Sumby, C. J.; Doonan, C. J.

Kinetically Controlled Porosity in a Robust Organic Cage Material. *Angew. Chem., Int. Ed.* **2013**, *125*, 3834–3837.

74- Zhang, G.; Presly, O.; White, F.; Oppel, I. M.; Mastalerz, M. A Permanent Mesoporous Organic Cage with an Exceptionally High Surface Area. *Angew. Chem., Int. Ed.* **2014**, *126*, 1542–1546.

75- Hong, S.; Rohman, M. R.; Jia, J.; Kim, Y.; Moon, D.; Kim, Y.; Ko, Y. H.; Lee, E.; Kim, K. Porphyrin Boxes: Rationally Designed Porous Organic Cages. *Angew. Chem., Int. Ed.* **2015**, *127*, 13439–13442.

76- Teng, B.; Little, M. A.; Hasell, T.; Chong, S. Y.; Jelfs, K. E.; Clowes, R.; Briggs, M. E.; Cooper, A. I. Synthesis of a Large, Shape-Flexible, Solvatomorphic Porous Organic Cage. *Cryst. Growth Des.* **2019**, *19*, 3647–3651.

77- Zhang, C.; Chen, C. Synthesis and Structure Of A Triptycene-Based Nanosized Molecular Cage. *J. Org. Chem.* **2007**, *72*, 9339-9341.

78- Ono, K.; Johmoto, K.; Yasuda, N.; Uekusa, H.; Fujii, S.; Kiguchi, M.; Iwasawa, N. Self-Assembly Of Nanometer-Sized Boroxine Cages From Diboronic Acids. *J. Am. Chem. Soc.* **2015**, *137*, 7015-7018.

79- Zhang, J.; Li, Y.; Yang, W.; Lai, S.; Zhou, C.; Liu, H.; Che, C.; Li, Y. A Smart Porphyrin Cage For Recognizing Azide Anions. *Chem. Commun.* **2012**, *48*, 3602-3604.

80- Bojdys, M.; Briggs, M.; Jones, J.; Adams, D.; Chong, S.; Schmidtmann, M.; Cooper, A. Supramolecular Engineering Of Intrinsic And Extrinsic Porosity In Covalent Organic Cages. *J. Am. Chem. Soc.* **2011**, *133*, 16566-16571.

81- Hasell, T.; Culshaw, J.; Chong, S.; Schmidtmann, M.; Little, M.; Jelfs, K.; Pyzer-Knapp, E.; Shepherd, H.; Adams, D.; Day, G.; Cooper, A. Controlling The Crystallization Of Porous Organic Cages: Molecular Analogs Of Isoreticular Frameworks Using Shape-Specific Directing Solvents. *J. Am. Chem. Soc.* **2014**, *136*, 1438-1448.

82- Klotzbach, S.; Beuerle, F. Shape-Controlled Synthesis And Self-Sorting Of Covalent Organic Cage Compounds. *Angew. Chem., Int. Ed.* **2015**, *54*, 10356-10360.

83- Icli, B.; Sheepwash, E.; Riis-Johannessen, T.; Schenk, K.; Filinchuk, Y.; Scopelliti, R.; Severin, K. Dative Boron–Nitrogen Bonds In Structural

Supramolecular Chemistry: Multicomponent Assembly Of Prismatic Organic Cages. *Chem. Sci.* **2011**, *2*, 1719-1721.

84- Wang, Q.; Zhang, C.; Noll, B.; Long, H.; Jin, Y.; Zhang, W. A Tetrameric Cage With d2h Symmetry Through Alkyne Metathesis. *Angew. Chem., Int. Ed.* **2014**, *53*, 10663-10667.

85- Wang, Q.; Yu, C.; Zhang, C.; Long, H.; Azarnoush, S.; Jin, Y.; Zhang, W. Dynamic Covalent Synthesis Of Aryleneethynylene Cages Through Alkyne Metathesis: Dimer, Tetramer, Or Interlocked Complex?. *Chem. Sci.* **2016**, *7*, 3370-3376.

86- Jones, J.; Hasell, T.; Wu, X.; Bacsa, J.; Jelfs, K.; Schmidtmann, M.; Chong, S.; Adams, D.; Trewin, A.; Schiffman, F.; Cora, F.; Slater, B.; Steiner, A.; Day, G.; Cooper, A. Modular And Predictable Assembly of Porous Organic Molecular Crystals. *Nature* **2011**, *474*, 367-371.

87- Swamy, S.; Bacsa, J.; Jones, J.; Stylianou, K.; Steiner, A.; Ritchie, L.; Hasell, T.; Gould, J.; Laybourn, A.; Khimyak, Y.; Adams, D.; Rosseinsky, M.; Cooper, A. A Metal−Organic Framework With A Covalently Prefabricated Porous Organic Linker. *J. Am. Chem. Soc.* **2010**, *132*, 12773-12775.

88- Buyukcakir, O.; Seo, Y.; Coskun, A. Thinking Outside The Cage: Controlling The Extrinsic Porosity And Gas Uptake Properties Of Shape-Persistent Molecular Cages In Nanoporous Polymers. *Chem. Mater.* **2015**, *27*, 4149-4155.

89- Zhang, J.-H.; Xie, S.-M.; Chen, L.; Wang, B.-J.; He, P.-G.; Yuan, L.-M. Homochiral Porous Organic Cage with High Selectivity for the Separation of Racemates in Gas Chromatography. *Anal. Chem*. **2015**, *87*, 7817–7824.

90- Brutschy, M.; Schneider, M.; Mastalerz, M.; Waldvogel, S. Porous Organic Cage Compounds As Highly Potent Affinity Materials For Sensing By Quartz Crystal Microbalances. *Adv. Mater.* **2012**, *24*, 6049-6052.

91- Hasell, T.; Cooper, A. Porous Organic Cages: Soluble, Modular And Molecular Pores. *Nat. Rev. Mater.* **2016**, *1*, 16053.

92- Mastalerz, M. Porous Shape-Persistent Organic Cage Compounds of Different Size, Geometry, and Function. *Acc. Chem. Res.* **2018**, *51*, 2411–2422.

93- Zhang, Y.; Zhan, T.-G.; Zhou, T.-Y.; Qi, Q.-Y.; Xu, X.-N.; Zhao, X. Fluorescence Enhancement through the Formation of a Single-Layer Two-Dimensional

Supramolecular Organic Framework and Its Application in Highly Selective Recognition of Picric Acid. *Chem. Commun.* **2016**, *52*, 7588–7591.

94- Chen, L.; Reiss, P. S.; Chong, S. Y.; Holden, D.; Jelfs, K. E.; Hasell, T.; Little, M. A.; Kewley, A.; Briggs, M. E.; Stephenson, A.; Thomas, K. M.; Armstrong, J. A.; Bell, J.; Busto, J.; Noel, R.; Liu, J.; Strachan, D. M.; Thallapally, P. K.; Cooper, A. I. Separation of Rare Gases and Chiral Molecules by Selective Binding in Porous Organic Cages. *Nat. Mater.* **2014**, *13*, 954–960.

95- Mitra, T.; Jelfs, K. E.; Schmidtmann, M.; Ahmed, A.; Chong, S. Y.; Adams, D. J.; Cooper, A. I. Molecular Shape Sorting Using Molecular Organic Cages. *Nat. Chem.* **2013**, *5*, 276–281.

96- Sun, J.-K.; Zhan, W.-W.; Akita, T.; Xu, Q. Toward Homogenization of Heterogeneous Metal Nanoparticle Catalysts with Enhanced Catalytic Performance: Soluble Porous Organic Cage as a Stabilizer and Homogenizer. *J. Am. Chem. Soc.* **2015**, *137*, 7063–7066.

97- Yilmaz, B.; Müller, U. Catalytic Applications of Zeolites In Chemical Industry. *Top. Catal.* **2009**, *52*, 888-895.

98- Bellussi, G.; Millini, R.; Pollesel, P.; Perego, C. Zeolite Science and Technology At Eni. *New J. Chem.* **2016**, *40*, 4061-4077.

99- Guisnet, M.; Magnoux, P. Fundamental Description Of Deactivation And Regeneration Of Acid Zeolites. *Catalyst Deactivation 1994, Proceedings of the 6th International Symposium* 1994, 53-68.

100- Christensen, C.; Johannsen, K.; Tornqvist, E.; Schmidt, I.; Topsoe, H.; Christensen, C. Mesoporous Zeolite Single Crystal Catalysts: Diffusion And Catalysis In Hierarchical Zeolites. *Catal. Today* **2007**, *128*, 117-122.

101- Guisnet, M.; Costa, L.; Ribeiro, F. Prevention Of Zeolite Deactivation By Coking. *J. Mol. Catal. A: Chem.* **2009**, *305*, 69-83.

102- Sholl, D.; Lively, R. Seven Chemical Separations To Change The World. *Nature* **2016**, *532*, 435-437.

103- Bosch, H.; De Haan, A. *Industrial Separation Processes*; De Gruyter: Boston, 2013. Pg. 2

104- Materials for Separation Technologies: Energy and Emission Reduction Opportunities; OSTI 1218755; US DOE Office of Energy Efficiency and Renewable Energy, Advanced Manufacturing Office: United States, 2005.

105- Reddy, C.; Fang, Y.; Rangaiah, G. Improving Energy Efficiency Of Distillation Using Heat Pump Assisted Columns. *Asia-Pac. J. Chem. Eng.* **2014**, *9*, 905-928.

106- Fu, J., Das, S., Xing, G., Ben, T., Valtchev, V. and Qiu, S. Fabrication of COF-MOF Composite Membranes and Their Highly Selective Separation of H_2/CO_2. *J. Am. Chem. Soc.* **2016,** 138, 7673-7680.

107- Uribe-Romo, F.; Hunt, J.; Furukawa, H.; Klöck, C.; O'Keeffe, M.; Yaghi, O. A Crystalline Imine-Linked 3-D Porous Covalent Organic Framework. *J. Am. Chem. Soc.* **2009**, *131*, 4570-4571.

108- Budd, P.; Msayib, K.; Tattershall, C.; Ghanem, B.; Reynolds, K.; McKeown, N.; Fritsch, D. Gas Separation Membranes from Polymers Of Intrinsic Microporosity. *J. Membr. Sci.* **2005**, *251*, 263-269.

109- Schulte-Schulze-Berndt, A.; Krabiell, K. Nitrogen Generation By Pressure Swing Adsorption Based On Carbon Molecular Sieves. *Gas Sep. Purif.* **1993**, *7*, 253-257.

110- Abdullah, A.; Idris, I.; Shamsudin, I.; Othman, M. Methane Enrichment From High Carbon Dioxide Content Natural Gas By Pressure Swing Adsorption. *J. Nat. Gas Sci. Eng.* **2019**, *69*, 102929.

111- Hasell, T.; Miklitz, M.; Stephenson, A.; Little, M.; Chong, S.; Clowes, R.; Chen, L.; Holden, D.; Tribello, G.; Jelfs, K.; Cooper, A. Porous Organic Cages For Sulfur Hexafluoride Separation. *J. Am. Chem. Soc.* **2016**, *138*, 1653-1659.

112- Evans, J.; Huang, D.; Hill, M.; Sumby, C.; Thornton, A.; Doonan, C. Feasibility Of Mixed Matrix Membrane Gas Separations Employing Porous Organic Cages. *J. Phys. Chem. C* **2014**, *118*, 1523-1529.

113- Robeson, L. Correlation Of Separation Factor Versus Permeability For Polymeric Membranes. *J. Membr. Sci.* **1991**, *62*, 165-185.

114- Robeson, L. The Upper Bound Revisited. *J. Membr. Sci.* **2008**, *320*, 390-400.

115- Zhang, J.; Xie, S.; Chen, L.; Wang, B.; He, P.; Yuan, L. Homochiral Porous Organic Cage With High Selectivity For The Separation Of Racemates In Gas Chromatography. *Anal. Chem.* **2015**, *87*, 7817-7824.

116- Hydrocarbon Processing: Efficient Separation Of Gas-Liquid Mixtures. *Filtr. Sep.* **2011**, *48*, 20-21.

117- U.S. Energy Information Agency. *Short Term Energy Outlook*; U.S. Energy Information Agency: Washington DC, 2020.

118- Li, B.; Zhang, Y.; Krishna, R.; Yao, K.; Han, Y.; Wu, Z.; Ma, D.; Shi, Z.; Pham, T.; Space, B.; Liu, J.; Thallapally, P.; Liu, J.; Chrzanowski, M.; Ma, S. Introduction Of Π-Complexation Into Porous Aromatic Framework For Highly Selective Adsorption Of Ethylene Over Ethane. *J. Am. Chem. Soc.* **2014**, *136*, 8654-8660.

119- Jiang, L.; Tian, Y.; Sun, T.; Zhu, Y.; Ren, H.; Zou, X.; Ma, Y.; Meihaus, K.; Long, J.; Zhu, G. A Crystalline Polyimide Porous Organic Framework for Selective Adsorption Of Acetylene Over Ethylene *J. Am. Chem. Soc.* **2018**, *140*, 15724-15730.

120- Jiang, L.; Wang, P.; Li, M.; Zhang, P.; Li, J.; Liu, J.; Ma, Y.; Ren, H.; Zhu, G. Construction Of A Stable Crystalline Polyimide Porous Organic Framework For C 2 H 2 /C 2 H 4 And CO 2 /N 2 Separation. *Chem. – Eur. J.* **2019**, *25*, 9045-9051.

121- Gonçalves, R.; de Oliveira, A.; Sindra, H.; Archanjo, B.; Mendoza, M.; Carneiro, L.; Buarque, C.; Esteves, P. Heterogeneous Catalysis By Covalent Organic Frameworks (COF): Pd(Oac)2@COF-300 In Cross-Coupling Reactions. *ChemCatChem* **2016**, *8*, 743-750.

122- Ding, S.; Gao, J.; Wang, Q.; Zhang, Y.; Song, W.; Su, C.; Wang, W. Construction of Covalent Organic Framework For Catalysis: Pd/COF-LZU1 In Suzuki–Miyaura Coupling Reaction. *J. Am. Chem. Soc.* **2011**, *133*, 19816-19822.

123- Maximov, A.; Zolotukhina, A.; Kulikov, L.; Kardasheva, Y.; Karakhanov, E. Ruthenium Catalysts Based on Mesoporous Aromatic Frameworks For The Hydrogenation Of Arenes. *React. Kinet., Mech. Catal.* **2016**, *117*, 729-743.

124- Rangel-Rangel, E.; Verde-Sesto, E.; Rasero-Almansa, A.; Iglesias, M.; Sánchez, F. Porous Aromatic Frameworks (PAFs) As Efficient Supports For N-Heterocyclic Carbene Catalysts. *Catal. Sci. Technol.* **2016**, *6*, 6037-6045.

125- Goesten, M.; Szécsényi, À.; de Lange, M.; Bavykina, A.; Gupta, K.; Kapteijn, F.; Gascon, J. Sulfonated Porous Aromatic Frameworks As Solid Acid Catalysts. *ChemCatChem* **2016**, *8*, 961-967.

126- Pal, R.; Sarkar, T.; Khasnobis, S. Amberlyst-15 In Organic Synthesis. *Arkivoc* **2012**, *2012*, 570-609.

127- Chen, P.; Sun, J.; Zhang, L.; Ma, W.; Sun, F.; Zhu, G. Porous Aromatic Framework (PAF-1) As Hyperstable Platform for Enantioselective Organocatalysis. *Sci. China Mater.* **2018**, *62*, 194-202.

128- Sun, J.; Jing, L.; Tian, Y.; Sun, F.; Chen, P.; Zhu, G. Task-Specific Design Of A Hierarchical Porous Aromatic Framework As An Ultrastable Platform For Large-Sized Catalytic Active Site Binding. *Chem. Commun.* **2018**, *54*, 1603-1606.

129- Argyle, M.; Bartholomew, C. Heterogeneous Catalyst Deactivation and Regeneration: A Review. *Catalysts* **2015**, *5*, 145-269.

130- Inventory of U.S. greenhouse gas emissions and sinks 1990-2017; U.S. Environmental Protection Agency: Washington, DC, 2019.

131- Van Dam, J. *Sustainable biomass production and use: lessons learned from the Netherlands programme sustainable biomass (NPSB) 2009-2013;* Report for Netherlands Enterprise Agency: BJ Utrecht, The Netherlands, May 2014

132- Johnson, T.; Joshi, A. Review of Vehicle Engine Efficiency and Emissions. *SAE Int. J. Engines* **2018**, *11*, 1307–1330.

133- Caton, J. A. Maximum Efficiencies for Internal Combustion Engines: Thermodynamic Limitations. *Int. J. Engine Res.* **2017**, *19*, 1005–1023.

134- Natural gas vehicles: Status, barriers, and opportunities; United States Dept. of Energy. Office of Scientific and Technical Information: Washington, D.C., 2010.

135- Bilgili, F.; Koçak, E.; Bulut, Ü. The Shale Gas Production and Economic Growth in Local Economies across the US. *Environ. Sci. Pollut. Res.* **2020**, *27*, 12001–12016.

136- Annual energy outlook 2020: with projections to 2050; Energy Information Administration: Washington, D.C., 2020.

137- Setzmann, U.; Wagner, W. A New Equation of State and Tables of Thermodynamic Properties for Methane Covering the Range from the Melting Line to 625 K at Pressures up to 100 MPa. *J. Phy. Chem. Ref. Data* **1991**, *20*, 1061–1155.

138- Sarıkoç, S. Fuels of the Diesel-Gasoline Engines and Their Properties. *Diesel and Gasoline Engines*; Viskup, R.; IntechOpen: London, 2020.

139- Mason, J. A.; Veenstra, M.; Long, J. R. Evaluating Metal–Organic Frameworks for Natural Gas Storage. *Chem. Sci.* **2014**, *5*, 32–51.

140- Greenhouse Emission Reductions and Natural Gas Vehicles: a Resource Guide on Technology Options and Project Development; United States. Office of Fossil Energy: Washington, D.C., 2002.

141- Gómez-Gualdrón, D. A.; Wilmer, C. E.; Farha, O. K.; Hupp, J. T.; Snurr, R. Q. Exploring the Limits of Methane Storage and Delivery in Nanoporous Materials. *J. Phys. Chem. C* **2014**, *118*, 6941–6951

142- Chui, S.; Lo, S.; Charmant, J.; Orpen, A.; Williams, I. A Chemically Functionalizable Nanoporous Material $[Cu_3(TMA)_2(H_2O)3]_n$. *Science* **1999**, *283*, 1148-1150.

143- Tsivadze, A.; Aksyutin, O.; Ishkov, A.; Knyazeva, M.; Solovtsova, O.; Men'shchikov, I.; Fomkin, A.; Shkolin, A.; Khozina, E.; Grachev, V. Metal-Organic Framework Structures: Adsorbents for Natural Gas Storage. *Russ. Chem. Rev.* **2019**, *88*, 925-978.

144- Li, B.; Wen, H.; Wang, H.; Wu, H.; Tyagi, M.; Yildirim, T.; Zhou, W.; Chen, B. A Porous Metal–Organic Framework with Dynamic Pyrimidine Groups Exhibiting Record High Methane Storage Working Capacity. *J. Am. Chem. Soc.* **2014**, *136*, 6207-6210.

145- Mahmoud, E.; Ali, L.; El Sayah, A.; Alkhatib, S.; Abdulsalam, H.; Juma, M.; Al-Muhtaseb, A. Implementing Metal-Organic Frameworks for Natural Gas Storage. *Crystals* **2019**, *9*, 406.

146- Li, B.; Wen, H.; Zhou, W.; Xu, J.; Chen, B. Porous Metal-Organic Frameworks: Promising Materials For Methane Storage. *Chem* **2016**, *1*, 557-580.

147- Yuan, Y.; Zhu, G. Porous Aromatic Frameworks As A Platform For Multifunctional Applications. *ACS Cent. Sci.* **2019**, *5*, 409-418.

148- Liu, S.; Josephson, T. R.; Athaley, A.; Chen, Q. P.; Norton, A.; Ierapetritou, M.; Siepmann, J. I.; Saha, B.; Vlachos, D. G. Renewable Lubricants with Tailored Molecular Architecture. *Sci. Adv.* **2019**, *5*, eaav5487.

149- Lange, J.-P.; Van Der Heide, E.; Van Buijtenen, J.; Price, R. Furfural-A Promising Platform for Lignocellulosic Biofuels. *ChemSusChem* **2011**, *5*, 150–166.

150- Gunanathan, C.; Milstein, D. Applications of Acceptorless Dehydrogenation and Related Transformations in Chemical Synthesis. *Science* **2013**, *341*, 1229712–1229712.

151- Yokoyama, T.; Yamagata, N. Hydrogenation of Carboxylic Acids to the Corresponding Aldehydes. *Appl. Catal., A* **2001**, *221*, 227–239.

152- Van Dam, J. *Sustainable biomass production and use: lessons learned from the Netherlands programme sustainable biomass (NPSB) 2009-2013;* Report for Netherlands Enterprise Agency: BJ Utrecht, The Netherlands, May 2014

153- Tripathi, N.; Hills, C. D.; Singh, R. S.; Atkinson, C. J. Biomass Waste Utilisation in Low-Carbon Products: Harnessing a Major Potential Resource. *Npj Clim. Atmos. Sci.* **2019**, *2*, 35.

154- Van Humbeck, J.; McDonald, T.; Jing, X.; Wiers, B.; Zhu, G.; Long, J. Ammonia Capture In Porous Organic Polymers Densely Functionalized With Brønsted Acid Groups. *J. Am. Chem. Soc.* **2014**, *136*, 2432-2440.

155- Liu, S.; Saha, B.; Vlachos, D. Catalytic Production of Renewable Lubricant Base Oils From Bio-Based 2-Alkylfurans And Enals. *Green Chem.* **2019**, *21*, 3606-3614.

156- Sathre, R.; Masanet, E. Prospective Life-Cycle Modeling Of A Carbon Capture And Storage System Using Metal–Organic Frameworks For CO_2 Capture. *RSC Adv.* **2013**, *3*, 4964-4975.

157- Wilmer, C.; Farha, O.; Bae, Y.; Hupp, J.; Snurr, R. Structure–Property Relationships Of Porous Materials For Carbon Dioxide Separation And Capture. *Energy Environ. Sci.* **2012**, *5*, 9849-9856.

158- Chen, L.; Morrison, C.; Düren, T. Improving Predictions Of Gas Adsorption In Metal–Organic Frameworks With Coordinatively Unsaturated Metal Sites: Model Potentials, Ab Initio Parameterization, And GCMC Simulations. *J. Phys. Chem. C* **2012**, *116*, 18899-18909.

159- Kökçam-Demir, Ü.; Goldman, A.; Esrafili, L.; Gharib, M.; Morsali, A.; Weingart, O.; Janiak, C. Coordinatively Unsaturated Metal Sites (Open Metal Sites) In Metal–Organic Frameworks: Design And Applications. *Chem. Soc. Rev.* **2020**, *49*, 2751-2798.

160- He, Y.; Zhou, W.; Yildirim, T.; Chen, B. A Series Of Metal–Organic Frameworks With High Methane Uptake And An Empirical Equation For Predicting Methane Storage Capacity. *Energy Environ. Sci.* **2013**, *6*, 2735-2744.

161- Cheng, F.; Li, Q.; Duan, J.; Hosono, N.; Noro, S.; Krishna, R.; Lyu, H.; Kusaka, S.; Jin, W.; Kitagawa, S. Fine-Tuning Optimal Porous Coordination Polymers Using Functional Alkyl Groups for CH_4 Purification. *J. Mater. Chem. A* **2017**, *5*, 17874-17880.

162- Eddaoudi, M.; Kim, J.; Rosi, N.; Vodak, D.; Wachter, J.; O'Keeffe, M.; Yaghi, O. Systematic Design Of Pore Size And Functionality In Isoreticular Mofs And Their Application In Methane Storage. *Science* **2002**, *295*, 469-472.

163- Zhu, Y.; Zhang, W. Reversible Tuning Of Pore Size And Co2adsorption In Azobenzene Functionalized Porous Organic Polymers. *Chem. Sci.* **2014**, *5*, 4957-4961.

164- Garibay, S.; Weston, M.; Mondloch, J.; Colón, Y.; Farha, O.; Hupp, J.; Nguyen, S. Accessing Functionalized Porous Aromatic Frameworks (PAFs) Through A De Novo Approach. *CrystEngComm* **2013**, *15*, 1515-1519.

165- Xue, D.; Wang, Q.; Bai, J. Amide-Functionalized Metal–Organic Frameworks: Syntheses, Structures and Improved Gas Storage And Separation Properties. *Coord. Chem. Rev.* **2019**, *378*, 2-16.

166- Chen, M.; Chen, S.; Chen, W.; Lucier, B.; Zhang, Y.; Zheng, A.; Huang, Y. Analyzing Gas Adsorption In An Amide-Functionalized Metal Organic Framework: Are The Carbonyl Or Amine Groups Responsible? *Chem. Mater.* **2018**, *30*, 3613-3617.

167- Suresh, V.; Bonakala, S.; Atreya, H.; Balasubramanian, S.; Maji, T. Amide Functionalized Microporous Organic Polymer (Am-MOP) For Selective CO2 Sorption and Catalysis. *ACS Appl. Mater. Interfaces* **2014**, *6*, 4630-4637.

168- Vitillo, J.; Savonnet, M.; Ricchiardi, G.; Bordiga, S. Tailoring Metal-Organic Frameworks For CO_2 Capture: The Amino Effect. *ChemSusChem* **2011**, *4*, 1281-1290.

169- Zheng, B.; Bai, J.; Duan, J.; Wojtas, L.; Zaworotko, M. Enhanced Co_2 binding Affinity Of A High-Uptake rht-Type Metal−Organic Framework Decorated With Acylamide Groups. *J. Am. Chem. Soc.* **2011**, *133*, 748-751.

170- Yuan, D.; Zhao, D.; Sun, D.; Zhou, H. An Isoreticular Series Of Metal-Organic Frameworks With Dendritic Hexacarboxylate Ligands And Exceptionally High Gas-Uptake Capacity. *Angew. Chem., Int. Ed.* **2010**, *49*, 5357-5361.

171- Aranovich, G.; Donohue, M. Analysis Of Adsorption Isotherms: Lattice Theory Predictions, Classification Of Isotherms For Gas–Solid Equilibria, And Similarities In Gas And Liquid Adsorption Behavior. *J. Colloid Interface Sci.* **1998**, *200*, 273-290.

172- Bracco, S.; Piga, D.; Bassanetti, I.; Perego, J.; Comotti, A.; Sozzani, P. Porous 3D Polymers for High Pressure Methane Storage and Carbon Dioxide Capture. *J. Mater. Chem. A* **2017**, *5*, 10328-10337.

173- Makal, T.; Li, J.; Lu, W.; Zhou, H. Methane Storage In Advanced Porous Materials. *Chem. Soc. Rev.* **2012**, *41*, 7761-7779.

174- Zhou, S.; Guo, C.; Wu, Z.; Wang, M.; Wang, Z.; Wei, S.; Li, S.; Lu, X. Edge-Functionalized Nanoporous Carbons for High Adsorption Capacity and Selectivity Of CO2 Over N2. *Appl. Surf. Sci.* **2017**, *410*, 259-266.

175- Ahmed, S.; Ramli, A.; Yusup, S.; Farooq, M. Adsorption Behavior of Tetraethylenepentamine-Functionalized Si-MCM-41 For CO 2 Adsorption. *Chem. Eng. Res. Des.* **2017**, *122*, 33-42.

176- Mafra, L.; Čendak, T.; Schneider, S.; Wiper, P.; Pires, J.; Gomes, J.; Pinto, M. Amine Functionalized Porous Silica for CO2/CH4 Separation By Adsorption: Which Amine And Why. *Chem. Eng. J.* **2018**, *336*, 612-621.

177- Ge, B.; Xu, Y.; Zhao, H.; Sun, H.; Guo, Y.; Wang, W. High Performance Gas Separation Mixed Matrix Membrane Fabricated By Incorporation Of Functionalized Submicrometer-Sized Metal-Organic Framework. *Materials* **2018**, *11*, 1421.

178- Cmarik, G.; Kim, M.; Cohen, S.; Walton, K. Tuning the Adsorption Properties Of Uio-66 Via Ligand Functionalization. *Langmuir* **2012**, *28*, 15606-15613.

179- Charles, C.; Bloch, E. High-Pressure Methane Storage and Selective Gas Adsorption In A Cyclohexane-Functionalised Porous Organic Cage. *Supramol. Chem.* **2019**, *31*, 508-513.

180- Gosselin, E.; Decker, G.; Antonio, A.; Lorzing, G.; Yap, G.; Bloch, E. A Charged Coordination Cage-Based Porous Salt. *J. Am. Chem. Soc.* **2020**, *142*, 9594-9598.

181- Jiang, S.; Jones, J.; Hasell, T.; Blythe, C.; Adams, D.; Trewin, A.; Cooper, A. Porous Organic Molecular Solids By Dynamic Covalent Scrambling. *Nat. Commun.* **2011**, *2*, 207.

182- Tagliabue, M.; Rizzo, C.; Millini, R.; Dietzel, P. D. C.; Blom, R.; Zanardi, S. Methane Storage on CPO-27-Ni Pellets. *J. Porous Mater.* **2010**, *18*, 289–296.

183- Jia, Z.; Li, H.; Yu, Z.; Wang, P.; Fan, X. Densification of MOF-5 Synthesized at Ambient Temperature for Methane Adsorption. *Matter. Lett.* **2011**, *65*, 2445–2447.

184- Peterson, G. W.; Decoste, J. B.; Glover, T. G.; Huang, Y.; Jasuja, H.; Walton, K. S. Effects of Pelletization Pressure on the Physical and Chemical Properties of the Metal–Organic Frameworks Cu3(BTC)2 and UiO-66. *Microporous and Mesoporous Mater.* **2013**, *179*, 48–53.